USGS
science for a changing world

Prepared in cooperation with Broward County Environmental Planning and Community Resilience Division, Florida

Sequence Stratigraphy, Seismic Stratigraphy, and Seismic Structures of the Lower Intermediate Confining Unit and Most of the Floridan Aquifer System, Broward County, Florida

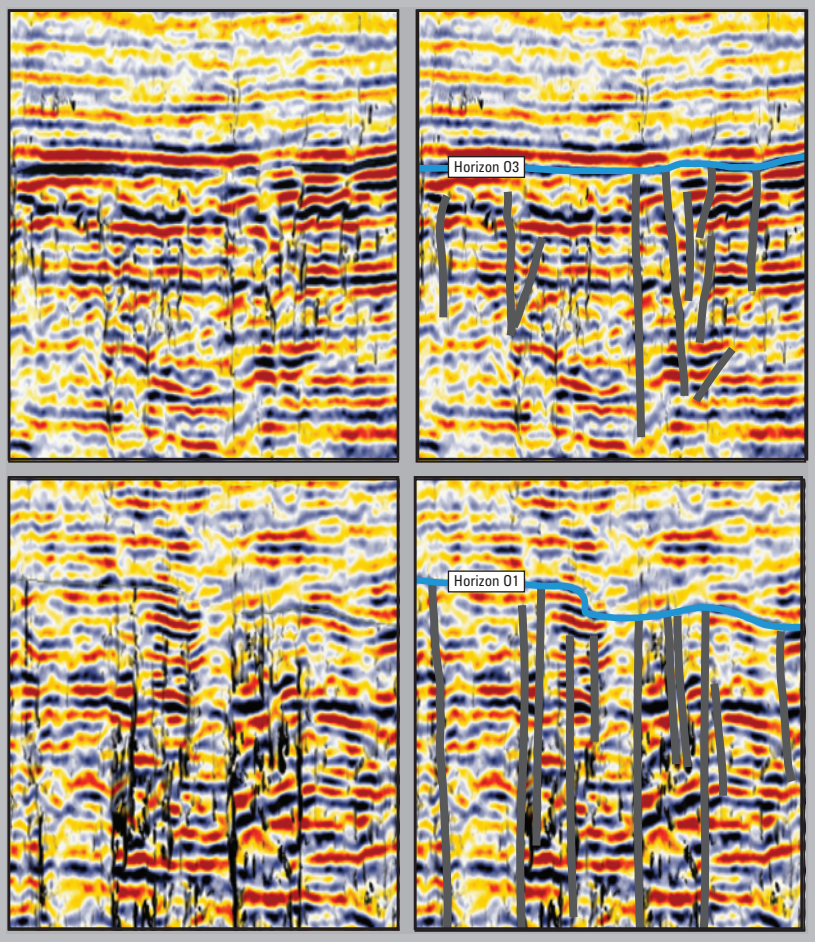

Scientific Investigations Report 2017–5109
Version 1.1

U.S. Department of the Interior
U.S. Geological Survey

Cover. Two parts of seismic-reflection profile S7 showing artificial-neural-network-based meta-attribute calculations applied. Uninterpreted profile segments are shown on the left and interpreted profile segments on the right. Further details are provided in figure 30*B*–*E* of this report.

Sequence Stratigraphy, Seismic Stratigraphy, and Seismic Structures of the Lower Intermediate Confining Unit and Most of the Floridan Aquifer System, Broward County, Florida

By Kevin J. Cunningham, Jared W. Kluesner, Richard L. Westcott, Edward Robinson, Cameron Walker, and Shakira A. Khan

Prepared in cooperation with Broward County Environmental Planning and Community Resilience Division, Florida

Scientific Investigations Report 2017–5109
Version 1.1

U.S. Department of the Interior
U.S. Geological Survey

U.S. Department of the Interior
RYAN K. ZINKE, Secretary

U.S. Geological Survey
William H. Werkheiser, Deputy Director,
exercising the authority of the Director

U.S. Geological Survey, Reston, Virginia:
First release: 2017
Revised: January 2018 (ver. 1.1)

Suggested citation:
Cunningham, K.J., Kluesner, J.W., Westcott, R.L., Robinson, Edward, Walker, Cameron, and Khan, S.A., 2018, Sequence stratigraphy, seismic stratigraphy, and seismic structures of the lower intermediate confining unit and most of the Floridan aquifer system, Broward County, Florida (ver. 1.1, January 2018): U.S. Geological Survey Scientific Investigations Report 2017–5109, 71 p., 21 pls., https://doi.org/10.3133/sir20175109.

ISSN 2328-0328 (online)

Acknowledgments

The authors thank Michael Zygnerski, Barbara Powell, and Jennifer Jurado of the Broward County Environmental Planning and Community Resilience Division for providing logistical support and guidance during the course of the project. Fran Henderson (retired) and Susan Bodmann of the Broward County Department of Planning and Environmental Protection-Water and Wastewater Services extended direction and logistical support. Timothy Welch of the City of Sunrise Utilities Department contributed useful advice during planning of the seismic-reflection survey. David Smith of Arcadis provided assistance in acquisition of well data from the City of Hollywood. Jonathan Arthur of the Florida Geological Survey granted permission for examination of rock core and cuttings from wells in Broward and Miami-Dade Counties, and David Paul and Jesse Hurd of the Florida Geological Survey furnished logistical support and guidance for the task. Amanda Leavitt and Ricardo Melendez, student services contractors, provided skillful assistance with processing core samples. Kevin Defosset, Cooperative Ecosystem Studies Units collaborator, helped with construction of two figures.

Dorothy Sifuentes of the U.S. Geological Survey (USGS) Caribbean-Florida Water Science Center offered supervisory direction throughout the study. Robert Renken, USGS emeritus, provided assistance in the early years of project development and planning. G. Lynn Wingard of the USGS Eastern Geology and Paleoclimate Science Center is thanked for her notes used in identification of an oyster of the Gryphaeidae family. Jacqueline Powell, USGS volunteer, assisted generously with core-sample processing and providing guidance in the identification of benthic foraminifers.

Contents

Plates

[Available for download at https://doi.org/10.3133/sir20175109]

Figures

Tables

Conversion Factors

Inch/Pound to International System of Units

Multiply	By	To obtain
	Length	
inch (in.)	2.54	centimeter (cm)
inch (in.)	25.4	millimeter (mm)
foot (ft)	0.3048	meter (m)
mile (mi)	1.609	kilometer (km)
	Area	
square mile (mi^2)	2.590	square kilometer (km^2)
	Volume	
cubic inch (in^3)	16.39	cubic centimeter (cm^3)
	Velocity	
foot per second (ft/s)	0.3048	meter per second (m/s)

Datum

Vertical coordinate information is referenced to the North American Vertical Datum of 1988 (NAVD 88).

Horizontal coordinate information is referenced to the North American Datum of 1983 (NAD 83).

Altitude, as used in this report, refers to distance above or below the vertical datum.

Supplemental Information

Concentrations of chemical constituents in water are given in milligrams per liter (mg/L).

Abbreviations

2D	two-dimensional
3D	three-dimensional
ASR	aquifer storage and recovery
Hz	hertz
kHz	kilohertz
RMS	reservoir management software
USGS	U.S. Geological Survey

Sequence Stratigraphy, Seismic Stratigraphy, and Seismic Structures of the Lower Intermediate Confining Unit and Most of the Floridan Aquifer System, Broward County, Florida

By Kevin J. Cunningham,[1] Jared W. Kluesner,[1] Richard L. Westcott,[2] Edward Robinson,[3] Cameron Walker,[4] and Shakira A. Khan[2]

Abstract

Deep well injection and disposal of treated wastewater into the highly transmissive saline Boulder Zone in the lower part of the Floridan aquifer system began in 1971. The zone of injection is a highly transmissive hydrogeologic unit, the Boulder Zone, in the lower part of the Floridan aquifer system. Since the 1990s, however, treated wastewater injection into the Boulder Zone in southeastern Florida has been detected at three treated wastewater injection utilities in the brackish upper part of the Floridan aquifer system designated for potential use as drinking water. At a time when usage of the Boulder Zone for treated wastewater disposal is increasing and the utilization of the upper part of the Floridan aquifer system for drinking water is intensifying, there is an urgency to understand the nature of cross-formational fluid flow and identify possible fluid pathways from the lower to upper zones of the Floridan aquifer system. To better understand the hydrogeologic controls on groundwater movement through the Floridan aquifer system in southeastern Florida, the U.S. Geological Survey and the Broward County Environmental Planning and Community Resilience Division conducted a 3.5-year cooperative study from July 2012 to December 2015. The study characterizes the sequence stratigraphy, seismic stratigraphy, and seismic structures of the lower part of the intermediate confining unit aquifer and most of the Floridan aquifer system.

Data obtained to meet the study objective include 80 miles of high-resolution, two-dimensional (2D), seismic-reflection profiles acquired from canals in eastern Broward County. These profiles have been used to characterize the sequence stratigraphy, seismic stratigraphy, and seismic structures in a 425-square-mile study area. Horizon mapping of the seismic-reflection profiles and additional data collection from well logs and cores or cuttings from 44 wells were focused on construction of three-dimensional (3D) visualizations of eight sequence stratigraphic cycles that compose the Eocene to Miocene Oldsmar, Avon Park, and Arcadia Formations. The mapping of these seismic-reflection and well data has produced a refined Cenozoic sequence stratigraphic, seismic stratigraphic, and hydrogeologic framework of southeastern Florida. The upward transition from the Oldsmar Formation to the Avon Park Formation and the Arcadia Formation embodies the evolution from (1) a tropical to subtropical, shallow-marine, carbonate platform, represented by the Oldsmar and Avon Park Formations, to (2) a broad, temperate, mixed carbonate-siliciclastic shallow marine shelf, represented by the lower part of the Arcadia Formation, and to (3) a temperate, distally steepened carbonate ramp represented by the upper part of the Arcadia Formation.

In the study area, the depositional sequences and seismic sequences have a direct correlation with hydrogeologic units. The approximate upper boundary of four principal permeable units of the Floridan aquifer system (Upper Floridan aquifer, Avon Park permeable zone, uppermost major permeable zone of the Lower Floridan aquifer, and Boulder Zone) have sequence stratigraphic and seismic-reflection signatures that were identified on cross sections, mapped, or both, and therefore the sequence stratigraphy and seismic stratigraphy were used to guide the development of a refined spatial representation of these hydrogeologic units. In all cases, the permeability of the four permeable units is related to stratiform megaporosity generated by ancient dissolution of carbonate rock associated with subaerial exposure and unconformities at the upper surfaces of carbonate depositional cycles of several

[1]U.S. Geological Survey.

[2]Cherokee Nation Businesses, Contractor to the U.S. Geological Survey.

[3]Jarer Biostrat, Inc., Contractor to the U.S. Geological Survey.

[4]Walker Marine Geophysical Company, Contractor to the Miami-Dade County Water and Sewer Department.

hierarchical scales ranging from high-frequency cycles to depositional sequences. Additionally, interparticle porosity also contributes substantially to the stratiform permeability in much of the Upper Floridan aquifer. Information from seismic stratigraphy allowed 3D geomodeling of hydrogeologic units—an approach never before applied to this area. Notably, the 3D geomodeling provided 3D visualizations and geocellular models of the depositional sequences, hydrostratigraphy, and structural features. The geocellular data could be used to update the hydrogeologic structure inherent to groundwater flow simulations that are designed to address the sustainability of the water resources of the Floridan aquifer system.

Two kinds of pathways that could enable upward cross-formational flow of injected treated wastewater from the Boulder Zone have been identified in the 80 miles of high-resolution seismic data collected for this study: a near-vertical reverse fault and karst collapse structures. The single reverse fault, inferred to be of tectonic origin, is in extreme northeastern Broward County and has an offset of about 19 feet at the level of the Arcadia Formation. Most of the 17 karst collapse structures identified manifest as columniform, vertically stacked sagging seismic reflections that span early Eocene to Miocene age rocks equivalent to much of the Floridan aquifer system and the lower part of the overlying intermediate confining unit. In some cases, the seismic-sag structures extend upward into strata of Pliocene age. The seismic-sag structures are interpreted to have a semicircular shape in plan view on the basis of comparison to (1) other seismic-sag structures in southeastern Florida mapped with two 2D seismic cross lines or 3D data, (2) comparison to these structures located in other carbonate provinces, and (3) plausible extensional ring faults detected with multi-attribute analysis. The seismic-sag structures in the study area have heights as great as 2,500 vertical feet, though importantly, one spans about 7,800 feet. Both multi-attribute analysis and visual detection of offset of seismic reflections within the seismic-sag structures indicate faults and fractures are associated with many of the structures. Multi-attribute analysis highlighting chimney fluid pathways also indicates that the seismic-sag structures have a high probability for potential vertical cross-formational fluid flow along the faulted and fractured structures. A collapse of the seismic-sag structures within a deep burial setting evokes an origin related to hypogenic karst processes by ascending flow of subsurface fluids. In addition, paleo-epigenic karst related to major regional subaerial unconformities within the Florida Platform generated collapse structures (paleo-sinkholes) that are much smaller in scale than the cross-formational seismic-sag structures.

Introduction

The source of drinking water in southeastern Florida primarily comes from the shallow Biscayne aquifer of the surficial aquifer system, whereas the Upper Floridan aquifer of the deeper Floridan aquifer system provides only a relatively minor volume (figs. 1 and 2). The Biscayne aquifer is a sole source aquifer in southeastern Florida (Federal Register Notice, 1979) and, as a protective measure, the South Florida Water Management District's Regional Water Availability Rule 1, adopted in 2007, limits urban water withdrawals from the Biscayne aquifer to pre-2006 levels (Broward Water Resources Task Force, 2010). In addition, legislation adopted by the State of Florida mandates the elimination of ocean outfalls of treated wastewater by 2025. These mandated changes have advanced the use of the more deeply buried Floridan aquifer system for the purposes of freshwater supply from the Upper Floridan aquifer and treated wastewater storage in the Boulder Zone of the Lower Floridan aquifer (fig. 2).

The year 1971 marked the beginning of the use of deep well injection of treated wastewater into the highly transmissive Boulder Zone in southern Florida (fig. 2, Meyer, 1974). Since the 1990s, however, wastewater injection into the Boulder Zone in southeastern Florida has been detected at three treated wastewater injection utilities in the brackish (brackish water contains dissolved-solids concentrations that range from 1,000 to 10,000 milligrams per liter) upper part of the Floridan aquifer system designated for potential use as drinking water (Maliva and others, 2007; Walsh and Price, 2010). At a time when usage of the Boulder Zone for treated wastewater disposal is increasing and utilization of the upper brackish part of the Floridan aquifer system for drinking water is intensifying, the possibility of upward movement of treated wastewater brings new urgency to understanding the nature of cross-formational fluid flow and identifying possible fluid pathways from the Boulder Zone to the upper brackish part of the Floridan aquifer system.

In Broward County, the Floridan aquifer system (figs. 1 and 2) is receiving increased attention as a result of regulatory restrictions on water-supply withdrawals and treated wastewater management practices. However, the integrity of the Floridan aquifer system for use either as a water-supply resource or wastewater repository (or both) is not well understood. Structural geologic anomalies (faults, fractures, and karst collapse structures) within the Floridan aquifer system in southeastern Florida are well documented (Cunningham and Walker, 2009; Cunningham and others, 2012; Reese and Cunningham, 2013, 2014; Cunningham, 2015) and present a potential risk for vertical cross-formational transport of undesirable fluids through the aquifer. The karst collapse structures are defined on seismic-reflection profiles as columniform, seismic-sag structures (McDonnell and others, 2007). Moreover, because of the risk posed by limited stratigraphic knowledge of the physical system and the presence of the structural geologic anomalies, the sustainability of the Floridan aquifer system as a source of groundwater and as a wastewater-injection reservoir remains uncertain (Broward Water Resources Task Force, 2010). In Broward County, some resource managers have expressed concern over a shortage of quality hydrogeologic data on which to base flow models used for evaluation of the potential efficacy of alternative

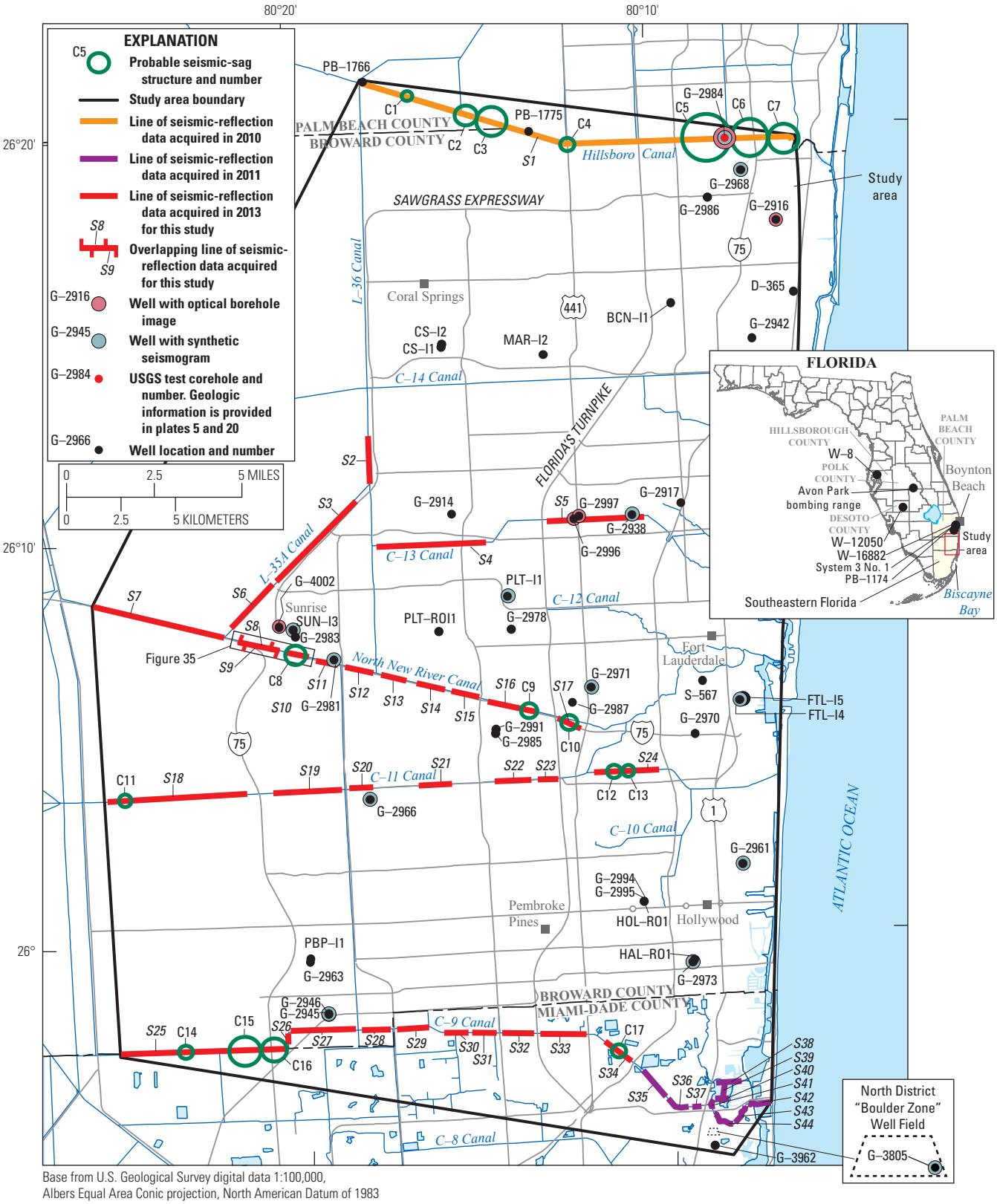

Base from U.S. Geological Survey digital data 1:100,000,
Albers Equal Area Conic projection, North American Datum of 1983

Figure 1. Location of southeastern Florida (inset map), and the eastern Broward County and northeastern Miami-Dade County study area. Shown are the locations of newly acquired (red lines) and existing (orange and purple lines) seismic-reflection surveys used in this cooperative study between the U.S. Geological Survey and the Broward County Environmental Planning and Community Resilience Division. Also shown are the locations of seismic-reflection profiles and seismic-sag structures observed on the profiles.

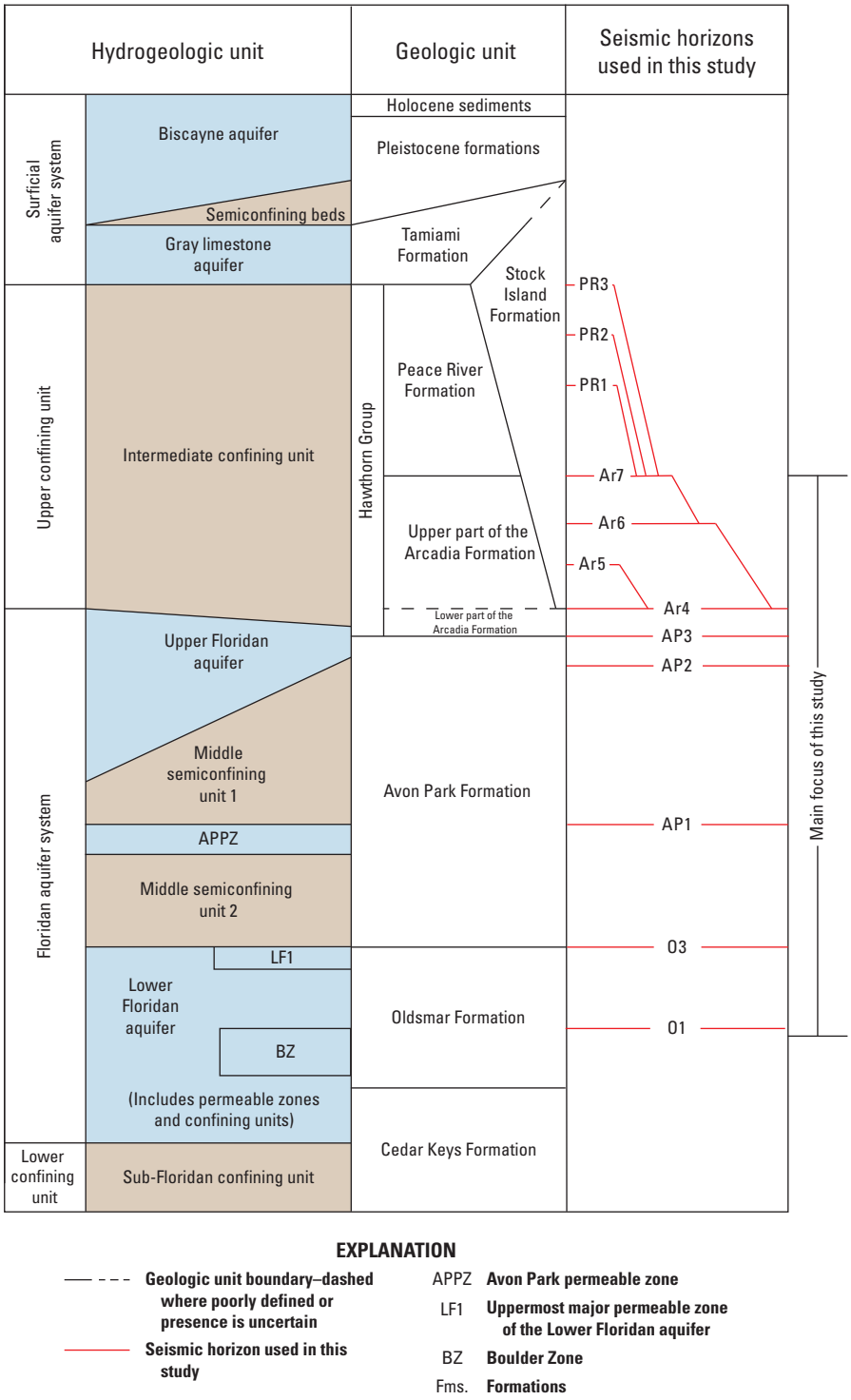

Figure 2. Relations between hydrogeologic units, geologic units, and seismic horizons in the eastern Broward County and northeastern Miami-Dade County study area (fig. 1). Modified from Miller (1986, 1990), Reese and Richardson (2008), Roberts-Ashby and others (2013), Reese and Cunningham (2014), and Cunningham (2015).

water-supply projects and of the sustainable use of the Floridan aquifer system (Broward Water Resources Task Force, 2010).

The Floridan aquifer system is present beneath the entire State of Florida and parts of adjacent States (Miller, 1986; Williams and Kuniansky, 2015). In southeastern Florida, the Floridan aquifer system is a regionally extensive, highly productive **karst**[1] carbonate aquifer, largely consisting of vertically stacked, meter-scale, high-frequency cycles composed mainly of limestone, but also dolomitic limestone and dolomite, especially in the lower part (Reese and Richardson, 2008; Reese and Cunningham, 2013, 2014). The Floridan aquifer system lies below the surficial aquifer system, the principal water supply for southeastern Florida, and is separated from it by the intermediate confining unit (fig. 2), which is hundreds of feet (ft) thick (Fish, 1988; Fish and Stewart, 1991; Reese and Wacker, 2009). The shallowest regionally extensive aquifer within the Floridan aquifer system is the Upper Floridan aquifer. A large part of the Upper Floridan aquifer throughout most of southeastern Florida is a U.S. Environmental Protection Agency-designated **Underground Source of Drinking Water**. The regionally widespread Lower Floridan aquifer lies beneath the Upper Floridan aquifer and is separated from it by hundreds of feet of primarily semiconfining, lower permeability carbonate rock (fig. 2). Within the Floridan aquifer system, salinity generally increases with depth. In southeastern Florida, the Upper Floridan aquifer typically contains brackish groundwater, and the groundwater salinity in the Lower Floridan aquifer is typically no higher than that of seawater (Reese, 1994; Miller, 1990).

The water-supply potential of the Floridan aquifer system in southeastern Florida is inadequately understood. Direct use of the Floridan aquifer system for water supply requires dilution with fresher water, or desalination by reverse osmosis, for example, because its groundwater is brackish or saline. An alternative use of the Floridan aquifer system for water supply is aquifer storage and recovery (ASR), a technology whereby freshwater is injected into an aquifer for storage and is later withdrawn. ASR has been applied in several locations in the Floridan aquifer system in southeastern Florida, but it has been used with limited success (Reese, 2002; Reese and Alvarez-Zarikian, 2007). The optimization of ASR water-supply yield requires knowledge of the spatial distribution of extensive permeable zones (that is, aquifer properties and stratigraphy) and their confinement, structural character, ambient water quality, and an appropriate source-water supply. Information is also limited regarding potential use of the lower parts of the Floridan aquifer system as a storage zone for injected treated wastewater. Treated wastewater injection may entail a risk of upward cross-formational transport of the treated wastewater from the injection zone used in Broward County—the highly permeable Boulder Zone (fig. 2). In Broward County, treated wastewater can migrate upward, enhanced because of its lower salinity and thus greater buoyancy than the native saline water of injection and confining zone strata. This upward migration of buoyant wastewater has been documented at seven wastewater treatment and injection facilities in Miami-Dade and Broward Counties (Maliva and others, 2007).

Sustainable development and management of the Floridan aquifer system for water supply is uncertain because of knowledge gaps in the stratigraphy and potential hydrologic connection between hydrologic units and potentially permeable structural features such as faults, fractures, and deep karst collapse structures (Cunningham and Walker, 2009; Cunningham and others, 2012; Reese and Cunningham, 2013, 2014; Cunningham, 2015). To address these concerns, the U.S. Geological Survey (USGS), in cooperation with Broward County Environmental Planning and Community Resilience Division, initiated a study in 2013 to better understand the controls on groundwater movement through the Floridan aquifer system in southeastern Florida. Karst collapse structures, faults, and fractures were identified and characterized to provide information for the reduction of uncertainty in the sustainable development of the Floridan aquifer system. **Seismic sequence** techniques coupled to **sequence stratigraphy** defined by existing borehole data provided an integrated methodology for improving the three-dimensional (3D) conceptualization of the hydrogeologic framework in the study area. In addition, this 3D conceptualization of the hydrogeologic framework can be used by water managers to (1) improve existing groundwater flow models, (2) evaluate the risk of upward migration of saline groundwater or treated wastewater, (3) aid in water-utility site selection, and (4) provide reasonable assurance to stakeholders and regulators that projects are scientifically defensible.

Purpose and Scope

This report characterizes the sequence stratigraphy, seismic stratigraphy, and seismic structures of the lower part of the intermediate confining unit and most of the Floridan aquifer, so water managers can better understand the hydrogeologic controls on groundwater movement through these hydrogeologic units (fig. 2). This hydrostratigraphic interval is defined at the top and bottom, respectively, by prominent seismic-reflection, geologic, and borehole geophysical horizons that mark the top of the Arcadia Formation and the uppermost part of a dolomite corresponding to the top of the Boulder Zone within a lower part of the Oldsmar Formation (fig. 2). A conceptual framework was produced as a 3D geomodel that is a computerized representation of the Earth below the study area in eastern Broward County and northeastern Miami-Dade County (fig. 1). The geomodel is designed to produce 3D visualizations of the conceptual framework of the **depositional sequences** of the lower part of the intermediate confining unit and most of the Floridian aquifer system, and to provide

[1]Terms shown in bold are defined in the glossary.

sequence stratigraphic surfaces and structural geobodies representative of columniform, karst collapse structures that can be assimilated within groundwater flow and constituent transport simulations. The study area occupies approximately 425 square miles (mi^2) that includes eastern Broward County and a small part of northeastern Miami-Dade County (fig. 1).

Approach

For this study, approximately 60 miles (mi) of newly acquired seismic-reflection data were combined with 20 mi of pre-existing seismic-reflection profiles along the Hillsboro Canal in Broward County (Cunningham, 2013; Reese and Cunningham, 2014) and within northeastern Miami-Dade County (Cunningham, 2015), and integrated with data from 45 nearby Floridan aquifer system wellbores (fig. 1, tables 1 and 2). The approach also included 3D mapping of the geologic, seismic-reflection, and hydrogeologic framework of a major part of the Floridan aquifer system, and identifying stratigraphic and structural characteristics that could either facilitate or preclude the sustainable use of the Floridan aquifer system as an alternate water supply or as a treated wastewater repository.

Previous Studies in Southeastern Florida

Notable studies that have focused on the Floridan aquifer system in southeastern Florida include Reese (1994), Reese and Memberg (2000), Reese and Richardson (2008), Reese and Cunningham (2013, 2014), and Cunningham (2014, 2015). The studies by Reese and Cunningham (2013, 2014) used borehole data acquired at 33 sites, including the G–2984 test corehole alongside the Hillsboro Canal, and seismic-reflection data acquired beneath the Hillsboro Canal (fig. 1). Their study refined the geologic and hydrogeologic framework of the Floridan aquifer system presented by Reese (1994). Interpretation of recent seismic-reflection data acquired in southeastern Florida by Cunningham and Walker (2009), Cunningham and others (2012), Reese and Cunningham (2013, 2014), and Cunningham (2013, 2014, 2015) contributed to (1) a refinement of the seismic-stratigraphic framework of the Floridan aquifer system and (2) an understanding of the possible influence of seismic-sag structures on groundwater flow in the Floridan aquifer system. Cunningham (2014) showed that at a deep injection well utility in eastern Broward County, upward cross-formational migration of fluids between the Boulder Zone and the uppermost major permeable zone of the Lower Floridan aquifer is possibly enhanced by faults, fractures, and karst dissolution associated with a seismic-sag structure having a karst collapse origin. Most recently, Cunningham (2015) used seismic-reflection and well data in Miami-Dade County to determine whether geologic factors may contribute to the upward migration of injected treated wastewater into the upper brackish part of the Floridan aquifer system. It was shown that seismic-reflection technology was effective for detailed mapping of permeable zones and semiconfining units of the Floridan aquifer system at a higher level of resolution than with well data alone. In addition, specific well data indicated it is plausible that a hydraulic connection along faults produced by karst collapse may contribute to the cross-formational upward transport of treated wastewater at the North District ”Boulder Zone” Well Field (figs. 1 and 2; Cunningham, 2015).

Methods of Investigation

A two-dimensional (2D), water-based, seismic-reflection dataset and data from 45 boreholes covering the approximately 425-mi^2 study area provided the foundation for this investigation. The dataset was utilized to develop a new seismic stratigraphic and sequence stratigraphic framework between the early Eocene dolomite that bounds the top of the Boulder Zone and the uppermost Miocene limestone of the Arcadia Formation within the middle part of the intermediate confining unit. Borehole geophysical logs and geological well data, such as core and well-cutting samples, validated seismic interpretations and supported the development of a 3D geomodel of the sequence stratigraphy of the study area.

Core Sample and Well Cutting Analysis

Borehole geophysical, geologic, and hydrogeologic data collected from 45 boreholes that partially penetrate the Floridan aquifer system were correlated with seismic-reflection profiles (fig. 1, tables 1 and 2) to produce a regional stratigraphic, hydrogeologic, and structural conceptual framework of the rocks from the middle of the intermediate confining unit to the top of the Boulder Zone. As part of a previous USGS investigation (Reese and Cunningham, 2013, 2014), the G–2984 test corehole was drilled by the Florida Geological Survey in 2009 to a depth of 1,307 ft alongside the Hillsboro Canal in Broward County (fig. 1). A core description of the Avon Park Formation and Arcadia Formation for the G–2984 test corehole was completed for this study (Cunningham and Robinson, 2017). A cursory comparison of the slabbed whole cores and cuttings from 10 additional wells in the study area was conducted to assess the continuity and correlation of selected rock units between coreholes, and evaluate sequence stratigraphy, depositional environments, lithostratigraphy, and foraminiferal biostratigraphy of the Oldsmar Formation, Avon Park Formation, Arcadia Formation, and Stock Island Formation (fig. 2).

For this study, analyses were conducted of core samples (either 2- or 4-inch [in.] diameter) obtained from 10 wells and cuttings from the G–3962 well used for lithologic analysis (table 2). Most of the core samples were slabbed and visually analyzed using a 10X-magnification hand lens and binocular microscope. Standard transmitted-light petrographic

Table 1. Seismic-reflection profile identifiers, year acquired, and county within which acquired for all seismic-reflection profiles used in this study.

[Data for lines S1-S34 are archived and available to the public in the Cunningham Walker (2017) data release. Data for lines S35-S44 are owned by Miami-Dade County and are not archived in the data release]

Seismic line identifier	Computer file name for seismic-reflection profile data	Year acquired	County
S1	Hillsboro_DSMF_With_Gaps_180_Phase_pass_null.sgy	2010	Broward
S2	L36_DSMF.sgy	2013	Broward
S3	L25A_DSMF.sgy	2013	Broward
S4	C13JUN43D_Phase_Rotate_Gaps.sgy	2013	Broward
S5	73D_merged2.sgy	2013	Broward
S6	L35A_DSMF.sgy	2013	Broward
S7	NNRW26APR_DSMF.sgy	2013	Broward
S8	NNRW2_DSMF.sgy	2013	Broward
S9	NNRE_DSMF.sgy	2013	Broward
S10	NNRCOM3D_V2_Extended_DSMF.sgy	2013	Broward
S11	NNRCOMM3D_DSMF.sgy	2013	Broward
S12	NNRFL3D_DSMF.sgy	2013	Broward
S13	NNRH3D_Phase_Rotate_3.5ms_Shift.sgy	2013	Broward
S14	NNR33D_Phase_Rotate.sgy	2013	Broward
S15	NNRR3D_Phase_Rotate.sgy	2013	Broward
S16	NNRU3D_Final_Stack_V2_Phase_Rotate.sgy	2013	Broward
S17	NNR25APR_DSMF.sgy	2013	Broward
S18	C11GB_DSMF_Gaps.sgy	2013	Broward
S19	C11OJ3D_DSMF_Phase_Rotate_Gaps_Header2.sgy	2013	Broward
S20	C11NH3D_DSMF_Phase_Rotate.sgy	2013	Broward
S21	C11P3D_DSMF.sgy	2013	Broward
S22	C11U113D_DSMF_Phase_Rotate.sgy	2013	Broward
S23	C11TPK3D_DSMF_Phase_Rotate.sgy	2013	Broward
S24	C11L3_DSMF.sgy	2013	Broward
S25	C9W_DSMF.sgy	2013	Broward
S26	NC9_DSMF.sgy	2013	Broward
S27	NC9EE_DSMF.sgy	2013	Broward
S28	C9P2_DSMF.sgy	2013	Broward
S29	C9F73D_DSMF_Phase_Rotate.sgy	2013	Miami-Dade
S30	C9D3D_DSMF_Phase_Rotate.sgy	2013	Miami-Dade
S31	C9E3D_DSMF_Phase_Rotate.sgy	2013	Miami-Dade
S32	C9SUN3D_DSMF_Phase_Rotate_Gaps.sgy	2013	Miami-Dade
S33	C9MG3D_DSMF_Phase_Rotate_Gaps.sgy	2013	Miami-Dade
S34	C9MGSW3D_DSMF_Phase_Rotate.sgy	2013	Miami-Dade
S35	NDBCP2_DSMF_Phase_Rotate.sgy	2011	Miami-Dade
S36	NDBC_DSMF_Phase_Rotate.sgy	2011	Miami-Dade
S37	NDCD_DSMF_Phase_Rotate.sgy	2011	Miami-Dade
S38	NDkl_DSMF_Phase_Rotate.sgy	2011	Miami-Dade
S39	NDhj_DSMF_Phase_Rotate.sgy	2011	Miami-Dade
S40	NDfg_DSMF_Phase_Rotate.sgy	2011	Miami-Dade
S41	NDde_DSMF_Phase_Rotate.sgy	2011	Miami-Dade
S42	NDDETWO_DSMF_Phase_Rotate.sgy	2011	Miami-Dade
S43	NDABC_DSMF_Phase_Rotate.sgy	2011	Miami-Dade
S44	NDQR_DSMF_Phase_Rotate.sgy	2011	Miami-Dade

Table 2. Well identifiers, locations, and information for all wells used in the study.

[USGS, U.S. Geological Survey; NA, not applicable; X, used; --, not used]

USGS local well identifier	Local identifier or other identifier(s)	USGS site identification number	State Plane Easting (feet)	State Plane Northing (feet)	Used for generating geomodel	Used in producing synthetic seismograms	Used to constrain horizon mapping on seismic-reflection profiles	Used to constrain mapping between seismic-reflection profiles	Used for lithology and cyclostratigraphy from core (Co) or cuttings (Cu)	Used for benthic forams
BCN–I1	IW–1	261538080092801	932258.00	701258.00	X	--	--	X	--	--
CS–I1	IW–1	261445080154801	897434.38	695155.44	X	--	--	X	--	--
CS–I2	IW–2	261445080154801	897567.65	695899.35	X	--	--	X	--	--
D–365	W–5144	261548080060201	950813.00	702547.00	X	--	--	X	--	--
FTL–I4	IW–4	260540080075001	941196.74	641362.15	X	--	--	X	Co[1, 2]	X
FTL–I5	Test Injection Well #5, G–2330A	260543080075601	940930.62	641347.25	--	X	--	--	--	--
G–2914	Springtree WTP ASR–1	261004080153801	898472.24	670243.67	X	--	X	X	--	--
G–2916	MW–1	261735080062502	948425.68	713399.83	X	--	--	X	--	--
G–2917	ASR–1	261030080091501	933072.18	671164.39	X	--	--	X	--	--
G–2938	BF–1, W–17103	261023080104401	925620.54	669564.64	X	X	X	X	--	--
G–2942	CS IW–1	261438080071201	944386.41	695710.68	X	--	--	X	--	--
G–2945	DZMW–1	255814080192801	878104.00	595573.89	X	X	X	X	--	--
G–2946	Miramar IW–2	255815080192801	878099.92	595685.94	--	X	--	--	Co[1,2]	--
G–2961	HOL–IW1, IW–1	260140080075701	941045.42	616690.57	X	X	--	X	--	--
G–2963	IW–1	255932080195601	875504.55	603509.64	X	--	--	X	--	--
G–2966	Concentrate Disposal #1, IW–1	260332080181001	885050.50	627681.58	X	X	X	X	--	--
G–2968	Deerfield Beach WTP IW–1	261852080072501	943289.00	720966.00	X	X	--	X	--	--
G–2970	Regional DZMW–1	260455080090901	934358.00	636421.00	X	--	--	X	--	--
G–2971	RO Concentrate IW–1	260609080115901	918833.00	643747.00	X	X	--	X	--	--
G–2973	IW–1	255916080092401	933148.85	602151.51	--	X	--	--	--	--
G–2978	CIW–1, IW–1	260739080140801	906973.00	652807.00	X	--	--	X	--	--
G–2981	Melaleuca Blending Test Well	260701080185101	880149.00	648805.00	X	X	X	X	--	--
G–2983	NA	260737080200502	874444.94	652428.06	X	--	X	X	--	--
G–2984	W–19318	261940080075001	940955.00	725754.00	X	X	X	X	Co[2, 3]	X
G–2985	FA PW–4, TPW1	260505080143901	904220.81	637211.94	X	--	X	X	--	--
G–2986	Supply Well FA–2	261813080082101	938174.20	716980.85	X	--	--	X	--	--
G–2987	Dixie–FAS1	260547080123001	915973.18	641513.40	X	--	X	X	--	--

Table 2. Well identifiers, locations, and information for all wells used in the study.—Continued

[USGS, U.S. Geological Survey; NA, not applicable; X, used; --, not used]

USGS local well identifier	Local identifier or other identifier(s)	USGS site identification number	State Plane Easting (feet)	State Plane Northing (feet)	Used for generating geomodel	Used in producing synthetic seismograms	Used to constrain horizon mapping on seismic-reflection profiles	Used to constrain mapping between seismic-reflection profiles	Used for lithology and cyclostratigraphy from core (Co) or cuttings (Cu)	Used for benthic forams
G–2991	City of Davie IW–1	260511080143801	904337.83	637787.13	--	--	--	--	Co[1]	--
G–2994	Hollywood WTP IW–1	260048080104201	926029.22	611424.74	--	--	--	--	Co[1, 2]	X
G–2995	Hollywood WTP DZMW–1	260050080104201	926000.12	611553.79	--	--	--	--	Co[2]	X
G–2996	Lauderdale Lakes FW–1	261020080121801	916901.37	669096.40	--	--	--	--	Co[2]	--
G–2997	Lauderdale Lakes FW–2	261025080121001	917616.52	669554.14	--	--	--	--	Co[2]	--
G–3805	Northeast Miami-Dade IW–3N	255505080085001	936435.72	576806.95	X	X	X	X	Co[1, 2]	X
G–3962	Biscayne Landing IW–1	255442080085701	935821.98	574447.42	--	--	--	X	Cu[4]	--
G–4002	City of Sunrise SGF–1	260753080203201	872000.93	653952.06	X	--	X	X	--	--
HAL–RO1	Supply Well 1	255918080092201	933450.82	602480.11	X	--	--	X	--	--
HOL–RO1	Supply Well 1	260047080104201	926025.54	611429.76	X	--	--	X	--	--
MAR–I2	IW–2	261427080130301	912836.52	693914.92	X	--	--	X	--	--
PB–1766	PBF–12, W–17986, HASR–DZMW	262107080174202	886662.23	735551.10	X	--	X	X	Co[3]	--
PB–1775	FAMW	262030080132301	911515.00	727503.00	X	--	X	X	--	--
PBP–I1	IW–1	2559360801195700	875612.77	603938.29	X	--	--	X	--	--
PLT–I1	North WWTP IW–1	260828080141201	906587.94	657713.65	X	X	--	X	--	--
PLT–ROI1	RO IW–1	260739080160801	896089.00	652702.00	X	--	--	X	--	--
S–567	W–150	260614080085401	935656.62	644363.83	X	--	--	X	--	--
SUN–I3	WWTP IW–3	260738080201001	874090.00	653487.00	X	X	X	X	--	--

[1]Core samples used for study of Oldsmar Formation.

[2]Core samples used for study of Avon Park Formation.

[3]Core samples used for study of Arcadia Formation.

[4]Samples from cuttings used for study of Stock Island Formation.

techniques were used to examine 454 thin sections. Cores and thin sections were analyzed to help determine lithofacies, vertical trends in lithofacies, sedimentary structures, cycle boundaries, and to assess how features varied laterally and correlated. Lithofacies were defined by allochem types, fabric, sedimentary structures, bedding type, and diagenetic features using a combination of classification schemes and terminology from Dunham (1962), Embry and Klovan (1971), and Lucia (1999). The rock color of dry core samples was recorded by comparing them to a Munsell rock-color chart (Geological Society of America, 1991). A semiquantitative field classification of ichnofabric (Droser and Bottjer, 1986, 1989) was used to record variations in the extent of bioturbation. All continuous cores collected for this study are archived either at the USGS Caribbean-Florida Water Science Center in Davie, Fla., or at the Florida Geological Survey Geologic Sample Repository in Tallahassee, Fla. Relations between lithofacies and petrophysical properties (porosity and permeability) were assessed by combining classifications and methods prescribed by Choquette and Pray (1970), and Lucia (1995, 1999).

Foraminiferal Paleontologic Analysis

Taxonomy of benthic and planktonic foraminifera from selected lithofacies was determined to assist in interpreting paleoenvironments and biostratigraphy. Foraminifera were examined by Jarer Biostrat, Inc., in 440 thin sections prepared from core samples acquired from the following wells: USGS G–2984 test corehole (Cunningham and Robinson, 2017), City of Hollywood "Boulder Zone" IW–1 (G–2994), City of Hollywood DZMW–1 (G–2995), City of Fort Lauderdale "Boulder Zone" IW–4 (FTL-I4), and Northeast Miami-Dade "Boulder Zone" Deep Well Field IW–3N (G–3805) injection well (fig. 1, table 2). Most thin sections were cut normal to bedding, but a few were cut parallel to bedding. Thin sections were examined by transmitted light using a Zeiss stereoscopic microscope and by counting selected taxa at magnifications ranging from 1.6X to 6.3X. Then the thin sections were examined using an AmScope 2000X LED Model SME-F8BH trinocular compound microscope for more detailed analysis and identification to the most useful practicable taxonomic level. Typical examples of identified taxa were imaged using an AmScope MU Series 10MP digital camera.

Seismic-Reflection Data Acquisition and Processing

During 2013, about 60 mi (97 kilometers [km]) of high-resolution, high-frequency, marine seismic-reflection data were acquired in canals in eastern Broward County (fig. 1) using a 1.5-ft (0.5-meter [m]) shallow-draft boat in water depths that ranged from about 7 to 15 ft (2.1 to 4.6 m). The data yielded 33 seismic-reflection profiles located along the C–9, C–11, C–13, L–35A, L–36, and North New River Canals (fig. 1). The data for seismic-reflection profiles S1 to S34 (fig. 1) are available at Cunningham and Walker (2017). Data were collected at a 0.25-millisecond sampling interval with variable record lengths and a common depth point bin size of 5.125 ft (4 m). A SeaMux3digital-data acquisition system, a dual air-gun source (two 10-cubic-inch [in.^{3}] air guns), and a 72-channel hydrophone streamer with 10.253-ft (3.125-m) receiver spacing were used to conduct the seismic survey. The acquisition digital sampling rate was 4 kilohertz (kHz), shot spacing was about 20.5 ft (6.25 m), and 0.5-millisecond resampling was conducted for processing. Real-time navigational positions were acquired in State Plane Florida East 0901 with a Trimble differential global positioning system receiver. Excel Geophysical Services performed post-acquisition processing of the seismic-reflection data. Processing steps included geometry, bandpass filtering, trace edits, noise attenuation, channel rejection, spherical divergence correction, notch filtering and odd harmonics, predictive deconvolution (2–6 millisecond gap), velocity analysis, normal move-out correction, muting trace balancing, stacking, and frequency-wave predictive and reject filtering. Post-processing of each seismic-reflection profile included calculation of full **dip steering** to constrain the local dip and azimuth of seismic reflections at every sample position where inline and cross line intersect (Tingdahl and others, 2001; Tingdahl and De Rooij, 2005). A dip-steered median filter was then applied to reduce random noise and enhance laterally continuous events, while preserving edges (Brouwer and Arnaud, 2011). This filtering also improves multitrace **seismic attribute** calculations, enhancing the imaging capabilities of seismic discontinuities such as faults and gas **chimneys** (Tingdahl and De Rooij, 2005). Post-processing also included phase rotation of some seismic-reflection profiles and display of the attribute **average energy**. The average energy displays assisted in correlation of some key seismic-reflections and their relationship to the vertical stacking of seismic reflections comprising selected seismic sequences. Generally, the seismic records are interpretable to 0.75 second two-way traveltime or approximately 3,300 ft below canal stage; one profile, S7 (fig. 1, table 1) has an interpretable record to 1.5 seconds two-way traveltime or about 8,500 ft below canal stage. One seismic-reflection profile, S1 (fig. 1, table 1), about 13 mi in length, acquired along the Hillsboro Canal in 2010 for a previous Broward County study (Reese and Cunningham, 2014) and 10 seismic-reflection profiles, S35–44 (fig. 1, table 1), approximately 7 mi in total length, acquired in northeastern Miami-Dade County during 2011 for a seismic-reflection study by Cunningham (2015) augmented the newer inventory of 33 seismic-reflection profiles (fig. 1).

Synthetic Seismogram Generation and Correlation

A synthetic seismogram is a one-dimensional (1D) model of acoustic energy traveling through the layers of

the Earth (pls. 1 and 2). Synthetic seismograms provide a means to calibrate seismic-reflection profiles to specific subsurface stratigraphic events observed in 1D core and geophysical log data acquired from wells. Independently, Abbott Geophysical Incorporated (10 wells, pl. 1) and Geokinetics Incorporated (4 wells, pl. 2) used velocity data only from 13 borehole-compensated sonic logs, and in one case (pl. 2) acoustic impedance calculated from both a velocity and density log, as input for specialized geophysical software to generate 14 synthetic seismograms (Cunningham and others, 2017). These seismograms allow idealized reflections generated from borehole data to be directly compared with reflections from the seismic data. The log data were converted to a synthetic seismic trace using synthetic-seismogram production software. For the 13 wells, where only velocity logs were used because of a lack of density logs, the synthetic seismogram modeling was run without density. This method is valid with the time relationship between horizons being accurate, because the time is related only to velocity, but reflector amplitude is not perfectly accurate (Ewing, 1997). There is an imperfection in amplitude in cases where only velocity data are used, because amplitude is based on impedance (velocity multiplied by density). The modeled or synthetic wiggle traces produced by Abbott Geophysical Incorporated were generated using an Ormsby wavelet with a frequency band of 5 to 250 hertz (Hz) and a taper between frequencies of 5 to 15 Hz and 200 to 250 Hz (pl. 1). Synthetic wiggle traces produced by Geokinetics Incorporated used an Ormsby wavelet with either a frequency band of 0 to 250 Hz or 0 to 260 Hz and a taper between frequencies of 0 to 3 and 200 to 250 Hz or 2 to 60 and 140 to 260 Hz, respectively (pl. 2). Eight synthetic seismograms were used to relate geologic and geophysical well data directly to the respective seismic-reflection data. The other six wells and accompanying synthetic seismograms were too far from the seismic lines to allow for direct correlation but helped in understanding the seismic response of the geologic and seismic boundaries, and the interval velocities. They were also used to generate velocity (time-depth) functions that allowed the 3D horizons to be vertically constrained between canals. Stratigraphic and hydrogeologic interfaces selected on the basis of borehole gamma ray and sonic velocity data (pls. 1 and 2). In some cases, resistivity data (pl. 2) were correlated to the synthetic-seismogram wavelets, and these synthetic wavelets were then fit to the true wavelet traces on seismic-reflection profiles. Caliper logs were used as an aid to identify where on the synthetic seismogram the wavelet traces may have had errors in the sonic velocity logs and, thus, an incorrect correlation between the synthetic wavelets and seismic-profile wavelets. The direct correlation of key traces on the synthetic seismograms to seismic-reflection profiles was not a perfect fit; however, some disparity is common between synthetic seismograms and seismic-reflection profiles (Bruns and others, 1994; Ewing, 1997) and in many cases is a consequence of imperfect modeling of synthetic seismograms.

Horizon Mapping, 3D Velocity Function, and Depth Conversion

In preparation of seismic-reflection horizon picking and mapping, each profile of the entire 2D seismic-reflection survey within the study area (fig. 1) was processed using OpendTect seismic-interpretation software. The processing consisted of dip steering (reflector directivity information) and median filtering of all profiles. The dip-steering was used to help guide picks in regions having good lateral **reflection continuity**. Horizons on each of the seismic-reflection profiles were generated by interpolation between user picks and dip-steering using OpendTect seismic-interpretation software. **Horizon-point data** were first picked manually and then extended using amplitude, phase, and dip-steering information. When the preset thresholds based on amplitude, phase, and dip-steering failed, auto tracking would stop and the horizon was manually picked. The horizons picked commonly correspond to seismic sequence and depositional sequence boundaries (figs. 3 and 4). In addition, well-based synthetic seismograms were used to help guide the correlation of well data to horizons on seismic-reflection profiles and the mapping of lithologic and hydrogeologic boundaries on seismic-reflection profiles.

Using the mapped 2D horizons, 3D horizons were generated using a 3D inverse distance gridding workflow within the OpendTect seismic-interpretation software and then projected and visualized across the study area. In order to generate the 3D surfaces in traveltime, well locations, well log data, and where available, synthetic seismograms were imported into the OpendTect seismic-interpretation software. Lithologic and hydrologic boundaries identified from wells near seismic-reflection profiles were time-depth (time in seconds and depth in feet) matched directly from the 2D horizon picks (aided by synthetic seismograms), whereas wells in regions with limited seismic data (for example, between canals) were time-depth matched using synthetic seismograms and where absent, the intersection point of the well location and the gridded 3D time horizons. The time values for these intersections were then matched to depth boundaries identified from the wells. This method provided time-depth values for each of the wells used in the velocity function, excluding outlier wells that produced unrealistic velocities when time-depth matched with the seismic horizons.

A velocity function for the study area (figs. 3 and 4) was generated using correlations between synthetic seismograms at selected wells and seismic-reflection profiles, as well as time matching of lithologic and hydrogeologic boundaries identified from well data and 3D horizon mapping in two-way traveltime. Stacked interval velocities (interval velocities calculated between horizons) were then calculated for six intervals between the land surface and horizon O3. This consisted of the following intervals between mapped horizons: O3-AP1, AP1-AP2, AP2-AP3, AP3-Ar4, Ar4-Ar7, (figs. 3 and 4) and Ar7-land surface. The average velocity across all wells for each horizon interval was 10,688 feet per second (ft/s) (O3-AP1); 7,722 ft/s (AP1-AP2); 7,416 ft/s (AP2-AP3); 7,121 ft/s (AP3-Ar4); 7,493 ft/s (Ar4-Ar7); and 5,888 ft/s (Ar7-land surface) (figs. 3 and 4).

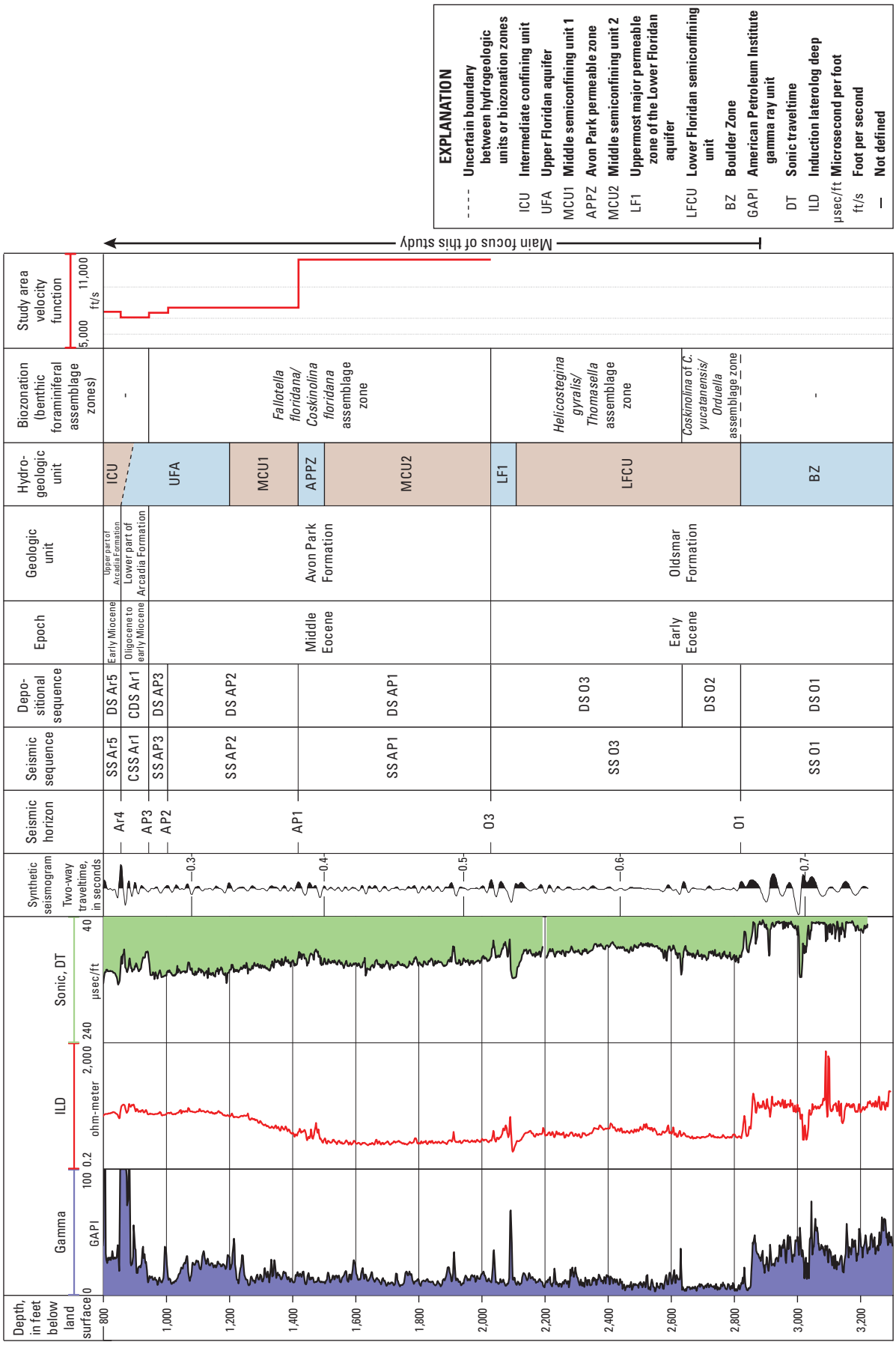

Figure 3. G-3805 well in the southeastern part of the study area (fig. 1) showing relations within the Floridan aquifer system between geophysical well logs, synthetic seismogram, seismic horizons, seismic sequences, depositional sequences, geologic data, hydrogeologic units, biozonation, and velocity function for the study area.

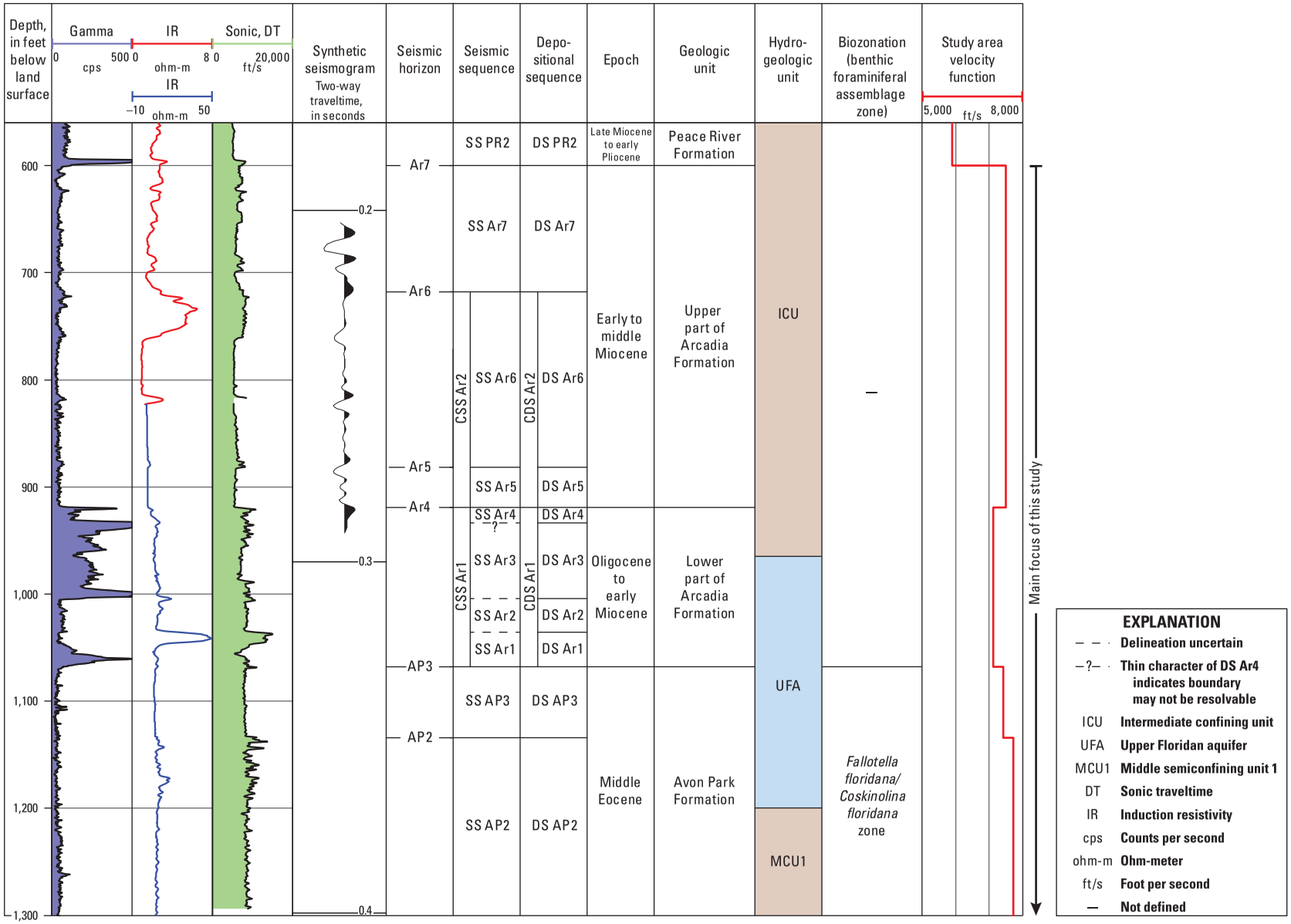

Figure 4. G–2984 well in the northeastern part of the study area (fig. 1) showing relations within a lower part of the intermediate confining unit and an upper part of the Floridan aquifer system between geophysical well logs, a synthetic seismogram, seismic horizons, seismic sequences, depositional sequences, geologic data, hydrogeologic units, biozonation, and velocity function for the study area.

The velocity function was formatted to x-coordinate, y-coordinate, interval velocity, and z-coordinate (two-way traveltime), and sorted by x-coordinate. The cell dimension for the gridded velocity volume, used for horizon depth conversion, was 200×400 ft. Following sorting, the velocity function was imported into the OpendTect seismic interpretation software and a 3D velocity model was generated using the volume-builder utility and the velocity-gridder workflow. The velocity gridder is a module in OpendTect that will create a volume out of a sparsely sampled dataset. The 3D gridding was applied to the time-depth relation of the velocity source instead of the amplitudes of the velocity source, preserving the time-depth relation and structure of the interval velocities provided. Because of the sparse distribution of data points across the study area, an inverse-distance interpolation algorithm was used.

Geomodeling

Seismic horizon and geologic well horizon data were used to develop geomodels using Roxar reservoir management software (RMS; Emerson Process Management, 2017). The Roxar RMS is designed for use in constructing geomodels for the petroleum industry but was well suited to the geomodeling needs of this study. Depth-converted x, y, and z seismic horizon point data along seismic-reflection profiles were exported from OpendTect, and along with x, y, and z 1D geologic well horizon data, in feet below land surface, both datasets were imported into Roxar RMS. The seismic horizon and geologic well pick datasets were converted into feet below NAVD 88. Eight horizon maps were generated by interpolating between horizon picks at wells and on seismic-reflection profiles using a Local B-spline algorithm for a single Oldsmar Formation seismic horizon (O3), three Avon Park Formation seismic horizons (AP1, AP2, and AP3), and the four Arcadia Formation seismic horizons (Ar4, Ar5, Ar6, and Ar7, figs. 3 and 4) with x and y grid increments of 50×50 ft and 100×100 ft, respectively. Seventeen seismic-sag structures were identified from seismic-reflection patterns (fig. 1). Regional horizon maps at the seismic-sag structures were manually shaped by adjusting the horizon point data and reinterpolating the horizons in Roxar RMS for a more detailed local horizon representation. The horizon shaping focused on three geometric seismic-reflection patterns at each of the seismic-sag structures: **inner sag width, shoulder width**, and the lowest point in the sag structure.

All stratigraphic units represented in the geomodel contained 3D grid cells (approximately 235×235 ft with varying thickness up to 88 ft) for rendering thickness and volume. Each 3D gridded cell has the capability to be interpolated and populated with an attribute value throughout the geomodel. Centroids and the attribute values for each cell could be exported from the geomodel and imported for use in other modeling programs such as MODFLOW (Harbaugh, 2005).

Seismic-Attribute Analyses

Following the pre-stack and post-stack processing steps, two 2D seismic-reflection profiles S–7 and S–1 (fig. 1, table 1), were imported into the OpendTect seismic-interpretation software for structural calculations, structural filtering, and seismic object detection of probable faults, fractures, and fluid-migration pathways (chimneys) by the use of artificial neural network-based **meta-attribute** calculations (Aminzadeh and de Groot, 2005). The neural-network meta-attribute methodology combines a predetermined set of parameterized seismic attributes into a single object probability attribute, which is used to detect and isolate seismic anomalies caused by geologic features, such as faults (Tingdahl and De Rooij, 2005), gas chimneys (Ligtenberg, 2005; Heggland, 2005; Connolly and Garcia, 2012; Brothers and others, 2014; Kluesner and Brothers, 2016), and gas-charged regions (Farfour and others, 2012) containing either hydrocarbon-based gas (for example, methane) or non-hydrocarbon-based gas (for example, carbon dioxide). Further, fluid-migration zones produce similar acoustic characteristics as gas-charged regions when imaged using seismic-reflection methods (Løseth and others, 2009).

As part of the post-processing workflow for all seismic-reflection profiles, dip steering was calculated for each seismic-reflection profile and a dip-steered median filter was applied to each profile. Multiple seismic attributes that highlight seismically discontinuous faults and fractures, and gas chimneys are used as input into the meta-attribute calculations (for example, vertical and horizontal similarity, average frequency, polar dip, and frequency wash-out ratio). A small percentage (typically less than 30 percent) of user picks of faults and non-faults, or chimneys and non-chimneys, were then used to supervise and train a neural network algorithm (Brouwer and others, 2011). Application of the neural-network algorithm enables the meta-attribute calculation to better distinguish between real faults and fractures, chimneys, and other more localized seismic discontinuities, such as other low-similarity, low-energy areas. After training, the chimney probability meta-attribute was calculated for the 2D seismic-reflection profiles S–7 and S–1 (fig. 1, table 1) and overlain onto the dip-steered median-filtered seismic-reflection profiles for visualization and interpretation of potential fluid migration pathways. Brouwer and others (2011) describe in detail the theory and practice of neural-network based meta-attribute analyses.

Geology and Sequence Stratigraphy

In the study area, a broad characterization was completed that focused on the geologic and sequence stratigraphic setting of the rocks and sediment that extend upward from the dolomite that composes an upper part of the Boulder Zone to the top of the Arcadia Formation within the middle

part of the intermediate confining unit, but also included a cursory conceptualization of the overlying Peace River Formation, Stock Island Formation, Tamiami Formation, Fort Thompson Formation, and Miami Limestone (figs. 3–6). This characterization utilized mainly whole core, cutting, and borehole geophysical information. The core and cutting information was selected from 11 wells (table 2). Continuously drilled whole core samples from the top of the Arcadia Formation to the upper approximately 300 ft of the Avon Park Formation from the G–2984 test core hole (figs. 1 and 4) were especially useful, because they provided an interval with thick continuity in the geologic record. The information was also used to refine mapping of hydrogeologic and geologic units that used 1D well data, thereby supporting an even more accurate mapping of these units within the more densely distributed 2D seismic-reflection data of the study area.

The hierarchy of cyclostratigraphy applied herein is based on the terminology and hierarchical scheme of Kerans and Tinker (1997, fig. 1.11), and presented from the highest cycle hierarchical order to the lowest, it includes high-frequency cycle, cycle set, depositional sequence, and composite depositional sequence. The hierarchical ordering of the cycle types indicates relative scale and position in the cycle hierarchy, but no particular time duration for each cycle type is inferred. Where the relative position of a specific cycle within this cycle hierarchy has a low level of confidence, the term "depositional cycle" is used.

Oldsmar Formation

An "Oldsmar limestone" was originally described from the Oldsmar well (Florida Geological Survey ascension number W–8) in Hillsborough County (fig. 1), as a lower Eocene limestone interval extending throughout the Florida peninsula and northern Florida (Applin and Applin, 1944). In the eastern Broward County and northeastern Miami-Dade County study area, the Oldsmar Formation lies above the carbonate and evaporite of the Cedar Keys Formation (Miller, 1986) and beneath limestone of the Avon Park Formation (figs. 2 and 3). Core samples acquired from five wells (City of Hollywood G–2994, City of Davie G–2991, City of Miramar G–2946, Fort Lauderdale Lohmeyer FTL-I4, and Northeast Miami-Dade G–3805; fig. 1, table 2) in the study area indicate that the Oldsmar Formation is a succession of shallow-marine platform carbonate rocks that are mainly limestone but dominated by dolomite beds in the basal and uppermost parts of the formation. High-frequency shallowing-upward cycles (Pratt and James, 1992) that grade in ascending order from subtidal to peritidal environments are most common. Typically, the uppermost part of the cycles are either intertidal lime mudstone or supratidal limestone breccia. The upper part of the shallowing-upward cycles, in some instances, are completely or partly replaced dolomite. Less common aggradational subtidal cycles are also present in the Oldsmar Formation. Common lime mudstone, wackestone, packstone, and grainstone that include smaller benthic foraminifera (including miliolids and rotaliids), peloids, larger benthic foraminifera, ostracods, and echinoids are common particles of the marine platform depositional setting of the Oldsmar Formation. The Oldsmar Formation ranges between about 900 and 1,200 ft in thickness.

Three depositional sequences are recognized within the Oldsmar Formation: depositional sequence O1, depositional sequence O2, and depositional sequence O3 (figs. 3, 5, and 6). Depositional sequence O1 is principally characterized by dense, brittle, fractured and cavernous dolomite (Miller, 1986; Meyer, 1989). This dolomite forms an important, extremely permeable hydrogeologic unit in the lower part of the Oldsmar Formation, the Boulder Zone, which is present throughout southern Florida (Miller, 1986; Meyer, 1989). Herein, seismic-reflection profiles indicate that the upper bounding surface of depositional sequence O1 commonly has a highly irregular, rugged paleotopography largely produced by **epigenic karst**.

The carbonate rock of depositional sequence O1 is equivalent to the Delray Dolomite—nomenclature assigned by Winston (1994, p. 28–29) as defined by a 375-ft vertical rock interval in the Palm Beach County System 3 No. 1 well (PB–1174) in southeastern Palm Beach County (fig. 1). Winston (1994) interpreted the Delray Dolomite as a basal dolomite of the Oldsmar Formation and inclusive of the Boulder Zone hydrogeologic unit. A younger and thinner dolomite unit (commonly about 100 ft in cumulative thickness) that contains minor limestone interbeds composes the dolomite cap of the uppermost Oldsmar Formation (fig. 5). For wells in southeastern Miami-Dade County, the stratigraphic position of the uppermost part of the Oldsmar Formation has been confused with that of the Delray Dolomite (for example, Dausman and others, 2009).

Depositional sequence O2 occurs above depositional sequence O1 and beneath depositional sequence O3 (figs. 3 and 5). The upper bounding surface of depositional sequence O2 is indicated on borehole geophysical logs by a substantial increase in gamma-ray values over a depth interval of about 6 ft (fig. 3). This thin interval was mapped by Reese and Richardson (2008, pl. 4) as the GLAUC gamma-ray geophysical log marker horizon in Broward and Miami-Dade Counties. Reese and Richardson (2008) identified the GLAUC marker horizon in the W–16882 well in Boynton Beach, Palm Beach County (fig. 1), where it is characterized by relatively high gamma-ray log values that correspond to glauconitic carbonate rock. The GLAUC marker horizon in the W–16882 well was correlated by Reese and Richardson (2008, pl. 4) to a high gamma-ray geophysical log marker horizon they assigned to the GLAUC marker horizon in three wells in Broward County and a fourth well in Miami-Dade County. These GLAUC marker horizons mapped by Reese and Richardson (2008, p. 4) correlate to the high gamma-ray marker that corresponds to the upper boundary of the depositional sequence O2 herein (fig. 3). It is plausible that the upper boundary of depositional sequence O2 is a drowning unconformity (Schlager, 1989) and that the

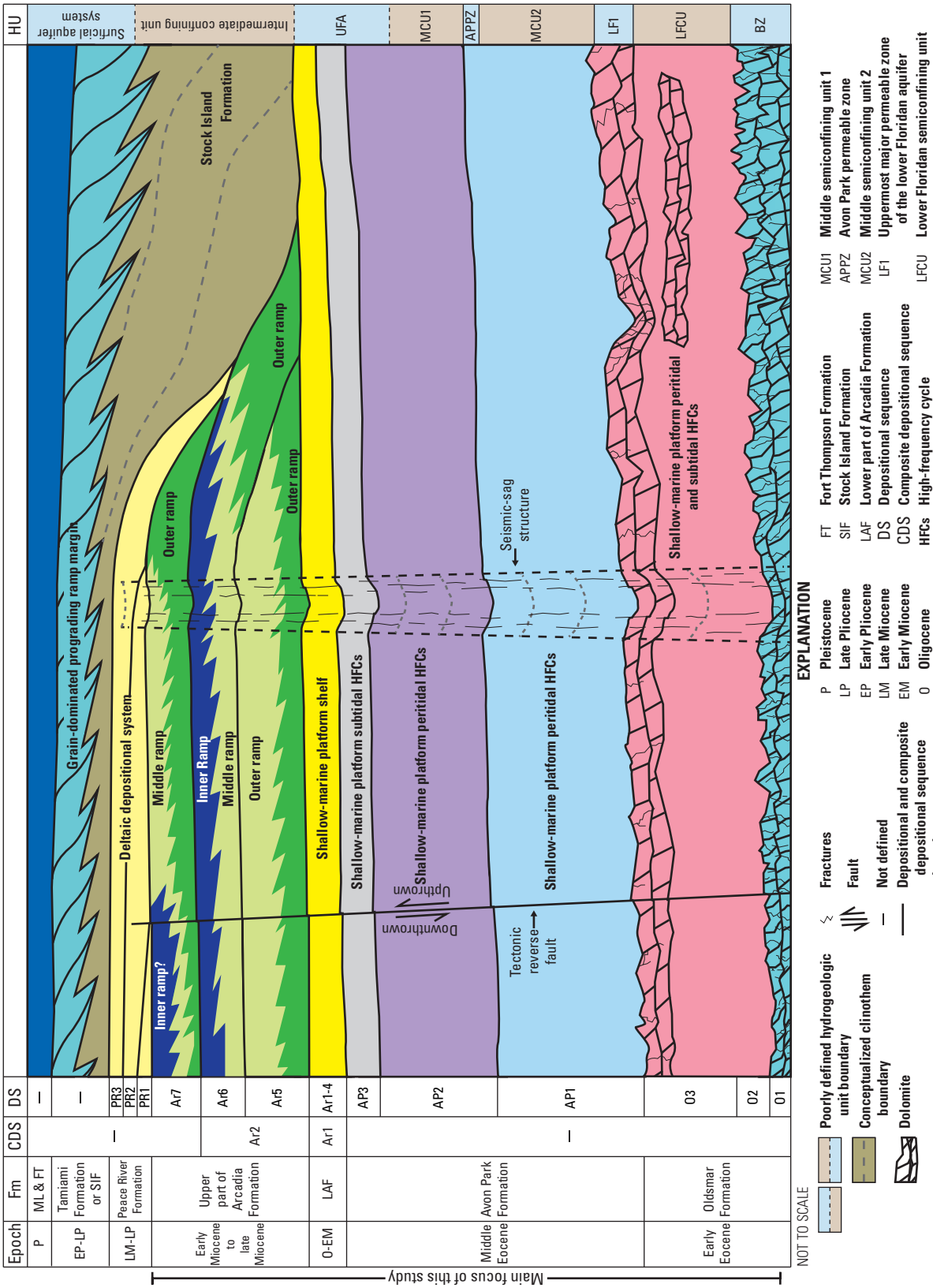

Figure 5. Conceptual west-to-east cross section across the study area that shows the Eocene to Pleistocene geologic units, depositional sequences, and hydrogeologic units.

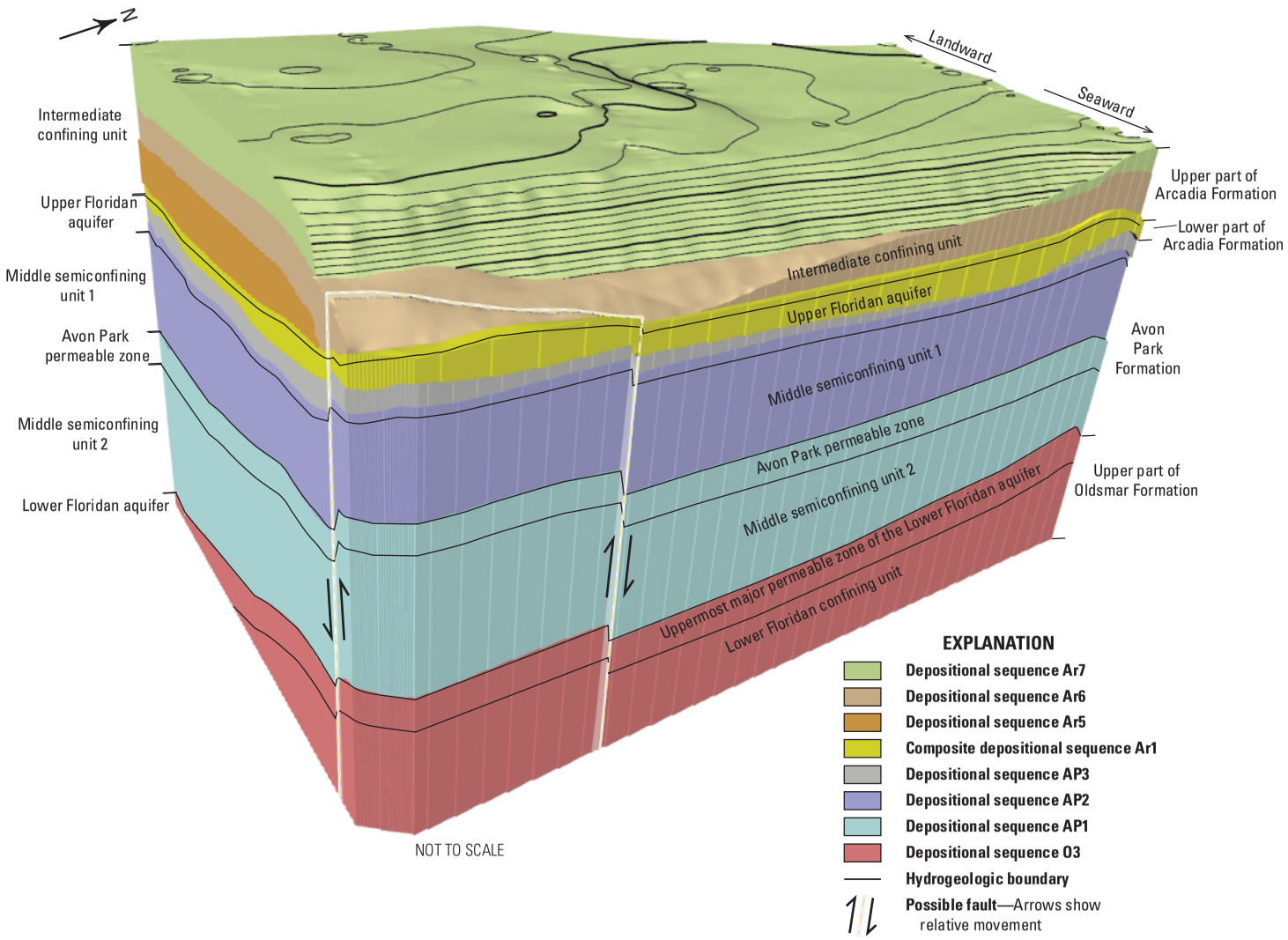

Figure 6. Subsurface geomodel of the study area with focus on the depositional sequences within the upper part of the Oldsmar Formation, shallow-marine platform carbonates of the Avon Park Formation, the sheet-like, widespread mixed carbonate and siliciclastic of the lower part of the Arcadia Formation, and three distally steepened carbonate ramps of the upper part of the Arcadia Formation. Also included are hydrogeologic units.

high gamma-ray values at the upper boundary throughout the study area are related to glauconite mineralization or mineralization by phosphorite, or both. These two radiogenic minerals are commonly associated with drowning unconformities (Godet, 2013).

Depositional sequence O3 lies above depositional sequence O2 and beneath the Avon Park Formation (figs. 3, 5, and 6). The upper bounding surface of depositional sequence O3 is a major hiatal unconformity (Miller, 1986, pl. 2) and corresponds to the upper surface of the Oldsmar Formation. The upper surface of depositional sequence O3 generally dips gently to the west about 0.2° (pls. 3*A*, *I*, and 4*A*). An aforementioned, moderately thick dolomite ranging from about 30 to approximately 200 ft in thickness composes the uppermost part of depositional sequence O3. Meyer (1989) also interpreted the upper boundary of this dolomite unit as the top of the Oldsmar Formation in southern Florida. The dolomite typically is associated with a marked increase in gamma ray, resistivity, and sonic velocity values compared to those for limestone at the base of the Avon Park Formation, for example, at the G–3805 and G–2991 wells (figs. 3 and 7). The typical gamma ray and sonic velocity log character is better shown than in figure 7 in a correlation chart of eastern Broward County by Reese and Cunningham (2014, pl. 2); however, they interpreted this dolomite to be within a lower part of the Avon Park Formation. It will be shown herein that seismic-reflection profiles provide evidence that the upper bounding surface of depositional sequence O3 is a very irregular epigenic karst exposure surface. The pore system of the dolomite unit was substantially impacted by epigenic karst, and is dominated by fractures and dissolution-enlarged voids (figs. 8 and 9). Selected cores from wells (table 2) suggest that, below the upper dolomite unit, carbonate peritidal-capped high-frequency cycles dominate depositional sequence O3 and that marine carbonate subtidal cycles are subordinate. The peritidal capped cycles commonly have a thin cap that has been partly or completely dolomitized. In some instances, the intertidal to supratidal uppermost part of the Oldsmar Formation peritidal cycles are directly underlain by sucrosic dolomite with relatively high intercrystalline porosity. The subtidal cycles are composed of mainly lime packstone and grainstone. The peritidal and subtidal high-frequency cycles plausibly stack into cycle sets or sequences that are potentially resolvable in the seismic-reflection profiles.

Applin and Applin (1944) included the use of biostratigraphic information to define the Oldsmar Formation in peninsular Florida, and herein, benthic foraminifer biostratigraphy is used as a supporting line of evidence for defining the lower and upper boundaries of depositional sequence O3 in the study area using data from the G–3805 well in northeastern Miami-Dade County (figs. 1, 3, and 10; table 3). Applin and Applin (1944) delineated the top of the Oldsmar Formation in peninsular Florida by the occurrence of abundant specimens of the benthic foraminifer *Helicostegina gyralis*. In the G–3805 well, three unique benthic foraminiferal biozones are present within depositional sequences O2 and O3, and the lower to middle part of the Avon Park Formation (figs. 3 and 10, table 3). The benthic foraminiferal biozones present within each of these three geologic intervals in ascending order are the *Coskinolina* cf. *yucatanensis*-*Orduella* assemblage zone, *Helicostegina gyralis*-*Thomasella* assemblage zone, and *Fallotella floridana*-*Coskinolina floridana* assemblage zone (figs. 4 and 10). Large-scale faunal turnovers at biozone boundaries tend to coincide with depositional sequence boundaries (Brandley and others, 1995; Goldman and Mitchell, 1998). Thus, the presence of unique larger benthic foraminiferal biozones within the depositional sequences O2 and O3, and the Avon Park Formation (fig. 4) provides corroborating evidence for the recognition of unconformities that represent the lower and upper boundaries of depositional sequence O3. Benthic foraminiferal analyses of whole cores acquired from the Hollywood G–2994 well (fig. 1, table 2) indicated the uppermost presence of *Gunteria floridana* is within about 60 ft below the upper bounding surface of the top of the Oldsmar Formation, suggesting that the upper part of the Oldsmar Formation is of latest early Eocene to earliest middle Eocene age (Cushman and Ponton, 1933; Loeblich and Tappan, 1987).

Avon Park Formation

Applin and Applin (1944) proposed the term "Avon Park limestone" for a section of "late middle Eocene" carbonate rock in a well at the Avon Park bombing range in Polk County (fig. 1). In the eastern Broward County and northeastern Miami-Dade County study area, limestone composing the Avon Park Formation lies above the limestone and dolomite of the Oldsmar Formation and beneath the mixed carbonate and siliciclastic rock and sediment of the lower part of the Arcadia Formation (figs. 3–6; Cunningham and Robinson, 2017). Both the upper and lower bounding surfaces of the middle Eocene Avon Park Formation are hiatal (Miller, 1986, pl. 2) and erosional unconformities (Cunningham and Robinson, 2017). Core samples acquired from eight wells (USGS test corehole G–2984, City of Hollywood G–2994 and G–2995, Lauderdale Lakes G–2996 and G–2997, City of Miramar G–2946, Fort Lauderdale Lohmeyer FTL-I4, and Northeast Miami-Dade G–3805; fig. 1, table 2) in the study area indicate that the Avon Park Formation is composed of a vertical succession of numerous high-frequency limestone cycles deposited on a shallow marine platform. The high-frequency cycles are of four types: (1) microbial laminite-capped grain-rich peritidal cycles; (2) rhizolith- and mud-capped micrite-rich peritidal cycles; (3) aggradational grain-rich subtidal cycles; and (4) *Glossifungites*-capped subtidal cycles (figs. 11 and 12). The Avon Park Formation ranges between about 960 and 1,410 ft in thickness.

In ascending order, the three major cycles that compose the Avon Park Formation are depositional sequences AP1, AP2, and AP3 (figs. 3 and 5). Depositional sequence AP1

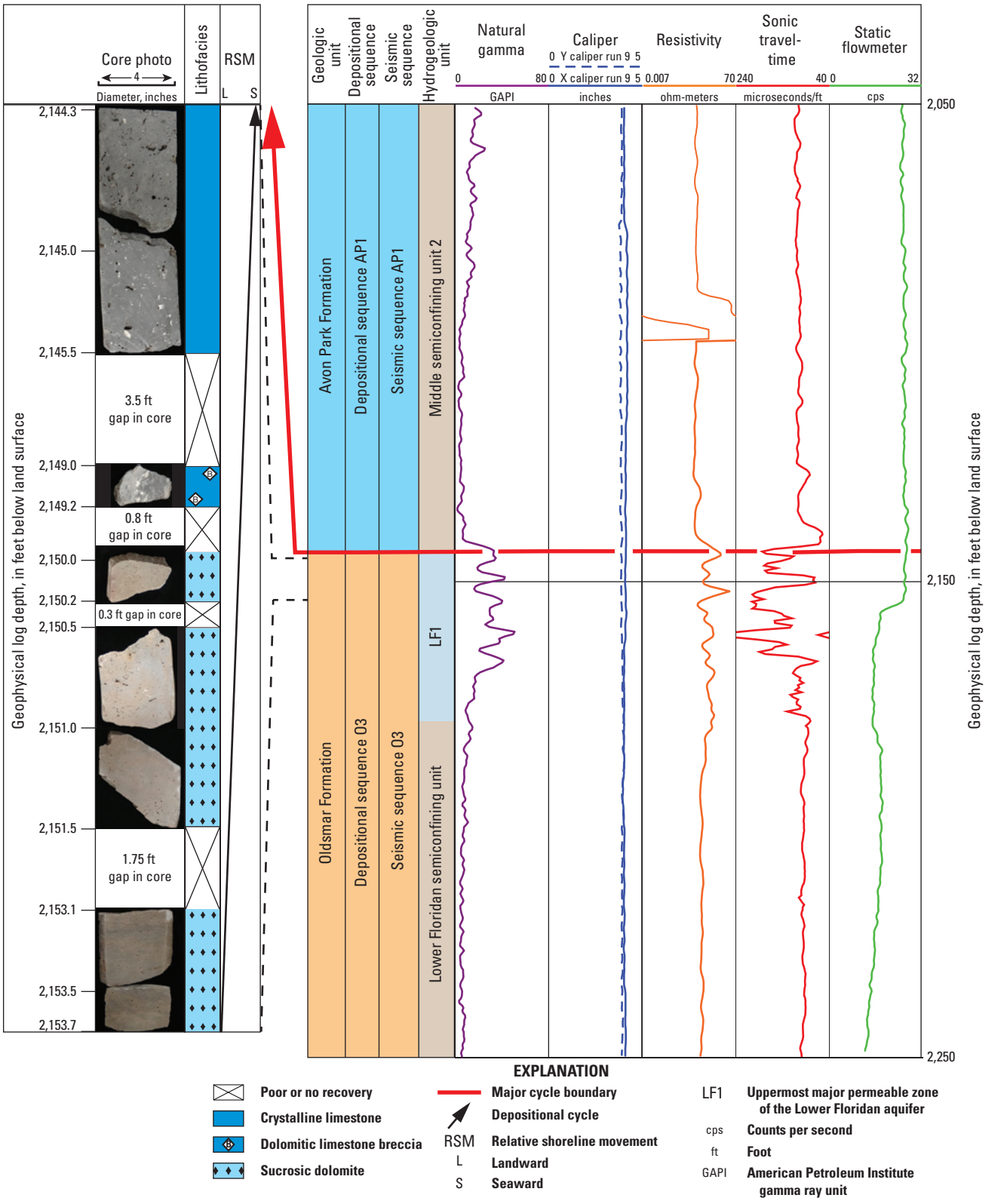

Figure 7. Lithologic and borehole geophysical data acquired from the G–2991 well located in the study area (fig. 1, table 2). A depositional sequence boundary separates depositional sequence O3 from superjacent depositional sequence AP1. Dense dolomite and limestone are present at the top of the Oldsmar Formation and compose the uppermost major permeable zone of the Lower Floridan aquifer in the study area.

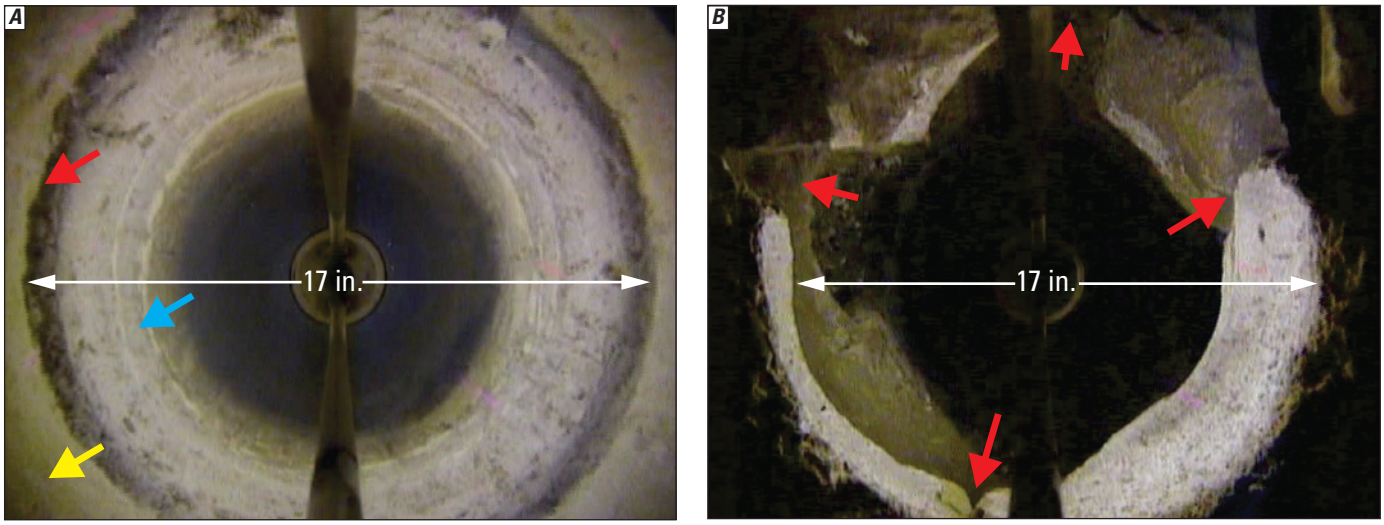

Figure 8. Borehole video images acquired in the G–2991 City of Davie IW–1 well (fig. 1). *A*, The contact (red arrow) between the rock that composes the depositional sequence O3 (cyan arrow) and overlying depositional sequence AP1 (yellow arrow) is shown. Note the absence of fracturing. *B*, Fractured dolomite (red arrows) of the uppermost part of the depositional sequence O3 and uppermost part of the Oldsmar Formation is shown. Solution enlarged fractures are parallel to maximum and minimum stress directions and borehole breakout.

Figure 9. A 4-inch-diameter core acquired in the G–2991 City of Davie IW–1 well (fig. 1) from the uppermost part of a dolomite that bounds the upper surface of the rocks of depositional sequence O3 and the top of the Oldsmar Formation (fig. 7). Red arrows point to two fractures that have an approximate dip of 45°. The fracture to the right appears to be solution enlarged. Blue arrows point to vuggy megaporosity.

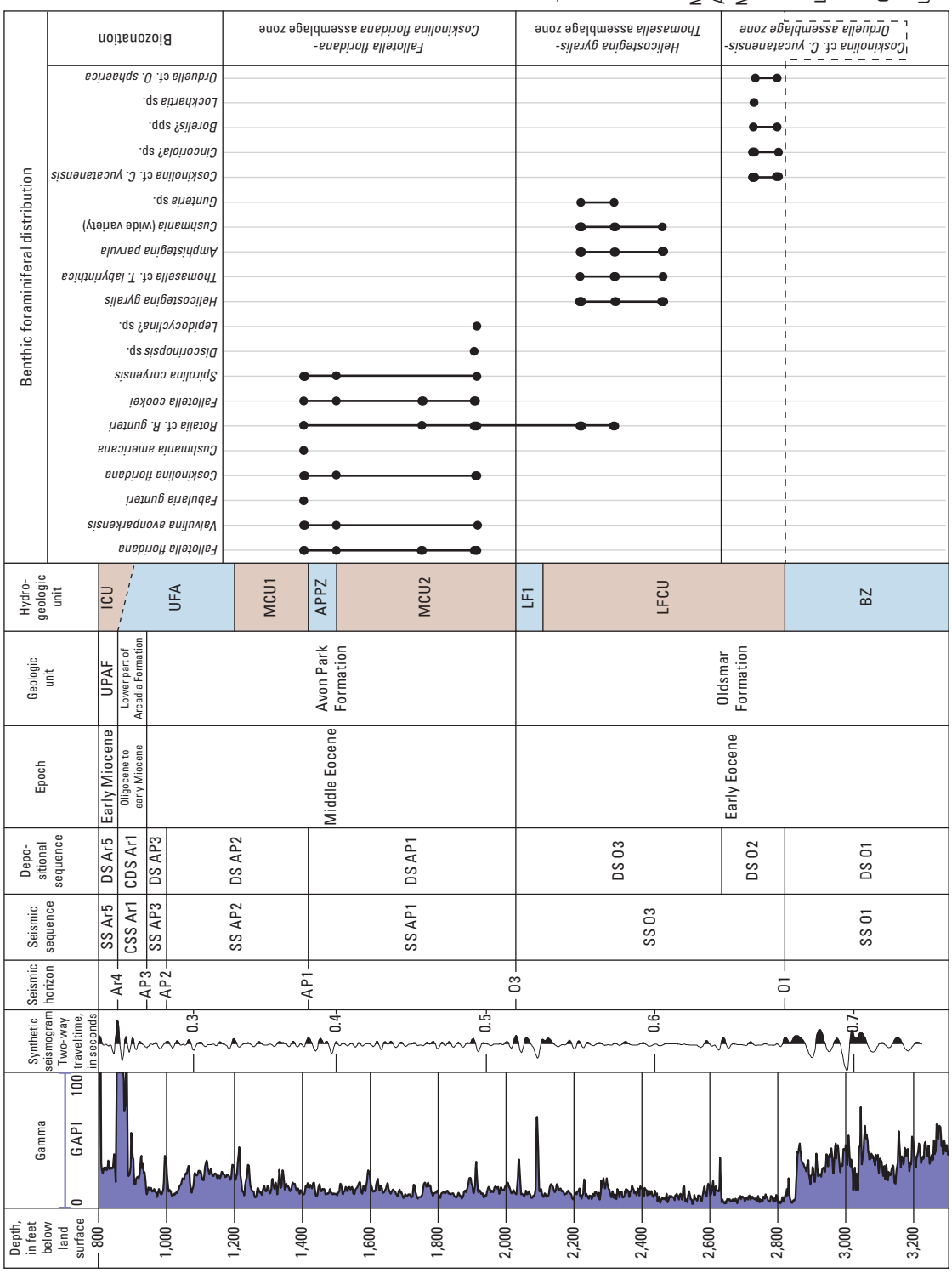

Figure 10. Detailed distribution of foraminifera in the G–3805 well (fig. 1, tables 2 and 3) and their corresponding assemblage zones for Oldsmar Formation depositional sequences O2 and O3, and the lower to middle part of the Avon Park Formation. Major faunal shifts occur at the lower and upper sequence boundaries of depositional sequence O3, providing supporting evidence for major unconformities at the lower and upper sequence boundaries of depositional sequence O3.

Table 3. Well G–3805 foraminiferal distribution chart (fig. 1).

[Poss., possibly; X, present; Xre, present but probably reworked occurrence; ?, uncertain occurrence; --, not present]

Depth (feet below land surface)	*Fallotella floridana*	*Valvulina avonparkensis*	*Fabularia gunteri*	*Coskinolina floridana*	*Coskinolina* sp.?	*Cushmania americana*	*Rotalia* cf. *gunteri*	*Fallotella cookei*	*Spirolina coryensis*	*Discorinopsis* sp.	*Lepidocyclina*?	*Helicostegina gyralis*	*Thomasella* n. sp.	*Amphistegina parvula*	*Cushmania* wide variety	*Amphistegina*? sp. thick walls	*Gunteria floridana*	*Coskinolina* cf. *C. elegans*	*Cincoriola*? sp.	*Borelis*? sp. or poss. *Globoflarina* sp.	*Lockhartia* sp.	Possible gypsinid	*Orduella* cf. *O. sphaerica*
1,404.20	X	X	X	X	--	X	X	--	X	--	--	--	--	--	--	--	--	--	--	--	--	--	--
1,405.30	--	--	--	--	--	--	--	--	--	--	--	--	--	--	--	--	--	--	--	--	--	--	--
1,406.15	X	X	--	X	--	--	--	X	--	--	--	--	--	--	--	--	--	--	--	--	--	--	--
1,406.55	--	--	--	--	--	--	--	--	--	--	--	--	--	--	--	--	--	--	--	--	--	--	--
1,407.00	--	X	--	--	--	--	--	--	--	--	--	--	--	--	--	--	--	--	--	--	--	--	--
1,408.00	X	X	--	--	--	--	--	--	--	--	--	--	--	--	--	--	--	--	--	--	--	--	--
1,409.20	--	--	--	--	--	--	--	--	--	--	--	--	--	--	--	--	--	--	--	--	--	--	--
1,409.70	--	X	--	X	--	--	--	--	X	--	--	--	--	--	--	--	--	--	--	--	--	--	--
1,411.00	--	--	--	--	--	--	--	--	--	--	--	--	--	--	--	--	--	--	--	--	--	--	--
1,501.10	X	X	--	X	--	--	--	X	--	--	--	--	--	--	--	--	--	--	--	--	--	--	--
1,501.40	--	--	--	--	--	--	--	X	X	--	--	--	--	--	--	--	--	--	--	--	--	--	--
1,502.20	--	--	--	--	--	--	--	X	--	--	--	--	--	--	--	--	--	--	--	--	--	--	--
1,751.60	X	--	--	--	--	--	--	--	--	--	--	--	--	--	--	--	--	--	--	--	--	--	--
1,752.70	X	--	--	--	--	--	X	X	--	--	--	--	--	--	--	--	--	--	--	--	--	--	--
1,753.30	--	--	--	--	--	--	--	--	--	--	--	--	--	--	--	--	--	--	--	--	--	--	--
1,754.00	--	--	--	--	--	--	--	--	--	--	--	--	--	--	--	--	--	--	--	--	--	--	--
1,754.20	X	--	--	--	--	--	--	X	--	--	--	--	--	--	--	--	--	--	--	--	--	--	--
1,756.40	?	--	--	--	--	--	--	X	--	--	--	--	--	--	--	--	--	--	--	--	--	--	--
1,906.50	--	--	--	--	--	--	Xre	--	--	--	--	--	--	--	--	--	--	--	--	--	--	--	--
1,906.90	X	--	--	--	--	--	X	X	--	X	--	--	--	--	--	--	--	--	--	--	--	--	--
1,908.10	--	--	--	--	--	--	--	--	--	--	--	--	--	--	--	--	--	--	--	--	--	--	--
1,909.90	X	--	--	--	--	--	X	X	--	--	--	--	--	--	--	--	--	--	--	--	--	--	--
1,910.10	--	--	--	--	X	--	X	--	--	X	--	--	--	--	--	--	--	--	--	--	--	--	--
1,911.60	X	--	--	--	--	--	X	--	--	--	--	--	--	--	--	--	--	--	--	--	--	--	--

Table 3. Well G–3805 foraminiferal distribution chart (fig. 1).—Continued

[Poss., possibly; X, present; Xre, present but probably reworked occurrence; ?, uncertain occurrence; --, not present]

Depth (feet below land surface)	*Fallotella floridana*	*Valvulina avonparkensis*	*Fabularia gunteri*	*Coskinolina floridana*	*Coskinolina* sp.?	*Cushmania americana*	*Rotalia* cf. *gunteri*	*Fallotella cookei*	*Spirolina coryensis*	*Discorinopsis* sp.	*Lepidocyclina*?	*Helicostegina gyralis*	*Thomasella* n. sp.	*Amphistegina parvula*	*Cushmania* wide variety	*Amphistegina*? sp. thick walls	*Gunteria floridana*	*Coskinolina* cf. *C. elegans*	*Cincoriola*? sp.	*Borelis*? sp. or poss. *Globoflarina* sp.	*Lockhartia* sp.	Possible gypsinid	*Orduella* cf. *O. sphaerica*
1,913.20	--	--	--	--	--	--	X	--	--	--	--	--	--	--	--	--	--	--	--	--	--	--	--
1,915.80	--	--	--	--	X	--	X	--	--	--	--	--	--	--	--	--	--	--	--	--	--	--	--
1,916.52	--	--	--	--	--	--	X	--	--	--	--	--	--	--	--	--	--	--	--	--	--	--	--
1,917.20	X	X	--	--	--	--	X	--	X	--	X	--	--	--	--	--	--	--	--	--	--	--	--
2,220.25	--	--	--	--	--	--	--	--	--	--	--	X	X	X	X	--	--	--	--	--	--	--	--
2,220.65	--	--	--	--	--	--	--	--	--	--	--	X	X	X	X	--	--	--	--	--	--	--	--
2,220.80	--	--	--	--	--	--	--	--	--	--	--	X	X	X	--	--	--	--	--	--	--	--	--
2,221.10	--	--	--	--	--	--	?	--	--	--	--	X	X	X	X	X		--	--	--	--	--	--
2,221.40	--	--	--	--	--	--	--	--	--	--	--	X	X	X	X	--	--	--	--	--	--	--	--
2,222.50	--	--	--	--	--	--	--	--	--	--	--	X	X	X	X	--	--	--	--	--	--	--	--
2,224.55	--	--	--	--	--	--	?	--	--	--	--	X	--	X	X	X	X	--	--	--	--	--	--
2,320.50	--	--	--	--	--	--	X	--	--	--	--	X	X	X	--	--	--	--	--	--	--	--	--
2,322.40	--	--	--	--	--	--	--	--	--	--	--	X	X	X	X	--	X	--	--	--	--	--	--
2,323.55	--	--	--	--	--	--	--	--	--	--	--	X	X	X	X	--	--	--	--	--	--	--	--
2,325.30	--	--	--	--	--	--	X	--	--	--	--	X	--	X	?	--	--	--	--	--	--	--	--
2,325.85	--	--	--	--	--	--	--	--	--	--	--	X	X	X	--	--	--	--	--	--	--	--	--
2,326.35	--	--	--	--	--	--	--	--	--	--	--	X	X	X	--	--	--	--	--	--	--	--	--
2,460.15	--	--	--	--	--	--	--	--	--	--	--	X	--	X	--	--	--	--	--	--	--	--	--
2,463.35	--	--	--	--	--	--	--	--	--	--	--	X	--	X	X	--	--	--	--	--	--	--	--
2,463.80	--	--	--	--	--	--	--	--	--	--	--	X	--	X	X	--	--	--	--	--	--	--	--
2,464.30	--	--	--	--	--	--	--	--	--	--	--	X	Xre	X	X	--	--	--	--	--	--	--	--
2,466.20	--	--	--	--	--	--	--	--	--	--	--	X	X	X	--	--	--	--	--	--	--	--	--
2,468.80	--	--	--	--	--	--	--	--	--	--	--	X	--	X	--	--	--	--	--	--	--	--	--
2,730.30	--	--	--	--	--	--	--	--	--	--	--	--	--	--	--	--	--	X	X	X	--	--	--

Table 3. Well G–3805 foraminiferal distribution chart (fig. 1).—Continued

[Poss., possibly; X, present; Xre, present but probably reworked occurrence; ?, uncertain occurrence; --, not present]

Depth (feet below land surface)	*Fallotella floridana*	*Valvulina avonparkensis*	*Fabularia gunteri*	*Coskinolina floridana*	*Coskinolina* sp.?	*Cushmania americana*	*Rotalia* cf. *gunteri*	*Fallotella cookei*	*Spirolina coryensis*	*Discorinopsis* sp.	*Lepidocyclina*?	*Helicostegina gyralis*	*Thomasella* n. sp.	*Amphistegina parvula*	*Cushmania* wide variety	*Amphistegina*? sp. thick walls	*Gunteria floridana*	*Coskinolina* cf. *C. elegans*	*Cincoriola*? sp.	*Borelis*? sp. or poss. *Globoflarina* sp.	*Lockhartia* sp.	Possible gypsinid	*Orduella* cf. *O. sphaerica*
2,731.50	--	--	--	--	--	--	--	--	--	--	--	--	--	--	--	--	--	--	--	--	--	--	--
2,732.70	--	--	--	--	--	--	--	--	--	--	--	--	--	--	--	--	--	X	X	--	X	X	--
2,732.74	--	--	--	--	--	--	--	--	--	--	--	--	--	--	--	--	--	X	X	X	--	X	X
2,732.79	--	---	--	--	--	--	--	--	--	--	--	--	--	--	--	--	--	X	X	X	X	--	--
2,732.87A	--	--	--	--	--	--	--	--	--	--	--	--	--	--	--	--	--	X	--	X	X	X	?
2,732.87B	--	--	--	--	--	--	--	--	--	--	--	--	--	--	--	--	--	X	--	X	X	--	--
2,733.05	--	--	--	--	--	--	--	--	--	--	--	--	--	--	--	--	--	--	--	X	?	--	--
2,733.13	--	--	--	--	--	--	--	--	--	--	--	--	--	--	--	--	--	X	--	X	X	--	--
2,733.24	--	--	--	--	--	--	--	--	--	--	--	--	--	--	--	--	--	X	--	?	X	--	--
2,733.29	--	--	--	--	--	--	--	--	--	--	--	--	--	--	--	--	--	--	X	?	X	--	X
2,734.25	--	--	--	--	--	--	--	--	--	--	--	--	--	--	--	--	--	X	--	--	X	X	X
2,734.30	--	--	--	--	--	--	--	--	--	--	--	--	--	--	--	--	--	--	--	--	X	--	X
2,735.20	--	--	--	--	--	--	--	--	--	--	--	--	--	--	--	--	--	X	--	--	--	X	--
2,736.60	--	--	--	--	--	--	--	--	--	--	--	--	--	--	--	--	--	X	X	--	X	--	X
2,737.20	--	--	--	--	--	--	--	--	--	--	--	--	--	--	--	--	--		--	--	--	--	--
2,737.79	--	--	--	--	--	--	--	--	--	--	--	--	--	--	--	--	--	X	--	--	--	--	X
2,800.60	--	--	--	--	--	--	--	--	--	--	--	--	--	--	--	--	--	X	--	--	--	--	X
2,801.30	--	--	--	--	--	--	--	--	--	--	--	--	--	--	--	--	--	X	--	X	X	--	--
2,801.60	--	--	--	--	--	--	--	--	--	--	--	--	--	--	--	--	--	X	--	--	--	--	--
2,803.35	--	--	--	--	--	--	--	--	--	--	--	--	--	--	--	--	--	X	--	--	--	--	--
2,804.60	--	--	--	--	--	--	--	--	--	--	--	--	--	--	--	--	--	X	X	--	--	--	--
2,806.00	--	--	--	--	--	--	--	--	--	--	--	--	--	--	--	--	--	X	--	--	--	--	--
2,806.30	--	--	--	--	--	--	--	--	--	--	--	--	--	--	--	--	--	X	X	--	--	--	--

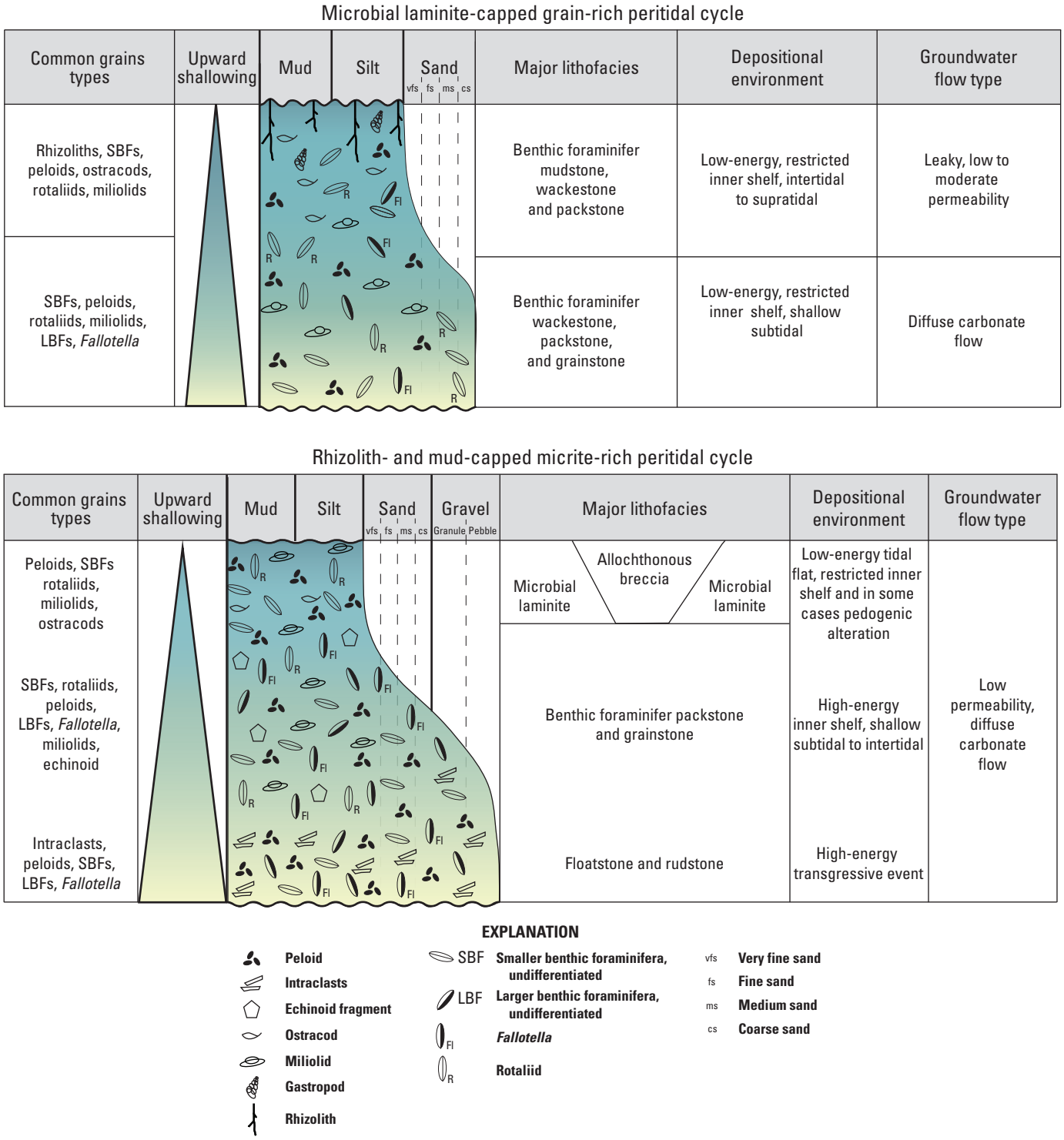

Figure 11. Two of four ideal high-frequency cycles defined for depositional sequences AP1 and AP2 using core and optical borehole-wall images from the G–2984 test corehole (pl. 5) and slabbed core from the wells: City of Hollywood G–2994 and G–2995, Lauderdale Lakes G–2996 and G–2997, City of Miramar G–2946, Fort Lauderdale Lohmeyer FTL-I4, and Northeast Miami-Dade G–3805 (fig. 1).

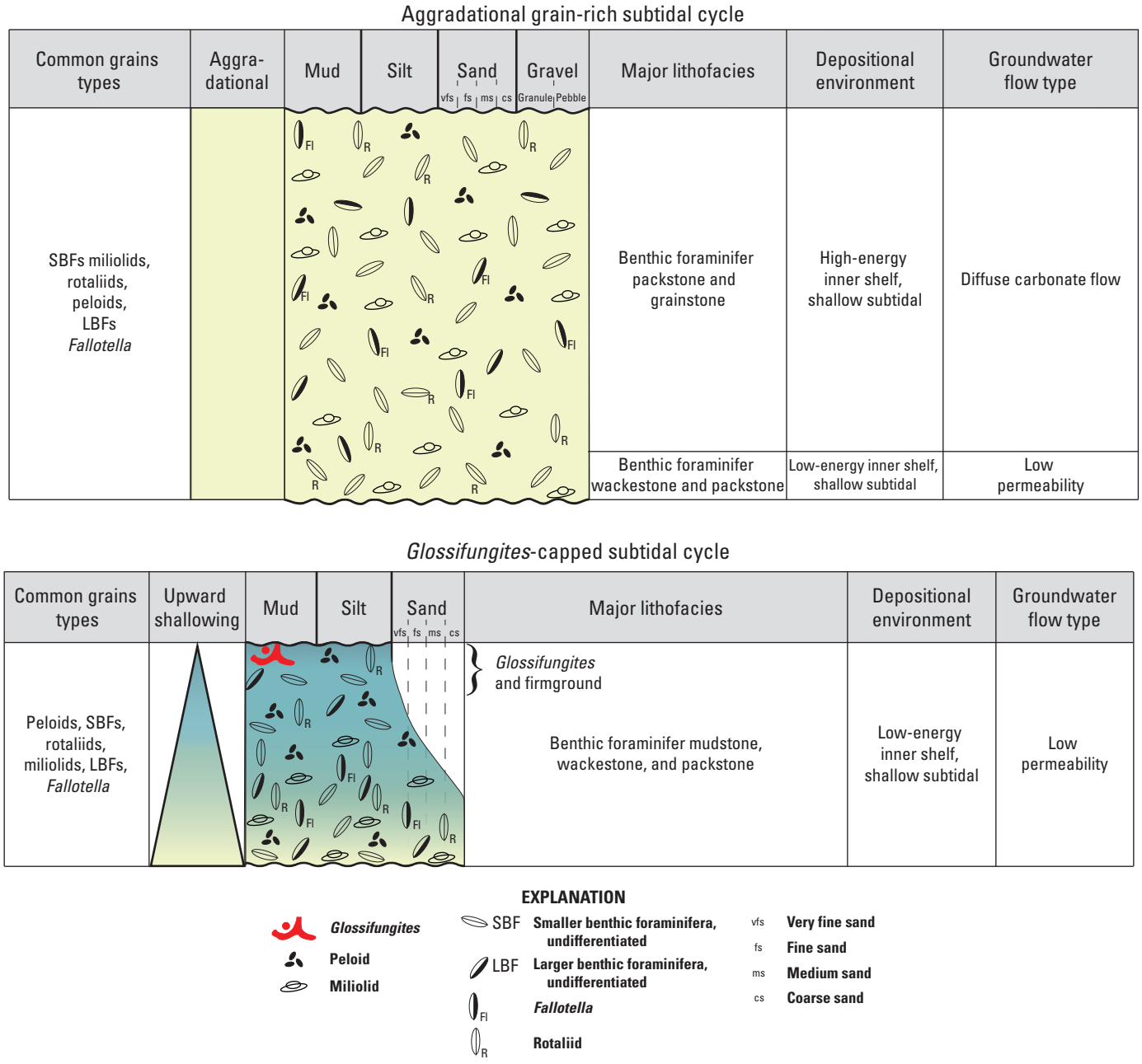

Figure 12. Two of four ideal high-frequency cycles defined for depositional sequence AP2, and AP3 using core and optical borehole-wall images from the G–2984 test corehole (pl. 5) and slabbed core from the wells: City of Hollywood G–2994 and G–2995, Lauderdale Lakes G–2996 and G–2997, City of Miramar G–2946, Fort Lauderdale Lohmeyer FTL-I4, and Northeast Miami-Dade G–3805 (fig. 1).

consists of limestone within the lower part of the Avon Park Formation (fig. 5). The overall upper bounding surface of depositional sequence AP1 generally dips toward the west about 0.1° (pls. 3*B*, *J*, and 4*B*). The geophysical log signature of the contact between depositional sequences AP1 and AP2 is typically a slight upward shift from relatively higher compressional sonic traveltimes in the upper part of depositional sequence AP1 to comparatively lower values at the base of depositional sequence AP2 (fig. 13; Reese and Cunningham, 2014, pls. 1–3). Similarly, the resistivity measured by borehole induction tools commonly show an abrupt upward shift from relatively higher values in the upper part of depositional sequence AP1 to comparatively lower values at the base of depositional sequence AP2 (fig. 13; Reese and Cunningham, 2014, pls. 1–3). It is notable that most examples provided in Reese and Cunningham (2014, pls. 1–3) show this geophysical log character more clearly than figure 13 herein.

The upper boundary of depositional sequence AP1 approximates the top of a major highstand progradational cycle in the G–4002 well (fig. 13). Digital borehole images in the G–4002 well indicate that peritidal cycles having a thick, rhizolith-bearing mud cap (fig. 13) are the dominant high-frequency cycle type in the uppermost part of seismic sequence AP1. The thickness of the rhizolith-bearing mud caps to cycles generally increases upward from the lower part of depositional sequence AP1 to form a cycle set within the depositional sequence made up of numerous shallowing-upward high-frequency cycles. The dense, rhizolith-bearing mud caps to cycles composing the cycle set appear to contribute substantially to higher measured sonic velocity and resistivity values, and the relative shift from higher to lower values upward across the boundary between the uppermost part of depositional sequence AP1 and the lowermost part of depositional sequence AP2. The application of **Walther's Law of facies** indicates that the upward increase in thickness of rhizolith-bearing mud (tidal flat) caps tracks an upward seaward shift in shoreline position, and the upper surface of the cycle set is both the termination of a regressive progradational depositional succession and the upper boundary of depositional sequence AP1.

Depositional sequence AP2 consists of limestone of the Avon Park Formation (fig. 5). The upper bounding surface of depositional sequence AP2 (fig. 14) mostly dips about 0.06°, largely toward the west (pls. 3*C*, *K*, and 4*C*). Core samples from six wells (USGS test corehole G–2984, City of Hollywood G–2994 and G–2995, City of Miramar G–2946, Fort Lauderdale Lohmeyer FTL-I4, and Northeast Miami-Dade G–3805; fig. 1, table 2) and digital borehole wall images from the test corehole G–3729 indicate that the platform carbonates that compose seismic sequence AP2 are characteristically vertically stacked, peritidal high-frequency cycles at a foot- to several-foot-scale (pl. 5; Cunningham and Robinson, 2017). Compared to the other five wells with core samples from short cored intervals, the continuously drilled core samples recovered from a long interval of the upper part of depositional sequence AP2 in the test corehole G–2984 were the most useful in characterizing the lithology and cyclostratigraphy of depositional sequence AP2 (pl. 5; Cunningham and Robinson, 2017). In the test corehole G–2984 core samples, three types of ideal high-frequency cycles (figs. 11 and 12) have been identified within the depositional sequence AP2: rhizolith- and mud-capped micrite-rich peritidal cycles; microbial laminite-capped grain-rich peritidal cycles; and *Glossifungites*-capped subtidal cycles (figs. 11 and 12; Cunningham and Robinson, 2017).

Depositional sequence AP3 consists of limestone of the uppermost part of the Avon Park Formation (fig. 5, pl. 5; Cunningham and Robinson, 2017). The upper bounding surface of depositional sequence AP3 (fig. 15) mostly dips toward the west about 0.05° (pls. 3*D*, *L*, and 4*D*). The upper sequence boundary of depositional sequence AP3 is a major unconformity where limestone of the middle Eocene Avon Park Formation (Miller, 1986) is overlain by a basal Oligocene part of the Arcadia Formation (fig. 15; Brewster-Wingard and others, 1997; Guertin and others, 2000; Cunningham and others, 2003; Cunningham and Robinson, 2017). The depositional textures and carbonate particles of the depositional sequence AP3 are largely indicative of deposition on the shallow subtidal, high-to-moderate energy inner platform of the Avon Park Formation (pl. 5, Cunningham and Robinson, 2017). The high-frequency cycle stacking pattern of seismic sequence AP3 indicates upward, progressive landward movement of the AP3 shoreline forming a transgressive systems tract that backstepped over the underlying depositional sequence AP2 (pl. 5). The aggradational, grain-rich, subtidal high-frequency cycle type is unique (figs. 14 and 15, pl. 5; Cunningham and Robinson, 2017) to the rocks that compose depositional sequence AP3 in the G–2984 test corehole. This aggradational cycle type is not found in core samples observed from depositional sequences AP1 and AP2.

Arcadia Formation

Scott (1988) formally proposed the name "Arcadia Formation" for a carbonate unit of the lower Hawthorn Group. The type section of the Arcadia Formation (Scott, 1988) is in the corehole W–12050, Hogan 1, DeSoto County, Florida (fig. 1). In the eastern Broward County and northeastern Miami-Dade County study area, continuously drilled core samples from the entire thickness of the Arcadia Formation from the G–2984 test corehole in northeastern Broward County and minor core samples from the PB–1766 well (fig. 1, table 2) provide the foundation for understanding the lithostratigraphy and sequence stratigraphy of the Arcadia Formation. This formation lies above the limestone of the Avon Park Formation (Reese and Cunningham, 2014; Cunningham, 2015) and beneath the siliciclastic rock and sediment of the Peace River Formation (fig. 5) throughout the study area, except in the easternmost part of the study area

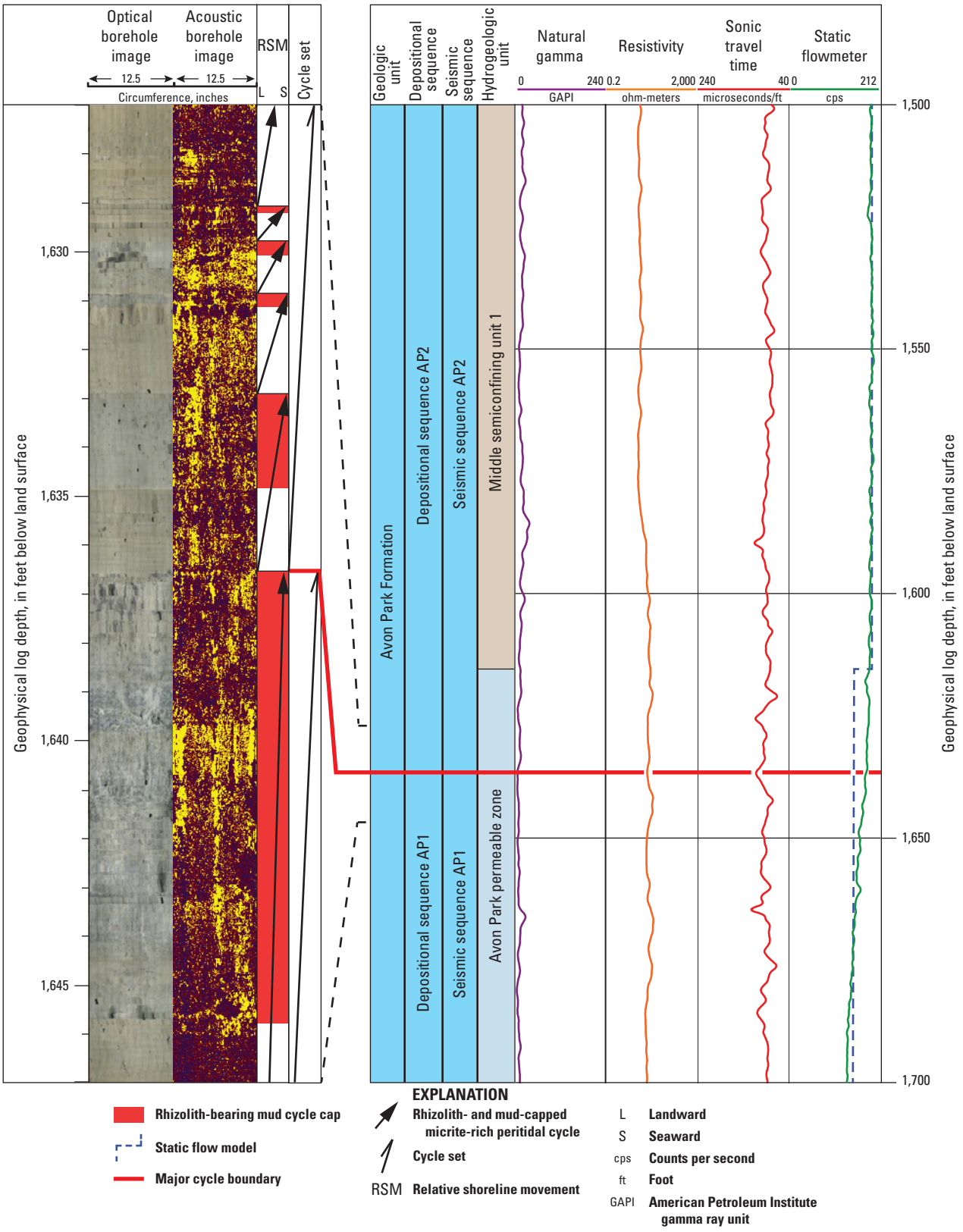

Figure 13. Boundary separating depositional sequence AP1 and superjacent depositional sequence AP2 in the G–4002 corehole located in the study area (fig. 1, table 2). Generally, multiple meter-scale, rhizolith- and mud-capped micrite-rich peritidal cycles compose the rock of the Avon Park permeable zone and overlying middle semiconfining unit of the upper part of the Floridan aquifer system. The top of the depositional sequence AP1 and seismic sequence AP1 are at or close to the top of the Avon Park permeable zone.

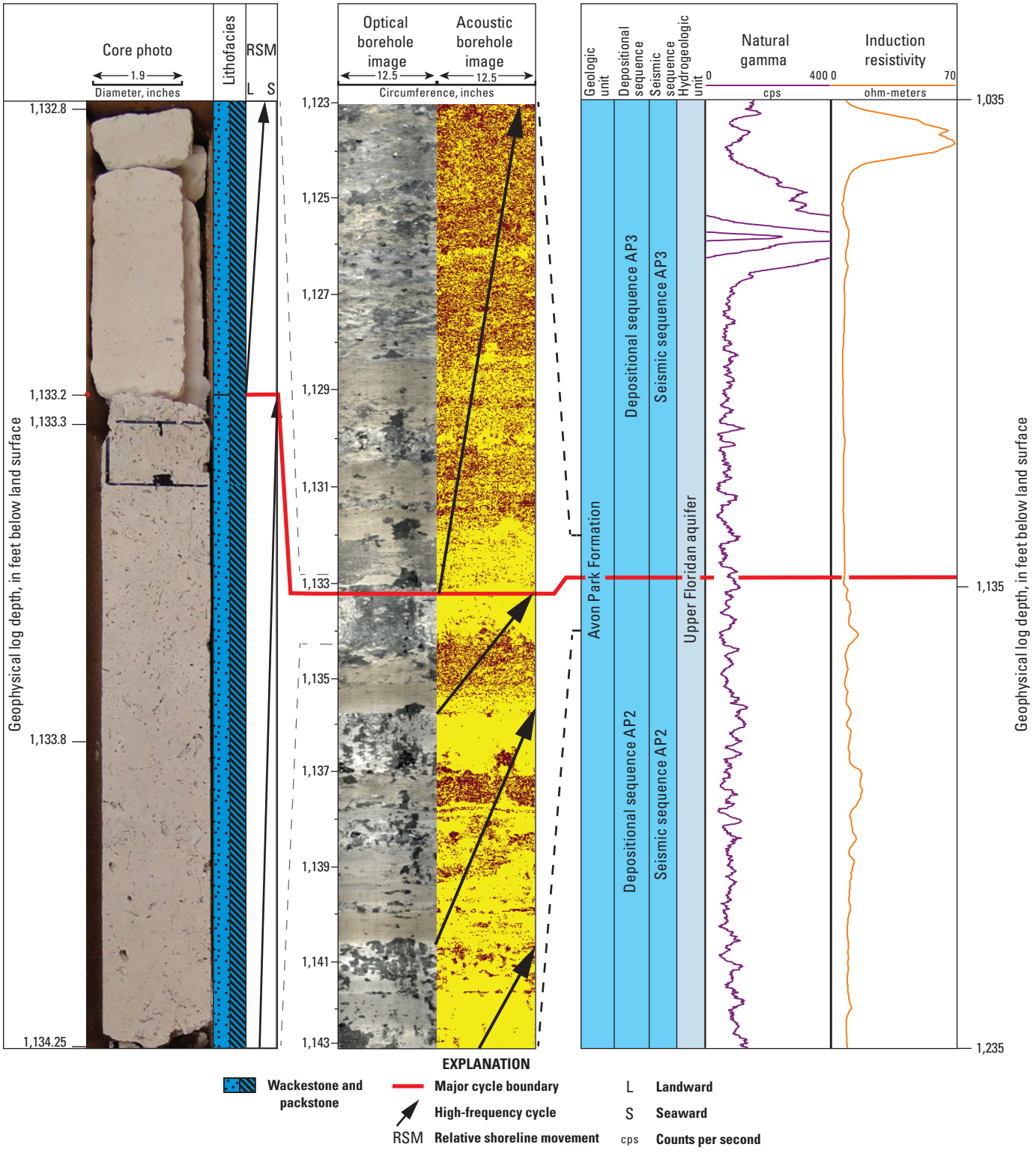

Figure 14. Boundary at the upper bounding surface of depositional sequence AP2 that separates it from depositional sequence AP3 in the G–2984 test corehole located in northeastern Broward County (fig. 1, table 2). Meter-scale, platform top, rhizolith- and mud-capped micrite-rich peritidal cycles of depositional sequence AP2 are overlain by thicker subtidal cycles of depositional sequence AP3 (pl. 5). The permeability of the Upper Floridan aquifer in the high-frequency cycles composing seismic sequence AP2 is dominantly related to karstic vuggy megaporosity within micrite-rich tidal-flat caps on high-frequency cycles, whereas the permeability of the limestone of the Avon Park Formation that composes seismic sequence AP3 is mainly related to interparticle porosity.

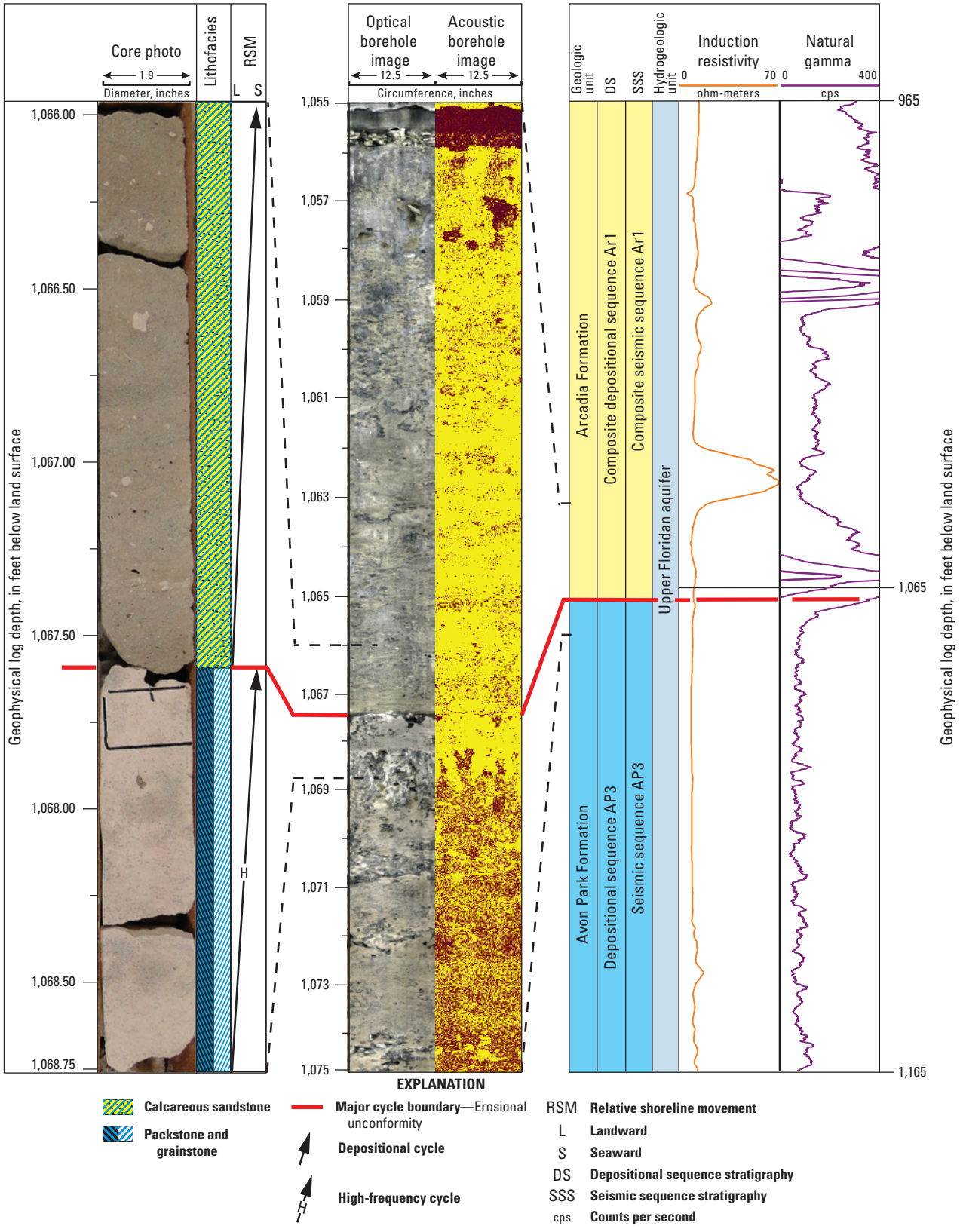

Figure 15. Boundary separating depositional sequence AP3 and superjacent composite depositional sequence Ar1 in the G–2984 test corehole located in northeastern Broward County (figs. 1, table 2). This depositional sequence boundary is equivalent to the upper seismic sequence boundary of seismic sequence AP3 (figs. 3 and 4, pls. 6–19). The Upper Floridan aquifer spans the rocks that compose depositional sequence AP3 and most, or in some cases all, of depositional **composite sequence** Ar1 (figs. 3 and 4; pls. 5 and 20).

where the Arcadia Formation is overlain by carbonate rock of the Stock Island Formation (figs. 1 and 5, pls. 18 and 19). The upper and lower bounding surfaces of the Arcadia Formation are both unconformities (figs. 15 and 16, pl. 20). The lower unconformity between the Avon Park and Arcadia Formations (fig. 15) is discussed more completely in Reese and Cunningham (2014, p. 7–8) and Cunningham (2015, p. 7–8). In the eastern part of the study area, the upper bounding surface of the Arcadia Formation (fig. 16) has a complex relationship between "stairstepping" stratal geometries and the overlying downlapping of strata of the Peace River and Stock Island Formations (figs. 1, 5, and 6; pls. 18 and 19). Both the upper and lower parts of the Arcadia Formation (fig. 5) are dominated by heterozoan particle assemblages (Cunningham and Robinson, 2017), indicating temperate water conditions during deposition (James, 1997).

In their report on eastern Broward County, Reese and Cunningham (2014) informally divided the Arcadia Formation into two lithostratigraphic units, the lower Arcadia Formation and the upper Arcadia Formation. Herein, however, the two units of Reese and Cunningham (2014) are referred as the "lower part of the Arcadia Formation" and the "upper part of the Arcadia Formation" (figs. 3 and 4), respectively. The lower part of the Arcadia Formation is composed of four aggradational depositional sequences: depositional sequence Ar1 through Ar4 (fig. 4, pl. 20). These four depositional sequences form composite depositional sequence Ar1 (fig. 4, pl. 20). The upper boundary of composite depositional sequence Ar1 is a phosphatized hardground related to a drowning unconformity at this sequence boundary (fig. 17; Reese and Cunningham, 2014, p. 17). Depositional sequences Ar1 through Ar4 are composed of subtidal shallow-marine mixed carbonate and siliciclastic rocks and sediments (pl. 20, Cunningham and Robinson, 2017) that are widespread throughout southeastern Florida. The lithostratigraphy and sequence stratigraphy of the depositional sequences Ar1 through Ar4 are more completely described by Reese and Cunningham (2014) and Cunningham and Robinson (2017).

The upper part of the Arcadia Formation consists of three depositional sequences: depositional sequences Ar5, Ar6, and Ar7 (figs. 4–6, pl. 20). Depositional sequences Ar5 and Ar6 form composite depositional sequence Ar2 (figs. 4 and 5, pl. 20). Depositional sequences Ar5 through Ar7 are three distally steepened carbonate ramps (figs. 5 and 6, pls. 3*F*-*H*, *N*-*P*, and 4*F*-*H*; compare to Pomar, 2001) that prograded eastward during their vertical and lateral accumulation. The eastern ramp margins of depositional sequences Ar5 through Ar7 terminate along an approximately north-south trend in eastern Broward County and northeastern Miami-Dade County (figs. 5 and 6, pls. 3*F*-*H*, *N*-*P*, and 4*F*-*H*). At the G–2984 test corehole, the composite depositional sequence Ar2 shallows upward from a deep offshore terrigenous mudstone representing an outer ramp environment in the basal part to bivalve floatstone and rudstone representing an inner ramp environment in the uppermost part (pl. 20; Cunningham and Robinson, 2017). Integration of the borehole data from the G–2984 test corehole and seismic-reflection data provided much of the basis for construction of a conceptual model in the form of a west-to-east cross section that includes the distribution of these environments within the composite depositional sequence Ar2 (fig. 5). Depositional sequence Ar5 represents a coarsening-upward, eastward prograding, outer ramp (figs. 5 and 6, pl. 3*F*, *N*, pl. 20; Cunningham and Robinson, 2017). The vertical lithofacies succession of the outer ramp is, in ascending order, the gradation from a terrigenous mudstone to interlaminated **marl** and foraminiferal wackestone (pl. 20). This vertical lithofacies succession, along with seismic-reflection profiles shown later herein, indicate the shallowing upward and eastward progradation of the depositional sequence Ar5 outer ramp. The fossil content of this ramp is dominated by smaller benthic foraminifera and globular planktonic foraminifera, with the density of foraminiferal specimens increasing upward (pl. 20; Cunningham and Robinson, 2017). The boundary between depositional sequences Ar5 and Ar6 is an erosional discontinuity (fig. 18). Depositional sequence Ar5 is capped by a *Thalassinoides*-dominated *Glossifungites* Ichnofacies and there is an abrupt shift in depositional textures from lime mudstone and wackestone to packstone across the boundary separating depositional sequences Ar5 and Ar6 (fig. 18, pl. 20; Cunningham and Robinson, 2017). The *Glossifungites* Ichnofacies "is a firmground suite of trace fossils that commonly demarcates erosional discontinuities in sedimentary successions" (MacEachern and Burton, 2000). Shown herein, a seismic-reflection profile (pls. 6 and 7) and core samples from the G–2984 test corehole (pl. 20) support the presence of a lowstand wedge at the ramp margin composed of a fining upward cycle at the base of depositional sequence Ar6 overlying depositional sequence Ar5. The fining-upward depositional cycle is composed of a vertical lithofacies succession that grades upward from packstone and grainstone at the base to overlying interlaminated to interbedded mudstone and wackestone (pl. 20). Common smaller benthic foraminifera and globular planktonic foraminifera, as well as minor ostracods and echinoid spines, mainly compose the assemblage of fossils. Overlying the wedge at the ramp margin are three depositional cycles that represent, in ascending order, transgressive to overlying highstand systems tracts of depositional sequence Ar6. The upper bounding surface of depositional sequence Ar6 is a vuggy emersion surface that was mineralized by phosphorite (fig. 19) during the formation of a later-stage drowning unconformity (Godet, 2013). The two depositional cycles above the lowstand wedge of depositional sequence Ar6 (pl. 20) contribute to the transgressive systems tract of depositional sequence Ar6. In general, the vertical lithofacies successions of the two depositional cycles grade upward from foraminifer wackestone and packstone to overlying foraminifer- and diatom-bearing marl. The particle composition of the marl, wackestone, and packstone is largely

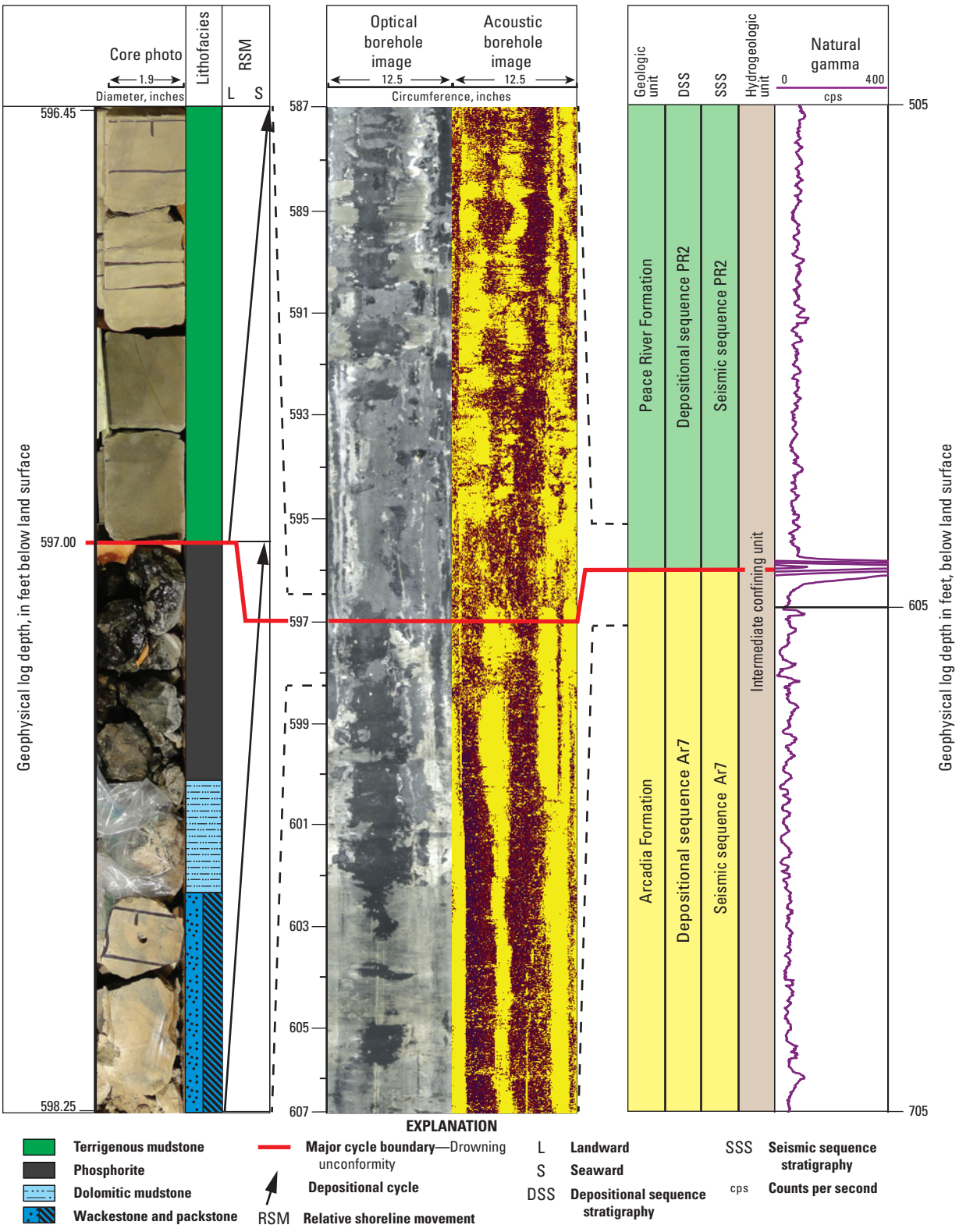

Figure 16. Boundary separating depositional sequence Ar7 and superjacent depositional sequences PR2 in test corehole G–2984 located in northeastern Broward County (figs. 1 and 4). Depositional sequence Ar7 and PR2 are equivalent to seismic sequences Ar7 and PR2, respectively. The thick phosphorite cap at the top of the outer ramp facies of depositional sequence Ar7 is indicative of a major drowning unconformity (Schlager, 1989; Godet, 2013). The flooding surface between depositional sequences Ar7 and PR2 is overlain by distal prodelta terrigenous mudstones of the Peace River Formation. The rocks and sediments that compose depositional sequences Ar7 and PR2 are part of the intermediate confining unit throughout much of the study area.

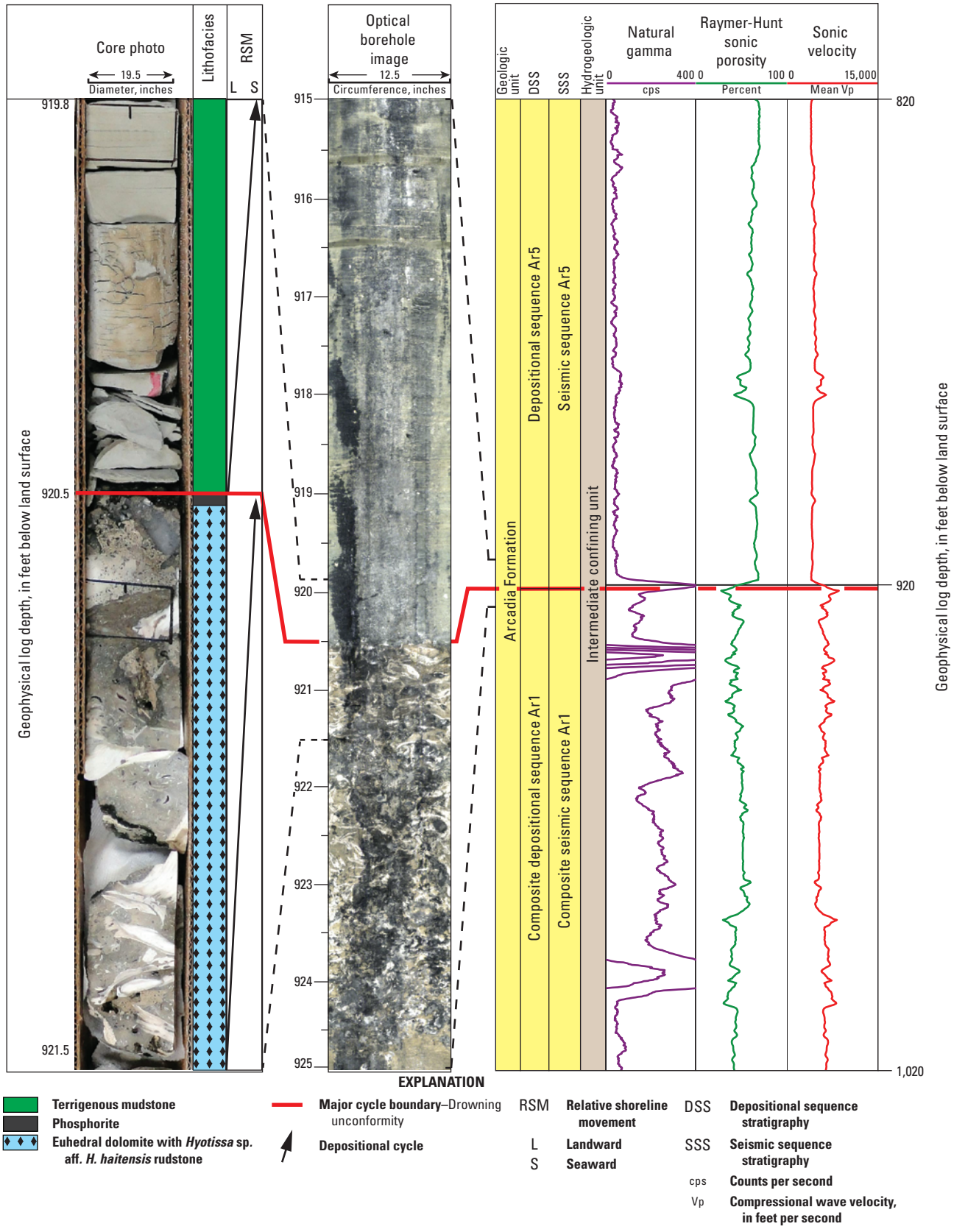

Figure 17. Uppermost part of composite depositional sequence Ar1, the lowermost part of the depositional sequence Ar5, and the boundary that separates them in the G–2984 test corehole located in northeastern Broward County (fig. 1, table 2, and pl. 20). The rocks shown are within the lower part of the intermediate confining unit.

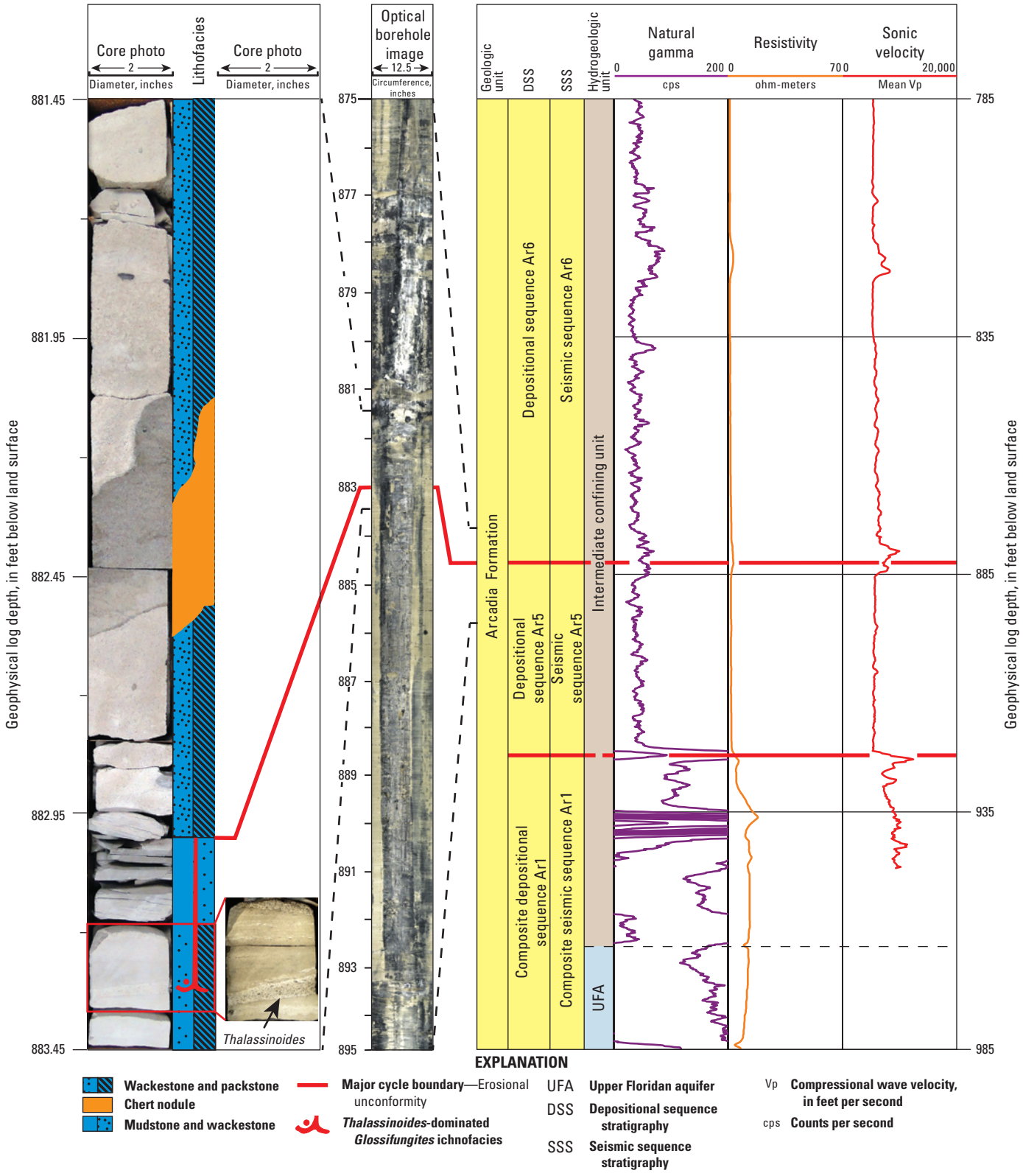

Figure 18. Boundary separating depositional sequences Ar5 and Ar6 in test corehole G–2984, located in northeastern Broward County (fig. 1, table 2, and pl. 20). A *Thalassinoides*-dominated *Glossifungites* Ichnofacies caps depositional sequence Ar5 and coincides with an erosional discontinuity at the top of depositional sequences Ar5. Depositional sequences Ar5 and Ar6 are equivalent to seismic sequences Ar5 and Ar6, respectively. The rocks that compose depositional sequences Ar5 and Ar6 represent part of the intermediate confining unit throughout much of the study area.

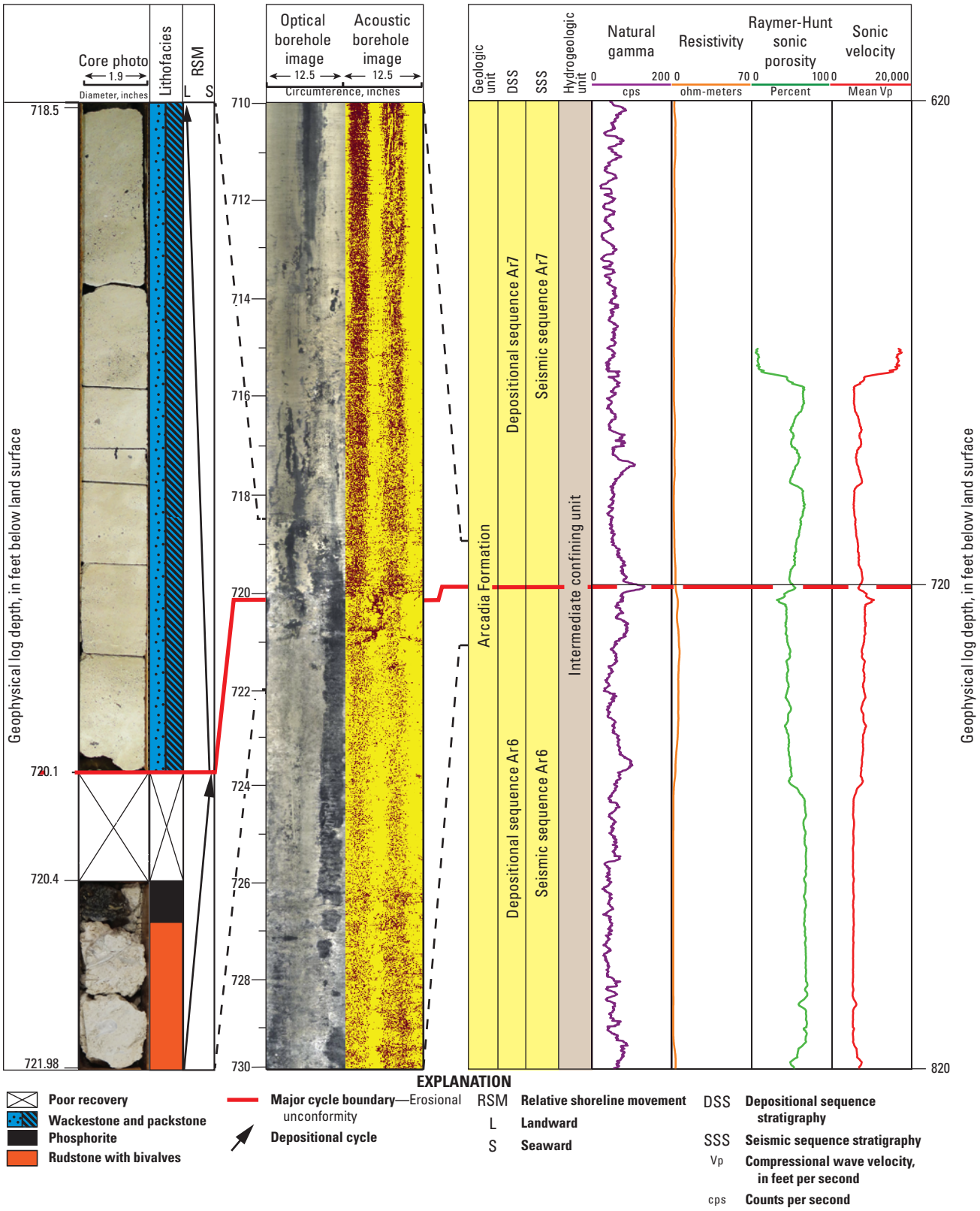

Figure 19. Boundary separating depositional sequences Ar6 and Ar7 in test corehole G–2984, located in northeastern Broward County (fig. 1, table 2, and pl. 20). Depositional sequences Ar6 and Ar7 are stratigraphically equivalent to seismic sequences Ar6 and Ar7, respectively. The rocks that compose depositional sequence Ar6 and Ar7 form part of the intermediate confining unit throughout the study area.

unidentified silt- to medium-sand-sized skeletal fragments, smaller benthic foraminifera, and globular planktonic foraminifera (pl. 20, Cunningham and Robinson, 2017). Diatoms are a unique component of the marl, and the skeletal fragments in the marl are typically silt- to very-fine-sand-sized (pl. 20 and Cunningham and Robinson, 2017). The uppermost depositional cycle of depositional sequence Ar6 is capped by a coarsening upward vertical lithofacies succession. In ascending order, the highstand part of the depositional cycle is composed of marl, marl interbedded with mudstone, bivalve wackestone and mud-dominated packstone, bryozoan floatstone, bivalve floatstone and rudstone, and phosphorite. The eastern, downward-sloping limit of the depositional sequence Ar6 ramp trends approximately north-south along the eastern part of the study area (pls. 3*G*, 4*G*).

At the G–2984 test corehole, depositional sequence Ar7 is composed of nine fining-upward, deepening-upward depositional cycles that represent an outer ramp environment (pl. 20). Two of the lowest three cycles contain marl, which occurs in the middle and upper parts of one cycle and in the upper part of the other, indicating deepening upward conditions during cycle development. The typical vertical lithofacies succession for each cycle is an upward change from wackestone and mud-dominated packstone in the lower part of the cycle to more dominant clay- or micrite-rich lithologies, such as marl, lime mudstone, or wackestone, in the upper part of the cycle (pl. 20; Cunningham and Robinson, 2017). Commonly, the lowermost part of each cycle contains a mixture of 5- to 7-percent silt and small, black, pebble-sized phosphorite grains, grading upward to a mixture of about 1- to 2-percent silt- and fine-sand-sized, black, phosphorite grains in the uppermost part of each cycle. The common fossil content of the cycles is dominated by silt-sized skeletal fragments, globular planktonic foraminifera, and smaller benthic foraminifera, and minor ostracods and echinoid spines. Each of the nine depositional cycles is capped by a burrowed firmground attributable to a *Thalassinoides*-dominated *Glossifungites* Ichnofacies (MacEachern and others, 2007, p. 49–52), wherein the burrow system is filled with sediment from the overlying phosphorite-pebble-bearing bed at the base of the overlying cycle. At the end of a transgressive accumulation phase of each deepening-upward cycle, a lowering of relative sea level dropped the storm wave base and caused submarine erosion. The seafloor erosion exposed dewatered firm lime muds, thus producing cycle-capping firmgrounds (MacEachern and others, 2007). The firmgrounds were colonized by *Thalassinoides*-forming crustaceans, followed by deposition of pebbly sediment during initial accumulation of the overlying cycle (pl. 20). The pebbly basal accumulation may have occurred during relative lowstand conditions when bottom currents intermittently eroded the seafloor and swept coarser sediment from more landward areas of the ramp to begin accumulation on the firmgrounds and fill burrows. Alternatively, this initial fill of burrows within the underlying cycle and initial accumulation of the overlying cycle may have occurred during early relative transgression, as conceptualized for a carbonate outer ramp of Early Cretaceous age in Argentina (Schwarz and Buatois, 2012).

The upper bounding surface of depositional sequence Ar7 is a hardground formed by mineralization of the original firmground by phosphorite and represents a major drowning unconformity. Shown later herein, seismic-reflection profiles support local submarine erosion or erosion during an emersion event of the upper bounding surface of depositional sequence Ar7 (pl. 20). The phosphatic hardground bounding the upper surface of the Arcadia Formation is usually well defined on gamma-ray borehole logs as a pronounced peak that is produced by high gamma-ray values (fig. 4; Reese and Cunningham, 2014, pls. 1–3). The depositional sequence Ar7 ramp margin terminates along an approximately north-south trend (pls. 3*H* and 4*H*) near the eastern coastal boundary of the study area.

Hydrogeology

A refined conceptualization of the hydrogeologic, geologic, depositional sequence, and seismic stratigraphic framework (figs. 3–6) of the intermediate confining system and Floridan aquifer system is critical to understanding the confinement and transport of treated wastewater at deep injection treated wastewater utilities in Broward County and elsewhere in southeastern Florida. This study focused on a lower part of the intermediate confining unit and most of the Floridan aquifer system in eastern Broward County and northeastern Miami-Dade County (figs. 1 and 2). That part of the Floridan aquifer system included in this investigation includes the Upper Floridan aquifer, middle semiconfining unit 1, Avon Park permeable zone, middle semiconfining unit 2, uppermost major permeable zone of the Lower Floridan aquifer, Lower Floridan semiconfining unit, and uppermost part of the Boulder Zone (fig. 2). These hydrogeologic units used herein were delineated in southeastern Florida by Reese and Richardson (2008) and Reese and Cunningham (2014), and provided the basis for defining a hydrogeologic framework using seismic reflection profiles. A more recent regional interpretation by Williams and Kuniansky (2015), which includes a different local hydrogeologic and geologic framework of the study area in Broward County and northeastern Miami-Dade County, was not used. It was found that the upper surfaces of each of the four permeable zones (Upper Floridan aquifer, uppermost major permeable zone of the Lower Floridan aquifer, Lower Floridan semiconfining unit, and Boulder Zone) generally correlated well with major seismic horizons, which correspond to major depositional sequence boundaries and seismic sequence boundaries (fig. 3). This relationship to upper depositional sequence boundaries indicates that all four permeable units of the Floridan aquifer system underlie, or approximately underlie, subaerial unconformity surfaces.

This is important, because it is shown later herein that the seismic expression of these unconformity surfaces, which form prominent seismic-reflection horizons, can be mapped continuously on seismic-reflection profiles. Elsewhere, sequence stratigraphy and seismic stratigraphy have been used broadly in the oil industry to effectively detect ancient subaerial exposure at unconformities and related secondary porosity (Budd and others, 1995), Detection of subaerial exposure at unconformities and related secondary porosity in southeastern Florida is at the upper surfaces of carbonate depositional cycles of several hierarchical scales ranging from high-frequency cycles to depositional sequences. Thus, the approach herein of using sequence stratigraphy and seismic stratigraphy provides a hydrologic-unit mapping approach superior to mapping with only well data.

More detailed information about the character of the hydrogeologic units within the study area is provided in Reese and Cunningham (2014). It is noteworthy, however, that the study described herein presents evidence for (1) epigenic karst contributing substantially to the development of enhanced porosity and permeability during paleo-subaerial exposure that is related to major depositional sequence boundaries and (2) **hypogenic karst** producing vertical, columniform, seismic-sag structures that have potential for cross-formational fluid flow. A relationship between secondary porosity and subaerial exposure related to unconformities and depositional sequence boundaries is well documented in carbonate hydrocarbon reservoirs around the world (Budd and others, 1995). This is especially the case for the increasing porosity and permeability of the uppermost major permeable zone of the Lower Floridan aquifer and Boulder Zone, where the evidence (unconformity related karst collapse, fracturing, and faulting) is on the scale imaged on seismic-reflection profiles. More subtle evidence is evident for small-scale dissolution features related to an unconformity along the upper surface of the sequence boundary (top of depositional sequence AP1) at or near the top of the Avon Park permeable zone (fig. 3) and minor exposure surfaces at the tops of high-frequency cycles below the sequence boundary. The relationship between unconformity-bound cycles (depositional sequences and high-frequency cycles) and the top of the Upper Floridan aquifer is more complex, because multiple unconformities and corresponding sequence boundaries are present within this aquifer in the lower part of the Arcadia Formation and upper part of the Avon Park Formation (figs. 3 and 4; Reese and Cunningham, 2014, figs. 8, 14, 21, 22, and 24).

Seismic Stratigraphy

The fundamental seismic stratigraphic analyses conducted for this study were identification and characterization of seismic-reflection termination, configuration, continuity, and amplitude produced by sedimentary strata (Mitchum and others, 1977). Twelve seismic sequences were identified within the study area. In ascending order, the seismic sequences are O1, O3, AP1, AP2, AP3, Ar1, Ar2, Ar3, Ar4, Ar5, Ar6, and Ar7 (figs. 3, 4, 20, and 21); however, seismic sequences Ar1 through Ar4 are tentatively defined, although the upper bounding surface of Ar4 is certain. In addition, two composite seismic sequences, Ar1 and Ar2, were identified and consist of seismic sequences Ar1 through Ar4, and Ar5 and Ar6, respectively (figs. 3–6, 20, and 21). These seismic sequences represent rock that comprises the hydrogeologic units from the middle of the intermediate confining unit downward into the Boulder Zone (figs. 3–6, 20, and 21). The interpretation of seismic-reflection data included mapping the altitude of the upper surfaces of eight of the seismic sequences (seismic sequences O1, Ar1, Ar2, and Ar3 were excluded) and characterization of subsurface seismic-sag structures and a single fault of probable tectonic origin within the study area (pls. 6–19, 21).

Seismic sequence stratigraphic analysis was used to broadly delineate and characterize seismic sequences mapped on seismic-reflection profiles acquired by the USGS (Cunningham, 2013, 2015; Reese and Cunningham, 2014) in eastern Broward and northeastern Miami-Dade Counties (fig. 1, table 1). The hydrogeologic framework of the Floridan aquifer system established by Reese and Richardson (2008) for central and southern Florida, and by Reese and Cunningham (2014) for eastern Broward County, was linked to five seismic sequences (O1, O3, AP1, AP2, and AP3) and part of composite seismic sequence Ar1 (figs. 2–4). The boundary between the intermediate confining unit and Floridan aquifer system commonly is within or near the top of composite seismic sequence Ar1 (figs. 3 and 4; Reese and Cunningham, 2014, pls. 1–3). Seismic sequences O1, O3, AP1, AP2, AP3, and part of composite seismic sequence Ar1 (typically depositional sequences Ar1 and Ar2, and uncommonly Ar3) compose a major part of the Floridan aquifer system (figs. 2–4). In the study area, the Upper Floridan aquifer (Reese and Cunningham, 2014) typically includes the lower to middle part of composite seismic sequence Ar1, all of seismic sequence AP3, and the upper part of seismic sequence AP2 (figs. 3 and 4). The top of the Avon Park permeable zone approximately corresponds to the top of seismic sequence AP1 (fig. 3). The top of the Lower Floridan aquifer and top of the uppermost major permeable zone of the Lower Floridan aquifer approximately corresponds to the top of seismic sequence O3 (figs. 2 and 3). The top of the Boulder Zone corresponds to the top of seismic sequence O1 (fig. 3). Seismic-reflection continuity below the base of the seismic sequence O3 was generally poor, with the exception of seismic-reflection profile S7 (figs. 1 and 21, table 1; Cunningham, 2014). In some cases on seismic-reflection profiles, the measurement and display of the attribute “average energy” was very useful in locating geologic features, such as the tops of seismic sequences O1, O3, AP1, AP2, and AP3, and top of composite seismic sequence Ar1 (figs. 2–4).

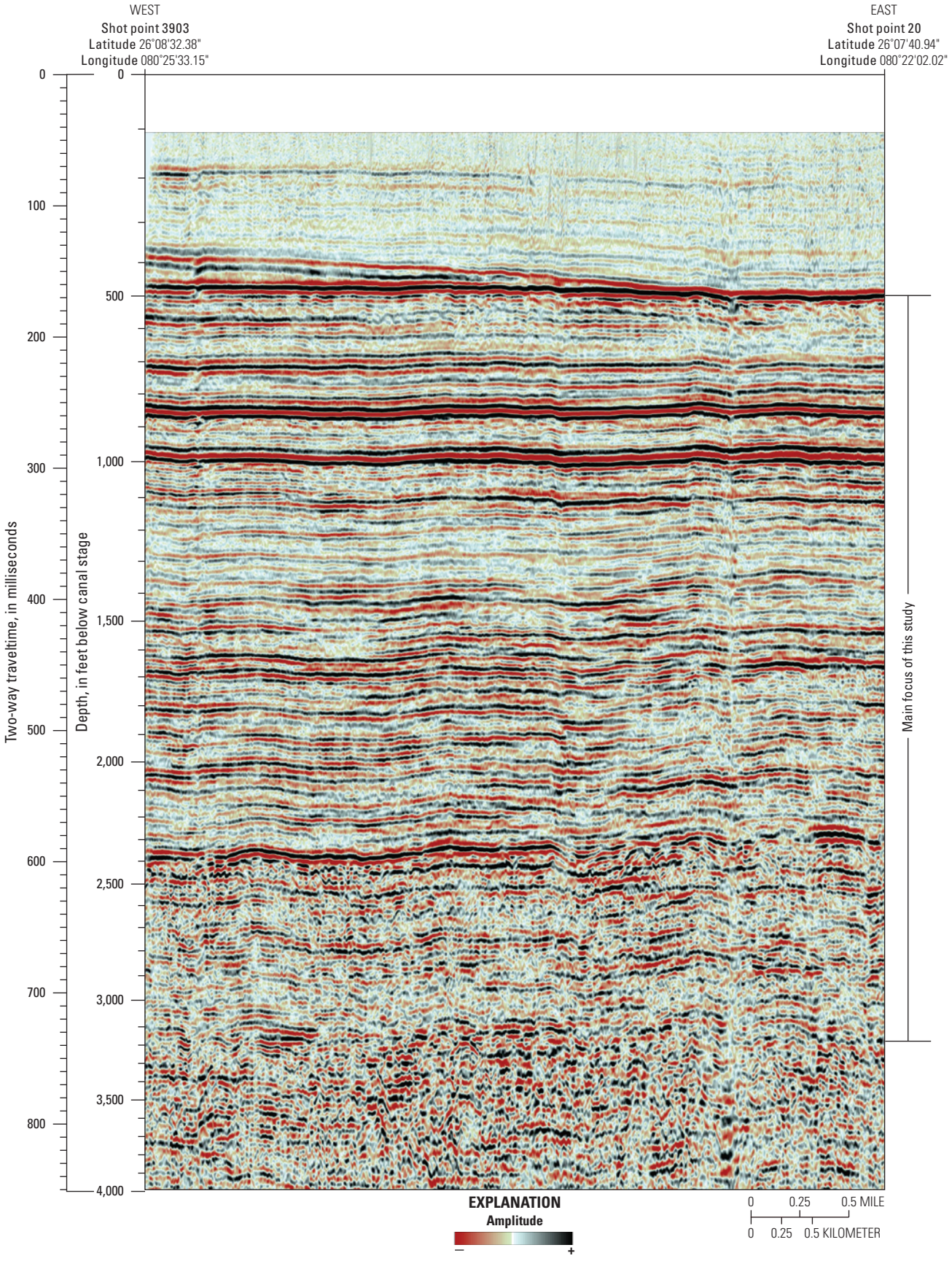

Figure 20. Uninterpreted seismic-reflection profile S7 (fig. 1, table 1).

The following sections describe and interpret the seismic and geologic character of the seven seismic sequences (O3, AP1, AP2, AP3, Ar5, Ar6, and Ar7) and one composite seismic sequence (Ar1) that are the focus of this study (fig. 3 and 4). The upper boundaries of all seismic sequences correspond to unconformities identified in seismic-reflection profiles and in well data such as whole cores, borehole image data, or both (figs. 7 and 13).

Seismic Sequence O3

Seismic sequence O3 is bounded by unconformities at its bottom and top (figs. 22 and 23). Two-way traveltime through seismic sequence O3 ranges from about 100 to approximately 190 milliseconds and its thickness ranges from about 600 to 1,100 ft. The lower boundary of seismic sequence O3 is underlain by seismic sequence O1 and the upper boundary is overlain by seismic sequence AP1. The attribute average energy is very useful in mapping the top of the seismic sequences O1 and O3, because it typically forms a traceable, continuous high-energy event (black end of high-energy attribute color range) where highly reflective, dense dolomite is present at the uppermost surfaces of seismic sequences O1 and O3. The upper surface of seismic sequence O3 generally dips gently toward the west (pls. 6–19). The lower bounding surface of seismic sequence O3 is discernable by a shift from relatively higher amplitudes and average energies for the upper part of the underlying seismic sequence O1 to lower amplitudes and average energies characterizing seismic reflections within the overlying lower part of seismic sequence O3 (figs. 22–24). Below the lower boundary of seismic sequence O3, some of the uppermost seismic-reflections of seismic sequence O1 terminate against faults (figs. 25 and 26). An irregular and hummocky seismic-reflection geometry is common for the upper bounding surface of seismic sequence O1, as well as semicontinuous seismic reflections (figs. 20–23, 25, and 26; pls. 8–19). Seismic reflections at the base of seismic sequence AP1, in some cases, exhibit onlap onto upper bounding seismic reflections of seismic sequence O3 (figs. 27 and 28)—a reflection termination relationship also noted by Cunningham (2015, fig. 8) in the offshore area of Miami-Dade County Biscayne Bay offshore area. Cunningham (2015, fig. 8) observed onlapping reflections within the base of seismic sequence AP1 that were local and infilling a structural depression about 4,000 ft wide. He concluded the structural depression represented collapse of ancient epigenic karst within the upper part of seismic sequence O3.

The upper boundary of seismic sequence O3 is marked by a shift from relatively low seismic-reflection amplitudes and low average energies within the lower part of seismic sequence AP1 to higher seismic-reflection amplitudes and average energies within the uppermost part of seismic sequence O3 (figs. 22–24). An irregular, hummocky, and locally faulted seismic-reflection geometry is common for the upper bounding surface of seismic sequence O3 (figs. 22, 23, 27, and 28; pls. 6–19). Locally, seismic reflections display erosional truncation along the top of seismic sequence O3 (figs. 27 and 28).

Seismic reflections in the upper part of seismic sequence O3 are semicontinuous on some profiles with abundant diffraction hyperbolas (figs. 22, 23, 27, and 28). In some cases, diffraction hyperbolas also occur within the middle part of seismic sequence O3 (figs. 22 and 23). In other cases, diffraction hyperbolas are associated with the uppermost part of seismic sequence O1 (figs. 25 and 26). Seismic-facies parameters (reflection terminations, reflection configurations, diffraction hyperbolas, amplitudes, average energies) similar to those just described are commonly found on seismic-reflection profiles that image other ancient karsted carbonate platform tops (for example, Janson and others, 2011; Zeng and others, 2011a, b; Decker and others, 2015). The semicontinuous seismic-reflections, for example, are very likely associated with discontinuities in the strata because of karst features that include collapsed strata. On some seismic-reflection profiles, reflection configurations that compose areas within the upper part of seismic sequence O3 are chaotic (figs. 27 and 28), plausibly indicating megabreccia fill of collapsed paleocave systems (Loucks, 1999; Zeng and others, 2011a, b).

The seismic-reflection character of seismic sequence O3 is mostly fair to good and composed mainly of continuous, parallel-even, wavy or contorted reflection configurations (pls. 6–19); however, the continuity of seismic-reflections within seismic sequence O3 generally decreases as the hummocky and chaotic reflection configuration patterns increase downward (figs. 22 and 23, pls. 6–19). Relatively high amplitudes are generally present in the uppermost part of seismic sequence O3, compared to somewhat lower amplitudes in the lower part (figs. 22 and 23, pls. 6–19).

Diffraction hyperbolas on seismic-reflection profiles can be useful indicators of vertical or high-angle fractures, karst dissolution features, or both (Bansal and others, 2002; Grasmueck and others, 2013; Bashir and others, 2015; Decker and others, 2015). Faulted seismic reflections are related to karst collapse (compare to Janson and others, 2011; Zeng and others, 2011a, b). The presence of faults and fractures within the rocks that compose seismic sequence O3 is further supported by artificial-neural-network-based meta-attribute calculations of seismic-reflection profile S7 (figs. 29 and 30). These neural network attributes help substantiate the stratigraphic interpretation and show that the probability of faults and fractures decreases upward in an abrupt, stepwise manner across the upper O3 seismic sequence boundary (figs. 29 and 30). This pattern is also observed at the boundary between seismic sequences O1 and O3 (figs. 29 and 30). Abrupt shifts in mechanical properties of the rocks composing the upper parts of seismic sequences O1 and O3 likely exist, with stratiform, brittle dolomite mainly composing the upper part of seismic sequences O1 and O3, and relatively less brittle limestone composing the lower part of seismic sequences O3 and AP1. Rock core and

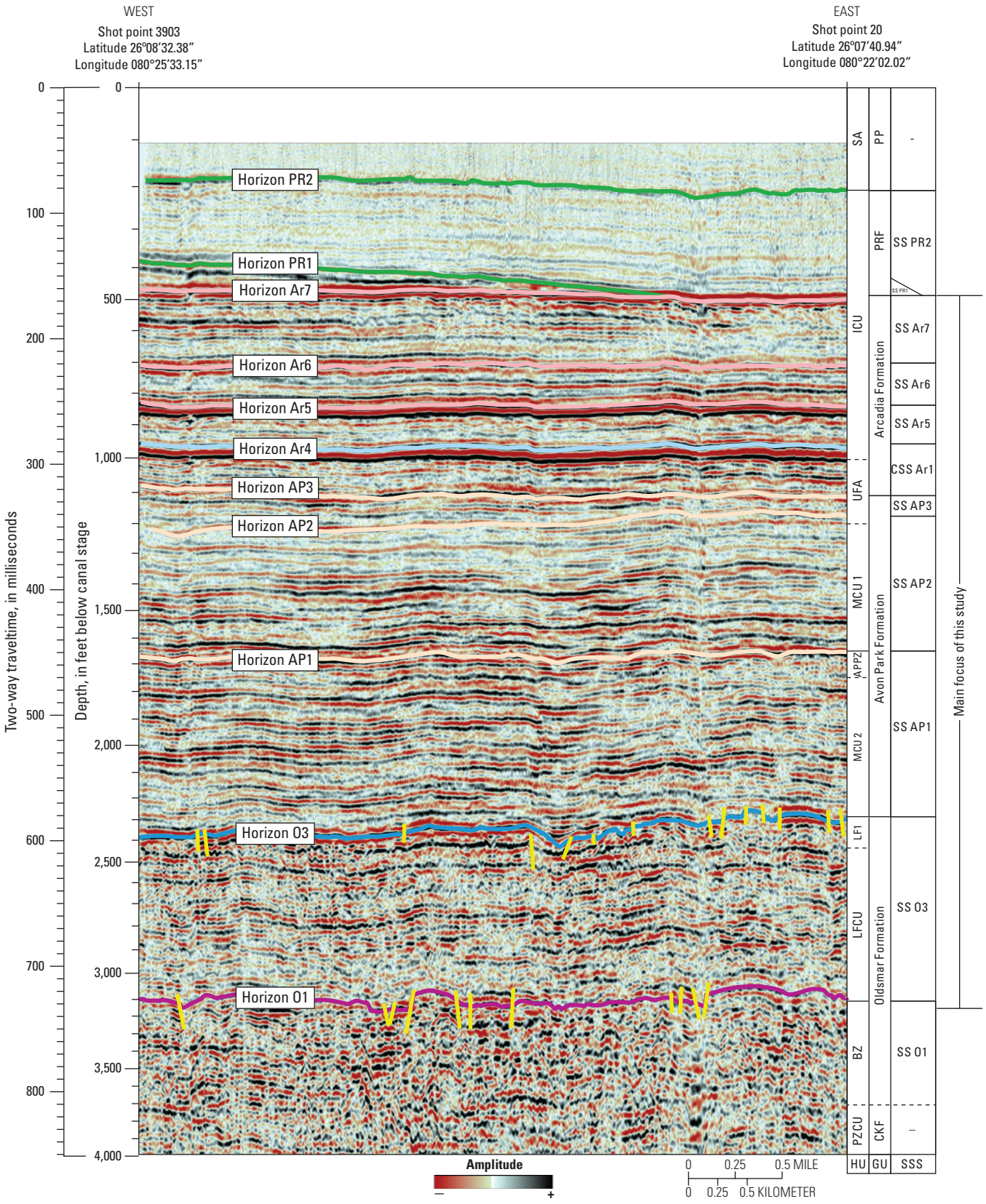

Figure 21. Interpreted seismic-reflection profile S7 (fig. 1, table 1) showing the seismic sequence stratigraphy that is the major focus of this study.

borehole-wall video images from the G–2991 City of Davie IW–1 well display fractures in dolomite from near the top of depositional sequence O3 (figs. 8 and 9), which provides physical corroborating evidence for the presence of fractures near the top of seismic sequence O3. The presence of faults, fractures, and karst within the dolomite in the upper part of the Oldsmar Formation and within the dolomite of the Boulder Zone indicate enhanced permeability in these two dolomite units.

Seismic Sequence AP1

Seismic sequence AP1 is superjacent to seismic sequence O3 and subjacent to seismic sequence AP2 (fig. 3, pls. 6–19). Typically, the uppermost seismic reflections of seismic sequence AP1 are comparatively distinct from seismic reflections above and below in that they have a noticeably higher amplitude (pls. 6–19) and average energy. In general, the good continuity of the two seismic-reflection attributes, amplitude and average energy, simplifies the mapping of the upper bounding surface of seismic sequence AP1. The uppermost seismic reflections of seismic sequence AP1 most commonly form an even to slightly wavy surface. Cunningham (2015) reported local cases where (1) erosional truncation of seismic reflections was observed below the upper bounding surface of seismic sequence AP1 and (2) seismic reflections of seismic sequence AP2 lapped onto the upper surface of seismic surface AP1, which provides evidence that the boundary is a seismic sequence boundary (Mitchum and others, 1977).

Seismic sequence AP1 is a sheet **seismic facies unit** (Mitchum and others, 1977, fig. 12) that is present throughout the study area (pls. 6–19). Sheets are one of the most common of shelf seismic facies units, and parallel patterns are the most common internal reflection configuration within these units in the study area. Two-way traveltime through seismic sequence AP1 ranges from about 80 to approximately 150 milliseconds and its thickness ranges from about 400 to 800 ft (pls. 6–19). The seismic-reflections assigned to seismic sequence AP1 generally have even, parallel to slightly wavy, parallel or subparallel reflection configuration patterns that, in some cases, grade into slightly hummocky to chaotic seismic-reflection patterns (figs. 20 and 21, pls. 6–19). The continuity of seismic-reflection patterns in seismic sequence AP1 is greater than that for underlying seismic sequence O3 and displays much less evidence for faulting and fracturing (figs. 22, 23, 27, and 30). Where seismic reflections are of very good quality and have very good continuity throughout the entire thickness of seismic sequence AP1, it is apparent that the seismic sequence is composed of multiple stacked reflections, that is cycle sets, wherein each set displays an upward increase in amplitude and average energy at the top of the seismic sequence (pls. 6–19), as described on seismic-reflection profiles in Miami-Dade County by Cunningham (2015, fig. 6*C–D*). The presence of a highly reflective average energy at the top of seismic sequence AP1 contributes to more accurate mapping as compared to only using reflection amplitude of the upper boundary of seismic sequence AP1. The stacked cyclicity of upward increasing reflection amplitudes, moderate to very good reflection continuity, and parallel reflection configurations are consistent with the seismic-reflection expression of vertical stacking of shallow-marine platform carbonates (Macurda, 1997).

Seismic Sequence AP2

Seismic sequence AP2 is superjacent to seismic sequence AP1 and subjacent to seismic sequence AP3 (fig. 3, pls. 6–19). Seismic sequence AP2 is a sheet seismic facies unit that is present throughout the study area. Two-way traveltime through seismic sequence AP2 ranges from about 80 to approximately 120 milliseconds, and its thickness ranges from about 350 to 550 ft. The reflection configurations of seismic sequence AP2 normally have horizontal, parallel seismic-reflection geometries with moderate to very good reflection continuity (figs. 20 and 21, pls. 6–19). Where seismic reflections are of good quality and have good continuity throughout the entire thickness of seismic sequence AP2 (pls. 6–19), it is apparent that the seismic sequence consists of multiple cycle sets of stacked seismic

EXPLANATION

- Fault
- Seismic horizon PR1 or PR2
- Seismic horizon Ar5, Ar6, or Ar7
- Composite seismic horizon Ar4
- Seismic horizon AP1, AP2, or AP3
- Seismic horizon O3
- Seismic horizon O1
- Uncertain boundary between hydrogeologic units, geologic units, and seismic sequence stratigraphic units

SA	Surficial aquifer
ICU	Intermediate confining unit
UFA	Upper Floridan aquifer
MCU 1	Middle semiconfining unit 1
APPZ	Avon Park permeable zone
MCU2	Middle semiconfining unit 2
LF1	Uppermost major permeable zone of the Lower Floridan aquifer
LFCU	Lower Floridan semiconfining unit
BZ	Boulder Zone
PZCU	Permeable zones and confining units of the Lower Floridan aquifer

PP	Pliocene and Pleistocene Formations
PRF	Peace River Formation
CKF	Cedar Keys Formation
SS PR2	Seismic sequence PR2
SS PR1	Seismic sequence PR1
SS Ar7	Seismic sequence Ar7
SS Ar6	Seismic sequence Ar6
SS Ar5	Seismic sequence Ar5
CSS Ar1	Composite seismic sequence Ar1

SS AP3	Seismic sequence AP3
SS AP2	Seismic sequence AP2
SS AP1	Seismic sequence AP1
SS O3	Seismic sequence O3
SS O1	Seismic sequence O1
HU	Hydrogeologic unit
GU	Geologic unit
SSS	Seismic sequence stratigraphy
–	Not defined

Figure 21. Interpreted seismic-reflection profile S7 (fig. 1, table 1) showing the seismic sequence stratigraphy that is the major focus of this study.—Continued

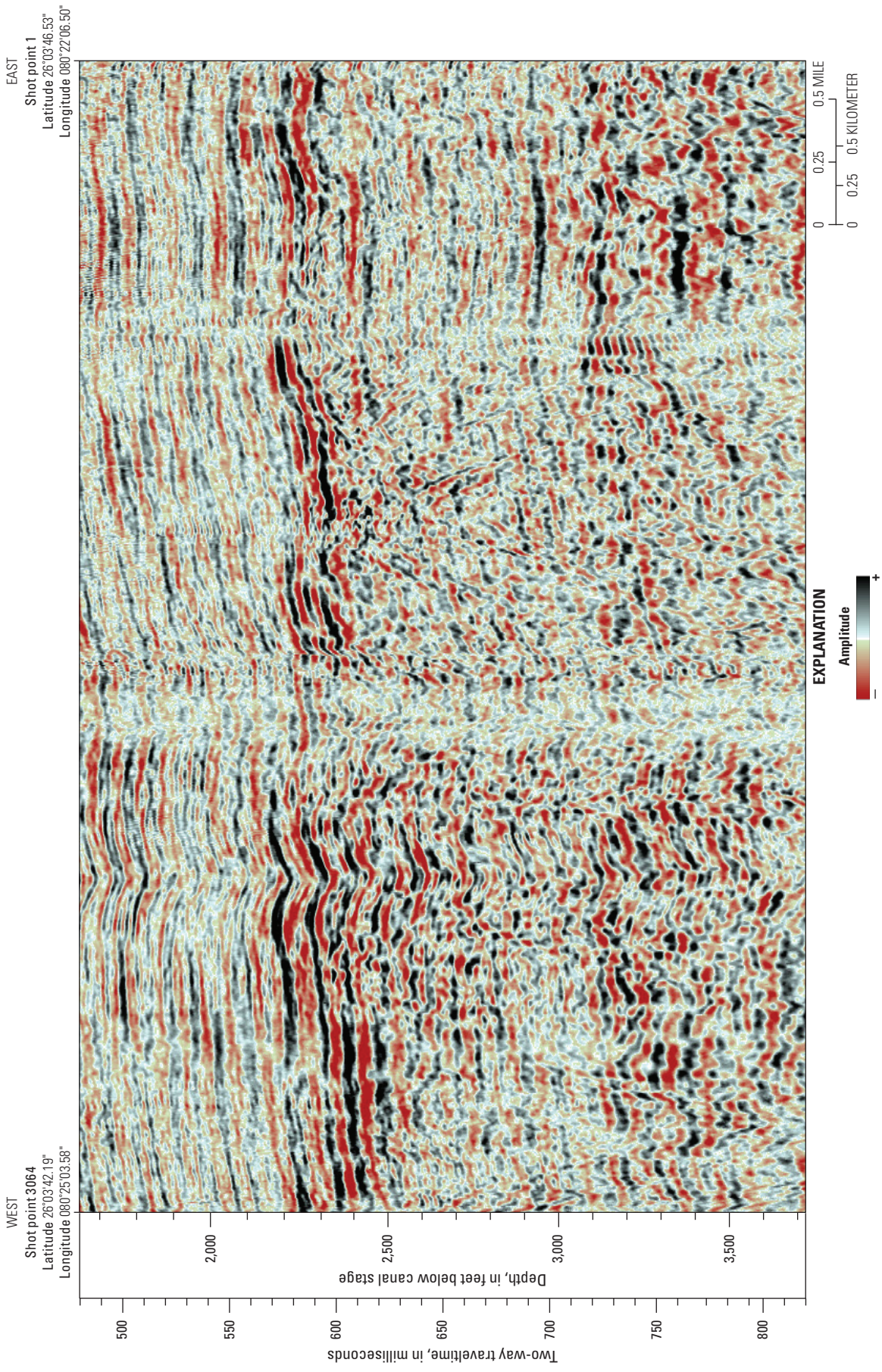

Figure 22. Uninterpreted part of seismic-reflection profile S18 (fig. 1, table 1) shown in figures 23 and 24.

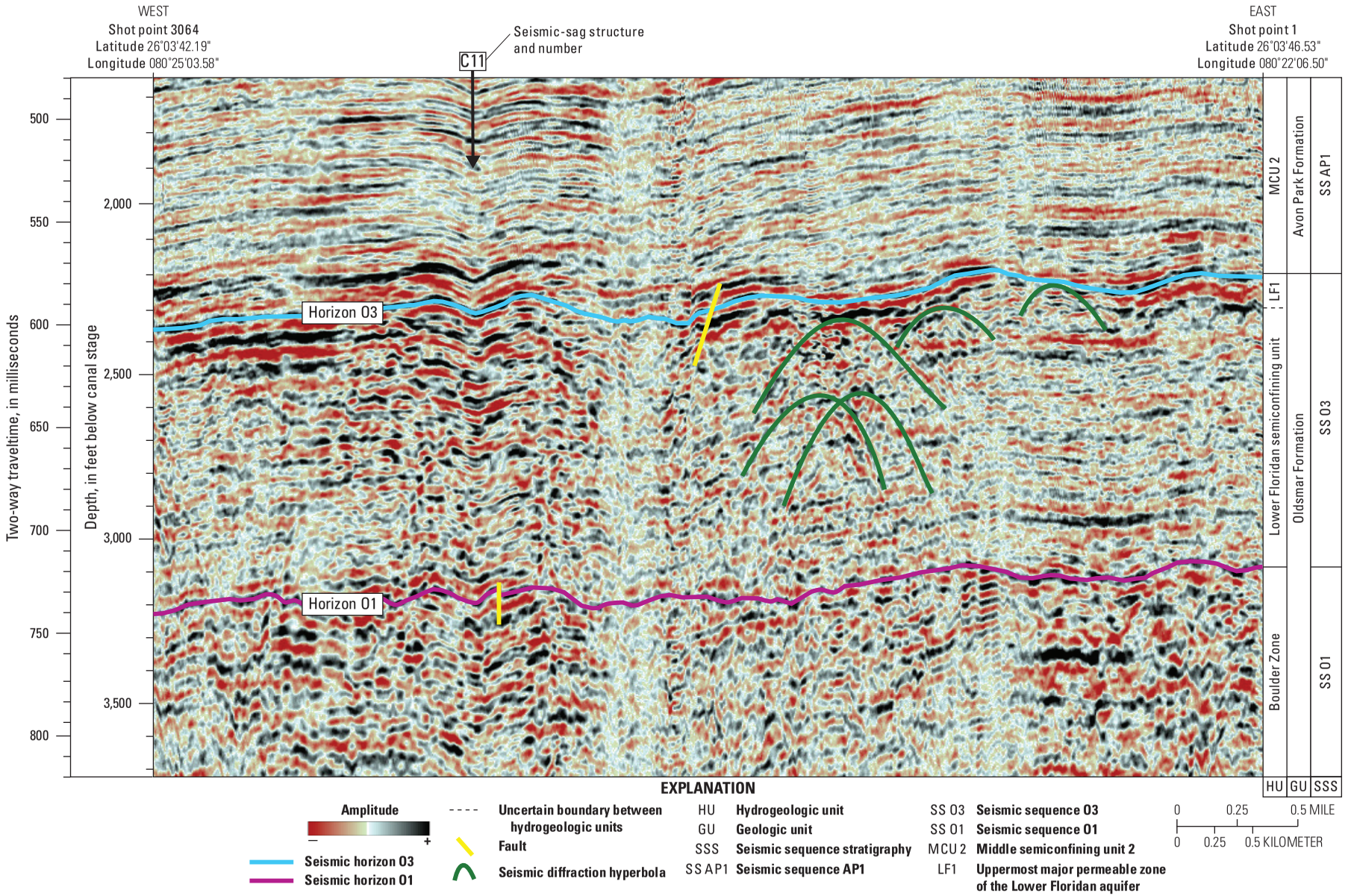

Figure 23. Interpreted part of seismic-reflection profile S18 (fig. 1, table 1) shown in figure 22. The profile shows that the upper bounding surface of seismic sequences O1 and O3 are irregular surfaces with local relief of about 12 milliseconds or 90 feet. The hummocky surfaces are related to regional karstification at the tops of depositional sequences O1 and O3 (fig. 2). Seismic sequence O1 is equivalent to the highly permeable Boulder Zone and the upper part of the seismic sequence O3 is equivalent to the top of the uppermost major permeable zone of the Lower Floridan aquifer (fig. 3). Diffraction hyperbolas probably indicate point-source reflections from steep fractures, karstic dissolution cavities, or both.

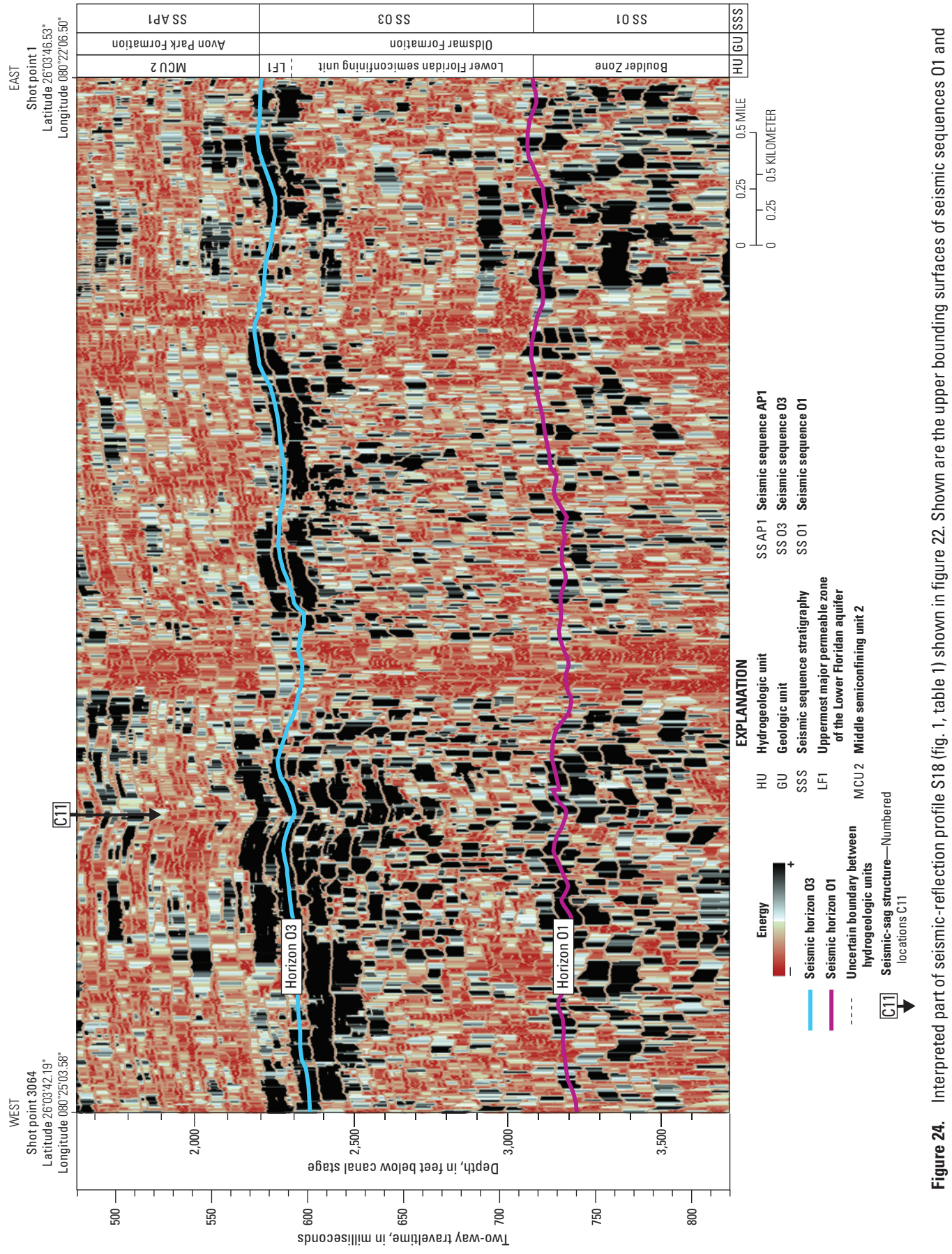

Figure 24. Interpreted part of seismic-reflection profile S18 (fig. 1, table 1) shown in figure 22. Shown are the upper bounding surfaces of seismic sequences O1 and O3. The seismic-reflection attribute shown here is average energy.

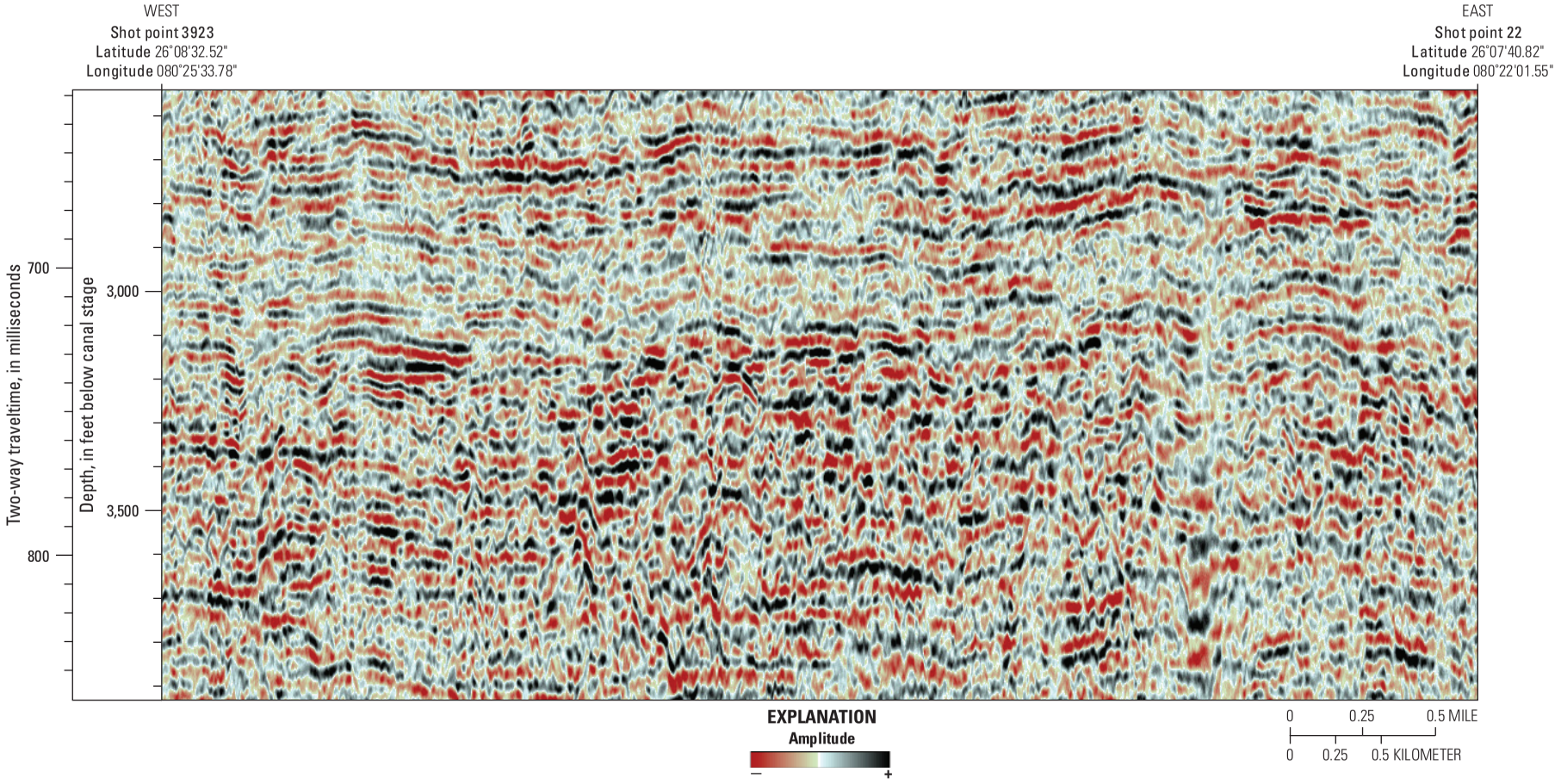

Figure 25. Uninterpreted part of seismic-reflection profile S7 (fig. 1, table 1) shown in figure 26.

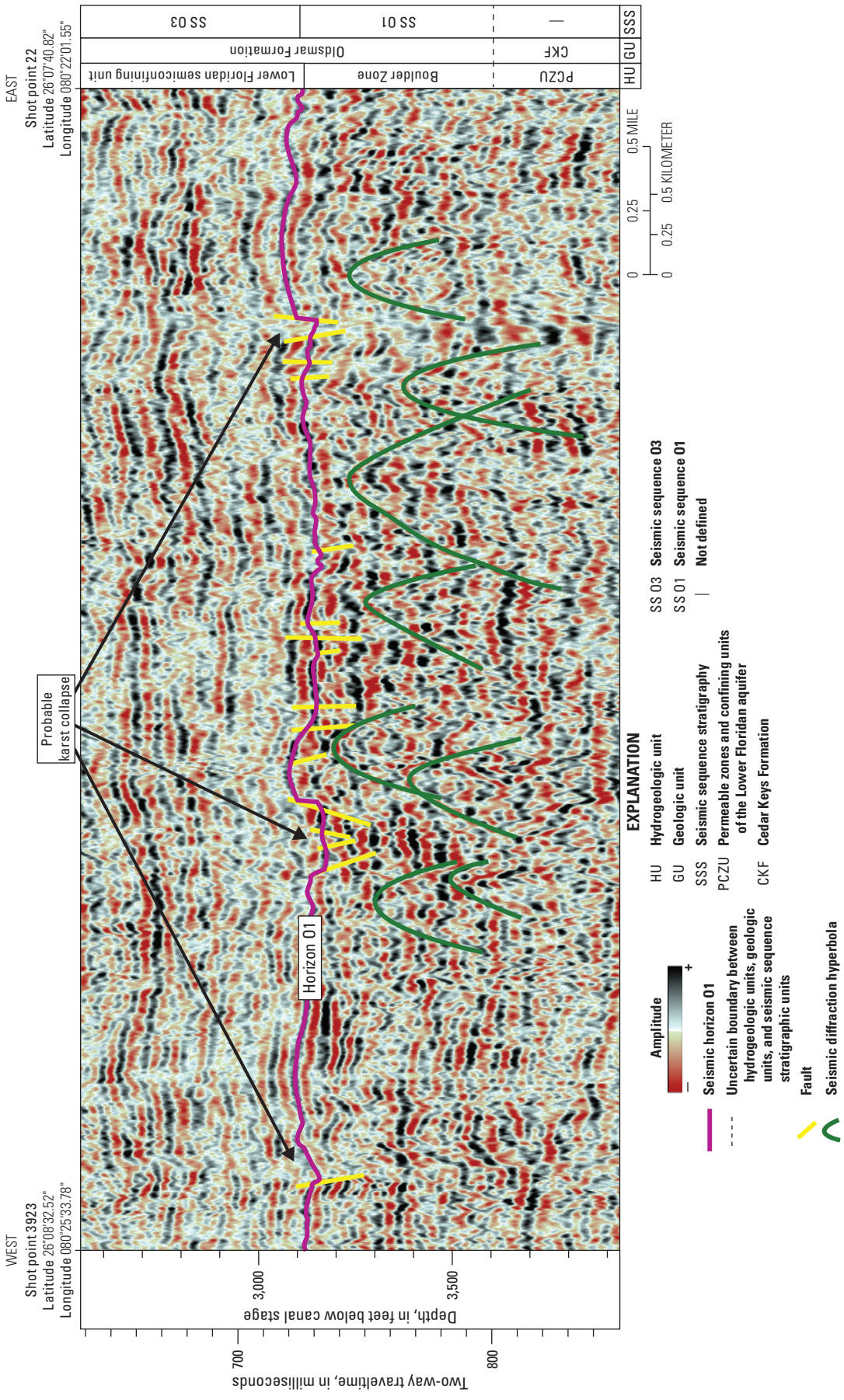

Figure 26. Interpreted part of seismic-reflection profile S7 (fig. 1, table 1) shown in figure 25. The profile shows that the upper bounding surface of seismic sequence O1 is an irregular surface having a local relief of about 10 milliseconds or 70 feet, which is related to regional karstification of depositional sequence O1. Seismic sequence O1 corresponds to the very permeable Boulder Zone of the Lower Floridan aquifer (fig. 3). Diffraction hyperbolas probably indicate steep fractures, karstic dissolution cavities, or both.

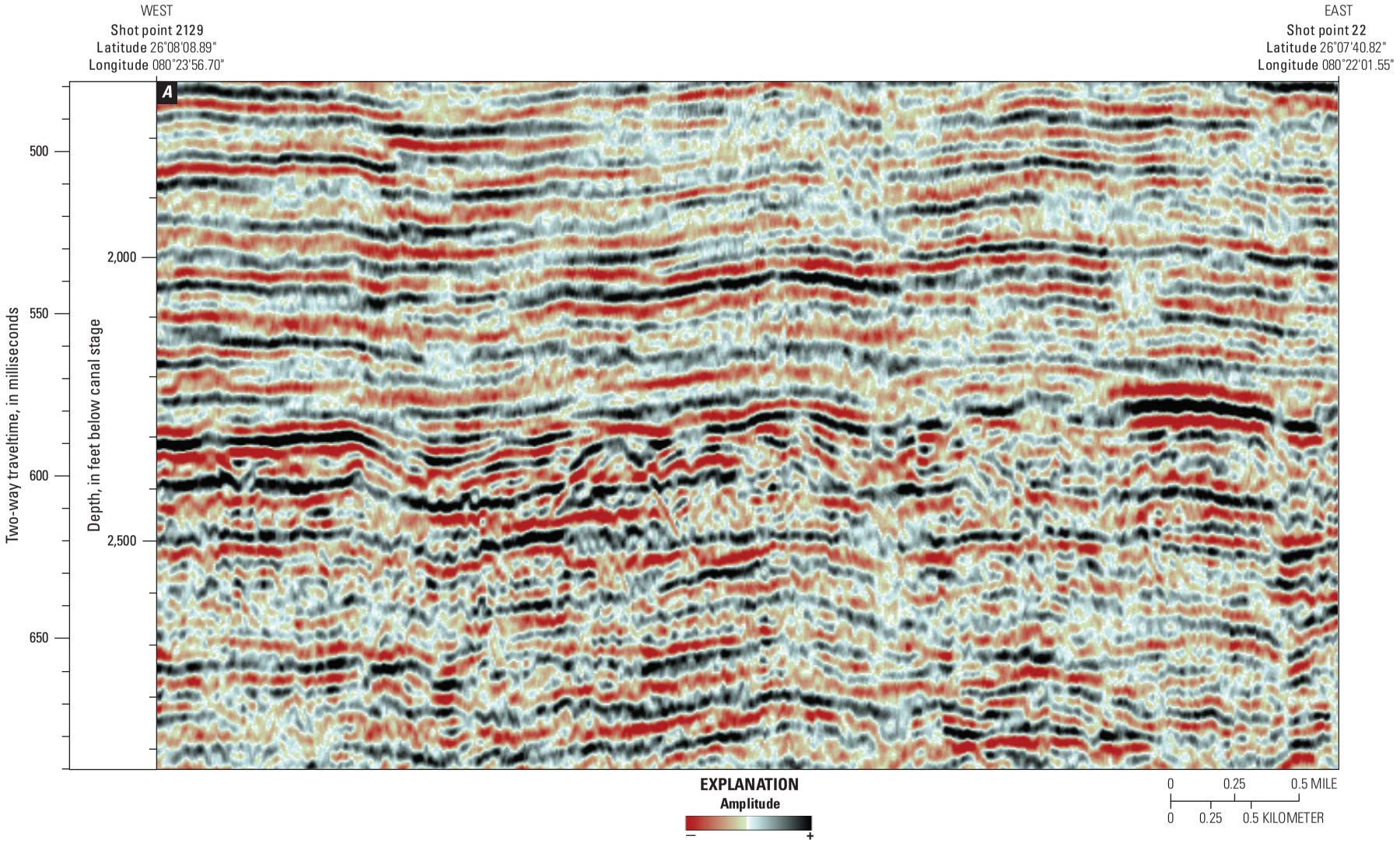

Figure 27. Uninterpreted part of seismic-reflection profile S7 (fig. 1, table 1) shown in figure 28

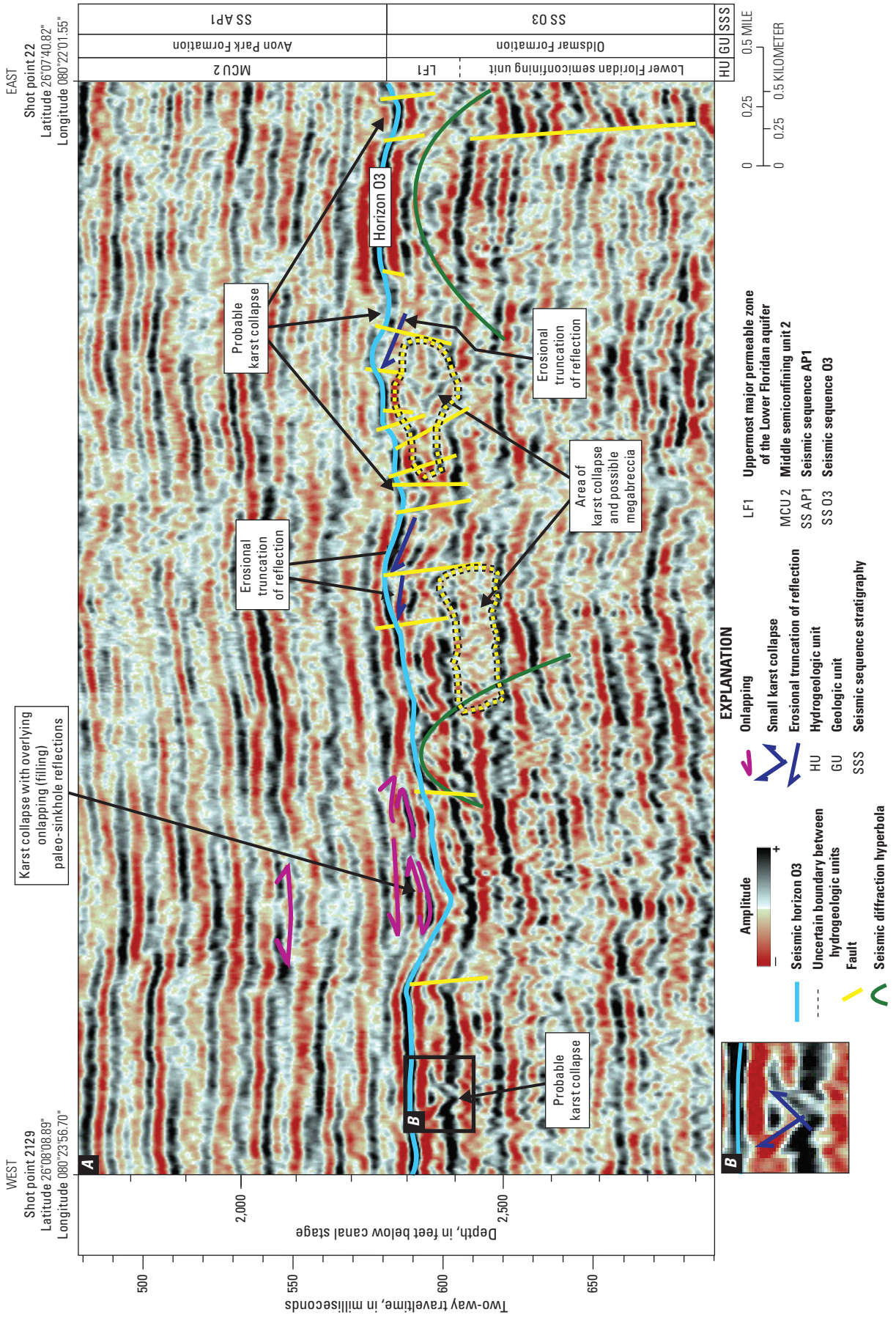

Figure 28. Interpreted part of seismic-reflection profile S7 (fig. 1, table 1) shown in figure 27. *A*, Profile showing upper bounding surface of the seismic sequences O3, characterized by an irregular, hummocky surface relief of about 12 milliseconds or 90 feet related to a regional karst unconformity. Faulting is commonly associated with the karst unconformity. The upper part of seismic sequence O3 represents the uppermost permeable major zone of the Lower Floridan aquifer that caps the Oldsmar Formation. Diffraction hyperbolas probably indicate steep fractures or karstic dissolution cavities or both. *B*, Inset showing small karst collapse (v-shaped seismic reflections) associated with the regional karst unconformity at the upper surface of seismic sequence O3.

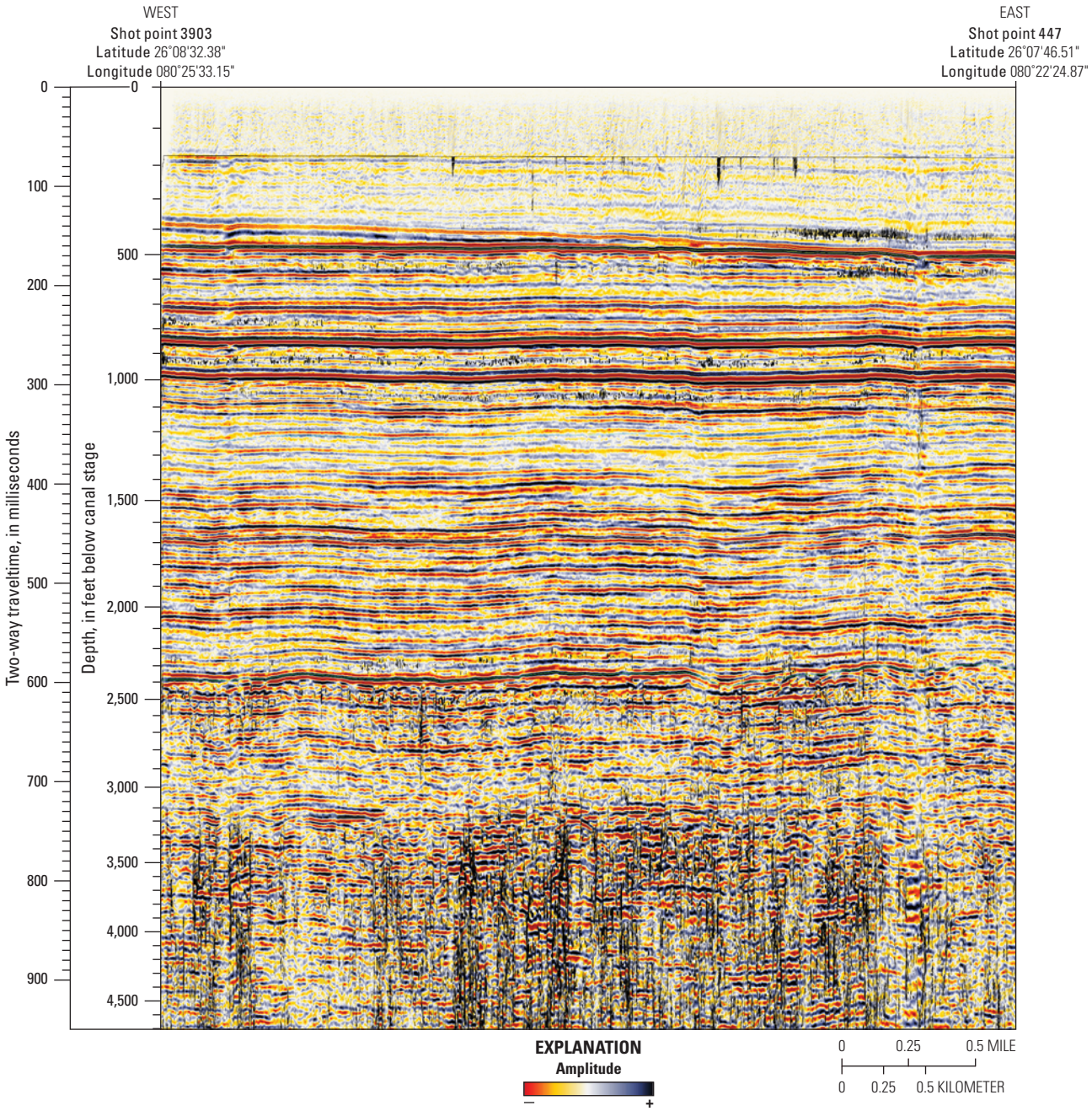

Figure 29. Uninterpreted seismic-reflection profile S7 (fig. 1, table 1) shown in figure 30.

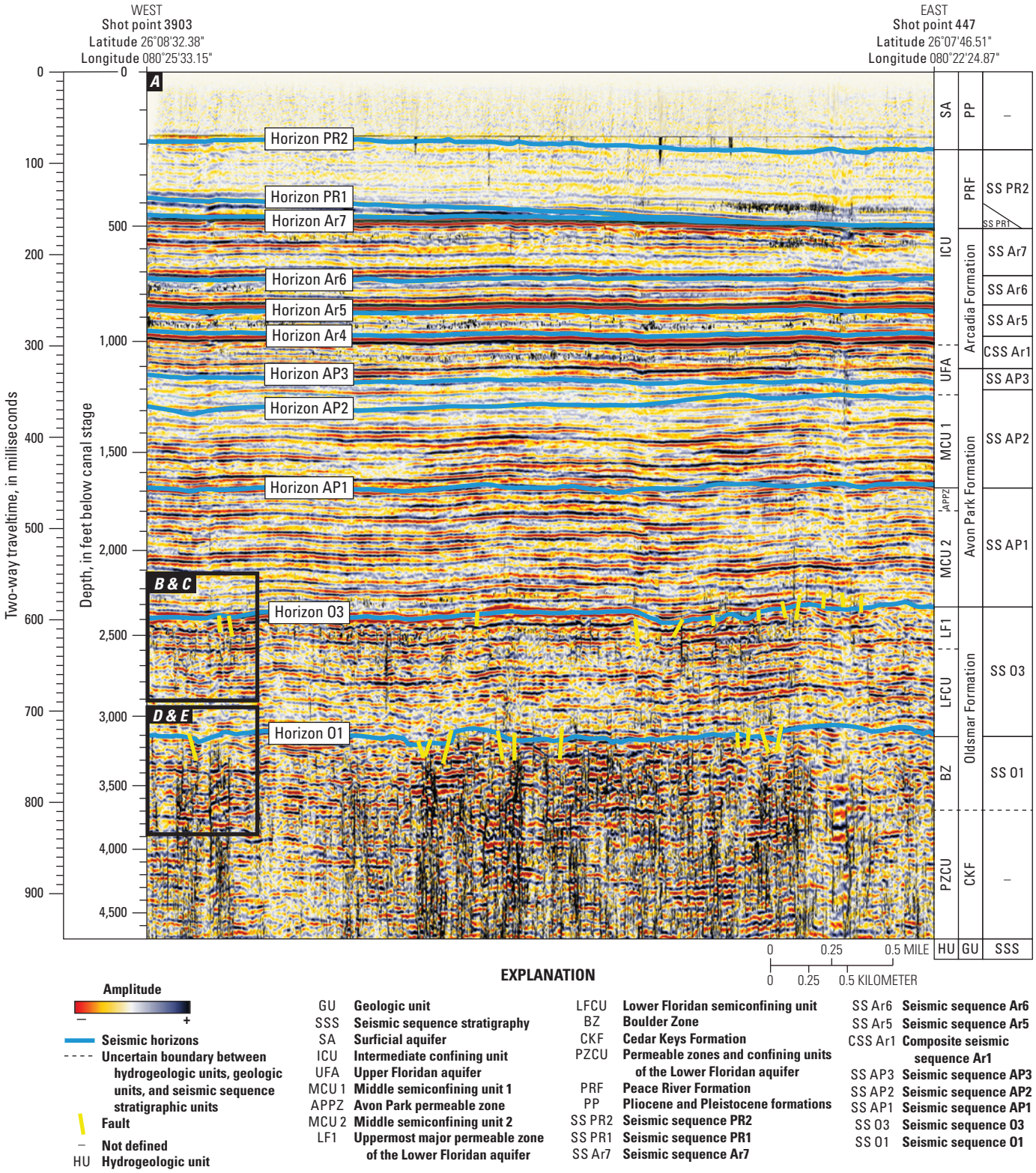

Figure 30. Interpreted seismic-reflection profile S7 (fig. 1, table 1) shown in figure 29. *A*, Profile showing artificial-neural-network-based meta-attribute calculations applied. *B-C*, Uninterpreted and interpreted inset of thin semivertical zones having a high-probability of faulting and fracturing, indicating the high-probability of influence of both of these structural features on enhanced permeability of the uppermost major permeable zone of the Lower Floridan aquifer. The density of these features in the overlying middle semiconfining unit 2 is low. *C-D*, Uninterpreted and interpreted inset of thin semivertical zones having a high-probability of faulting and fracturing, indicating the high-probability of influence of both of these structural features on enhanced permeability of the Boulder Zone. The density of these features in the overlying Lower Floridan confining unit is low.

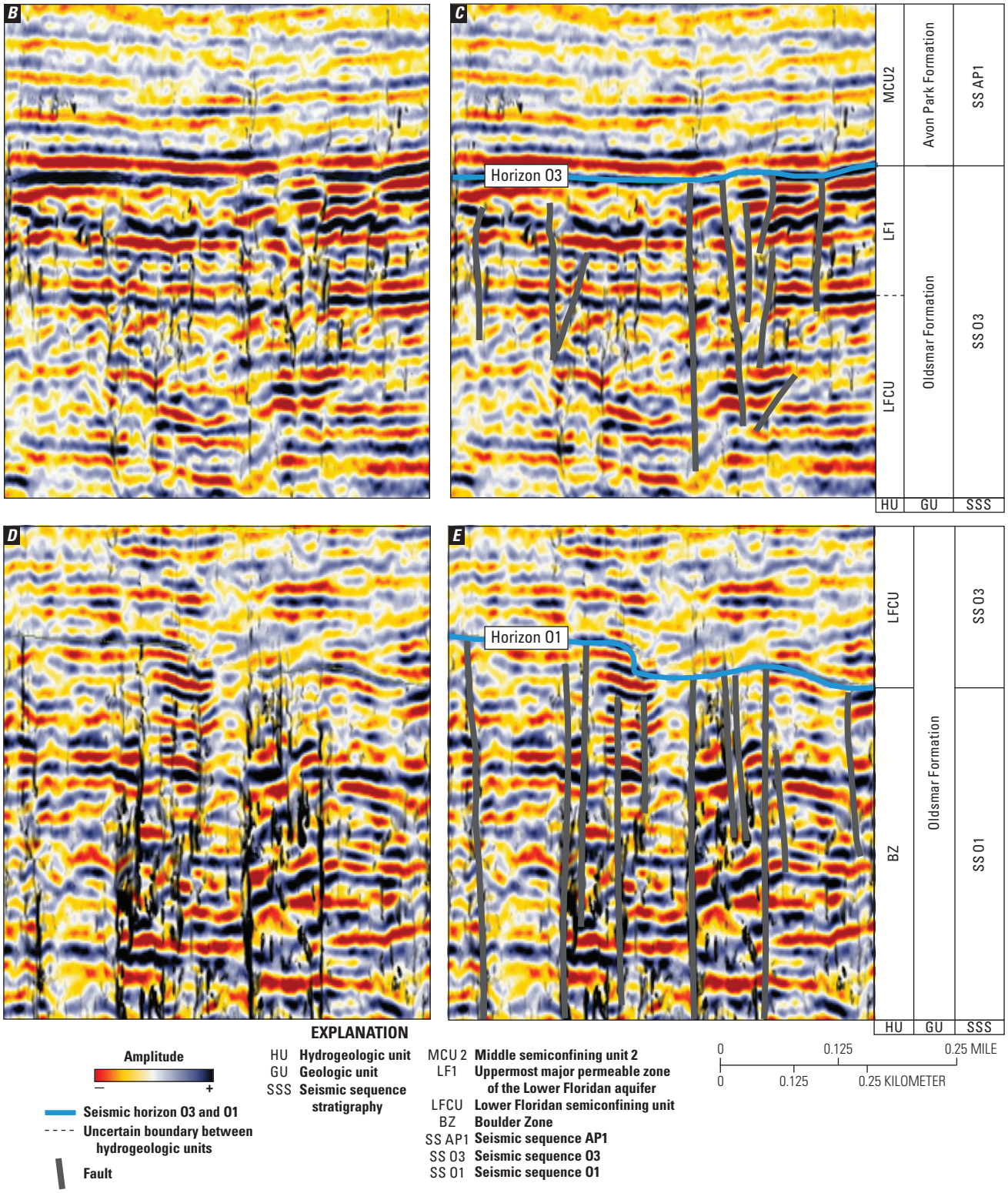

Figure 30. Interpreted seismic-reflection profile S7 (fig. 1, table 1) shown in figure 29. *A*, Profile showing artificial-neural-network-based meta-attribute calculations applied. *B-C*, Uninterpreted and interpreted inset of thin semivertical zones having a high-probability of faulting and fracturing, indicating the high-probability of influence of both of these structural features on enhanced permeability of the uppermost major permeable zone of the Lower Floridan aquifer. The density of these features in the overlying middle semiconfining unit 2 is low. *C-D*, Uninterpreted and interpreted inset of thin semivertical zones having a high-probability of faulting and fracturing, indicating the high-probability of influence of both of these structural features on enhanced permeability of the Boulder Zone. The density of these features in the overlying Lower Floridan confining unit is low.—Continued

reflections, wherein each set displays an upward increase in amplitude, as described on seismic-reflection profiles in Miami-Dade County by Cunningham (2015, fig. 6*A, B*). There is much less evidence for faulting and fracturing within seismic sequences AP1 and AP2 compared to the deeper seismic sequence O3 (figs. 29 and 30). Stacked, cyclical, upward-increasing reflection amplitudes, moderate to very good reflection continuity, and parallel reflection configurations are consistent with the seismic-reflection expression of vertical stacking of shallow-marine platform carbonates (Macurda, 1997).

Seismic Sequence AP3

Seismic sequence AP3 is superjacent to seismic sequence AP2 and subjacent to composite seismic sequence Ar1 (figs. 3 and 4, pls. 6–19). Seismic sequence AP3 is a sheet seismic facies unit that is present throughout the study area (pls. 6–19). Two-way traveltime through seismic sequence AP3 ranges from about 10 to approximately 40 milliseconds and its thickness ranges from about 35 to 140 ft (pls. 6–19). The reflection configurations of seismic sequence AP3 generally have horizontal, parallel seismic-reflection geometries with moderate to very good reflection continuity (figs. 31 and 32, pls. 6–19). Seismic sequence AP3 was not delineated in Miami-Dade County by Cunningham (2015); however, it was first identified by correlation of depositional sequence AP3 in test corehole G–2984 onto seismic-reflection profile S1 (Reese and Cunningham, 2014). In most instances, the seismic reflections above and below the lower boundary of seismic sequence AP3 have a parallel reflection configuration. The boundary can be challenging to delineate on seismic-reflection profiles (pls. 6–19). In general, the seismic reflections below and above the AP2-AP3 seismic sequence boundary have parallel seismic reflections (pls. 6–19). In some cases, however, the upper boundary of seismic sequence AP2 is overlain by seismic reflection terminations at the base of seismic sequence AP3 that display onlap onto the boundary (figs. 31 and 32) providing evidence for a seismic sequence boundary. Locally, seismic-reflections at the top of seismic sequence AP3 can display erosional truncation of seismic-reflections (for example figs. 31 and 32), thereby providing evidence for a seismic sequence boundary. Seismic synthetics (pls. 1 and 2) and optical borehole-wall images of the depositional sequence boundaries at five wells (G–2916, G–2984, G–2996, G–2997, and G–4002) (fig. 1, table 2) were used to help delineate the lower and upper seismic sequence boundaries on selected seismic-reflection profiles.

Composite Seismic Sequence Ar1

Composite seismic sequence Ar1 is superjacent to seismic sequence AP3 and subjacent to composite seismic sequence Ar5 (fig. 4, pls. 6–19). Composite seismic sequence Ar1 is composed of four tentatively defined seismic sequences, Ar1, Ar2, Ar3, and Ar4 (upper seismic sequence boundaries of Ar1, Ar2, and A3 are uncertain), which are correlated to four depositional sequences in the lower part of the Arcadia Formation (fig. 4, Reese and Cunningham, 2014; Cunningham, 2015; Cunningham and Robinson, 2017). Composite seismic sequence Ar1 is a sheet seismic facies unit (Mitchum and others, 1977) composed of mainly high- to moderate-amplitude, continuous, parallel reflection configurations where seismic-reflection data are good to excellent, and continuous-to-discontinuous hummocky reflection configurations where seismic-reflection data are fair (figs. 20, 21, 31, and 32; pls. 6–19). Sheet seismic facies are one of the most common of the shelf seismic facies units (Mitchum and others, 1977), and parallel patterns are the most common internal reflection configuration within these units in the study area. Some seismic-reflection profiles exhibit very minor local onlap or downlap of composite seismic sequence Ar1 reflections, terminating onto the upper bounding surface of seismic sequence AP3. In general, however, the basal Ar1 seismic reflections of composite seismic sequence Ar1 are parallel to its lower boundary. The uppermost seismic reflection of composite seismic sequence Ar1 is continuous where the seismic-reflection data are fair to excellent, except in a few local areas where the upper seismic reflections are terminations indicative of erosional truncation. Two-way traveltime through composite seismic sequence Ar1 ranges from about 10 to approximately 50 milliseconds, and its thickness ranges from about 40 to 200 ft (pls. 6–19).

Seismic Sequence Ar5

Seismic sequence Ar5 is superjacent to composite seismic sequence Ar1 and subjacent to composite seismic sequence Ar6 (fig. 4, pls. 6–19). Seismic sequence Ar5 is a bank seismic facies unit (Mitchum and others, 1977; Alley, 1987), where the eastern paleo-seaward termination of the bank seismic facies unit trends approximately north-south in eastern Broward County and northeastern Miami-Dade County (pls. 6, 7, 18, and 19). Banks are one of the most common of shelf seismic facies units (Mitchum and others, 1977), and parallel and prograding patterns are the most typical internal reflection configurations within these units in the study area. Seismic sequence Ar5 is composed mainly of high-amplitude, continuous, parallel reflections exhibiting high amplitudes where seismic-reflection data are good to excellent, and continuous-to-discontinuous hummocky reflection configurations where seismic-reflection data are fair (pls. 6–19). In the western part of the study area, reflection configurations are parallel to the boundary between seismic sequence Ar5 and composite seismic sequence Ar1 (pls. 6–17). In the eastern part of the study area, seismic reflections of seismic sequence Ar5 display downlap onto composite seismic sequence Ar1 (pls. 6, 7, 14, 15, 18, and 19). The

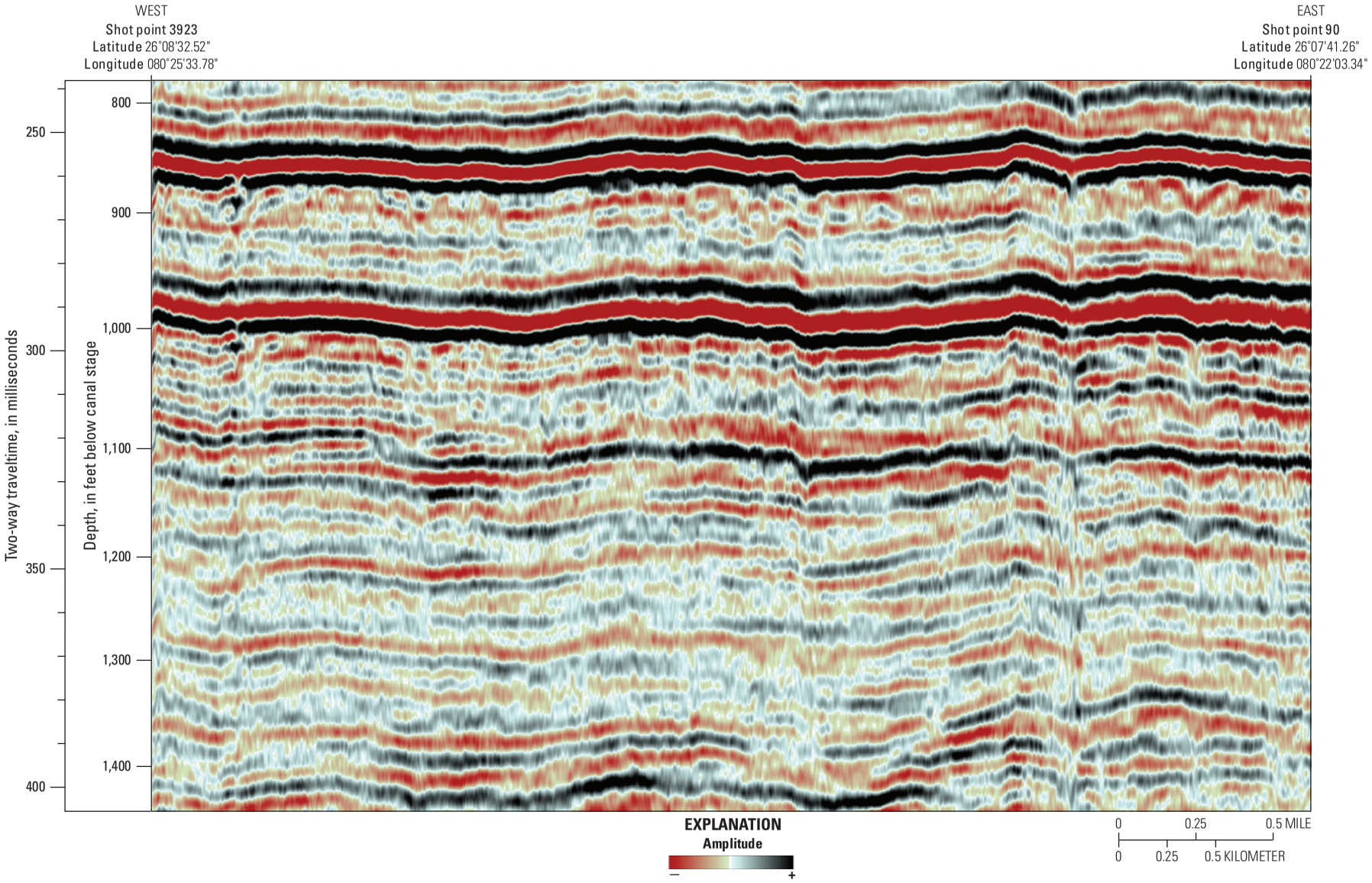

Figure 31. Uninterpreted part of seismic-reflection profile S7 (fig. 1, table 1) shown in figure 21.

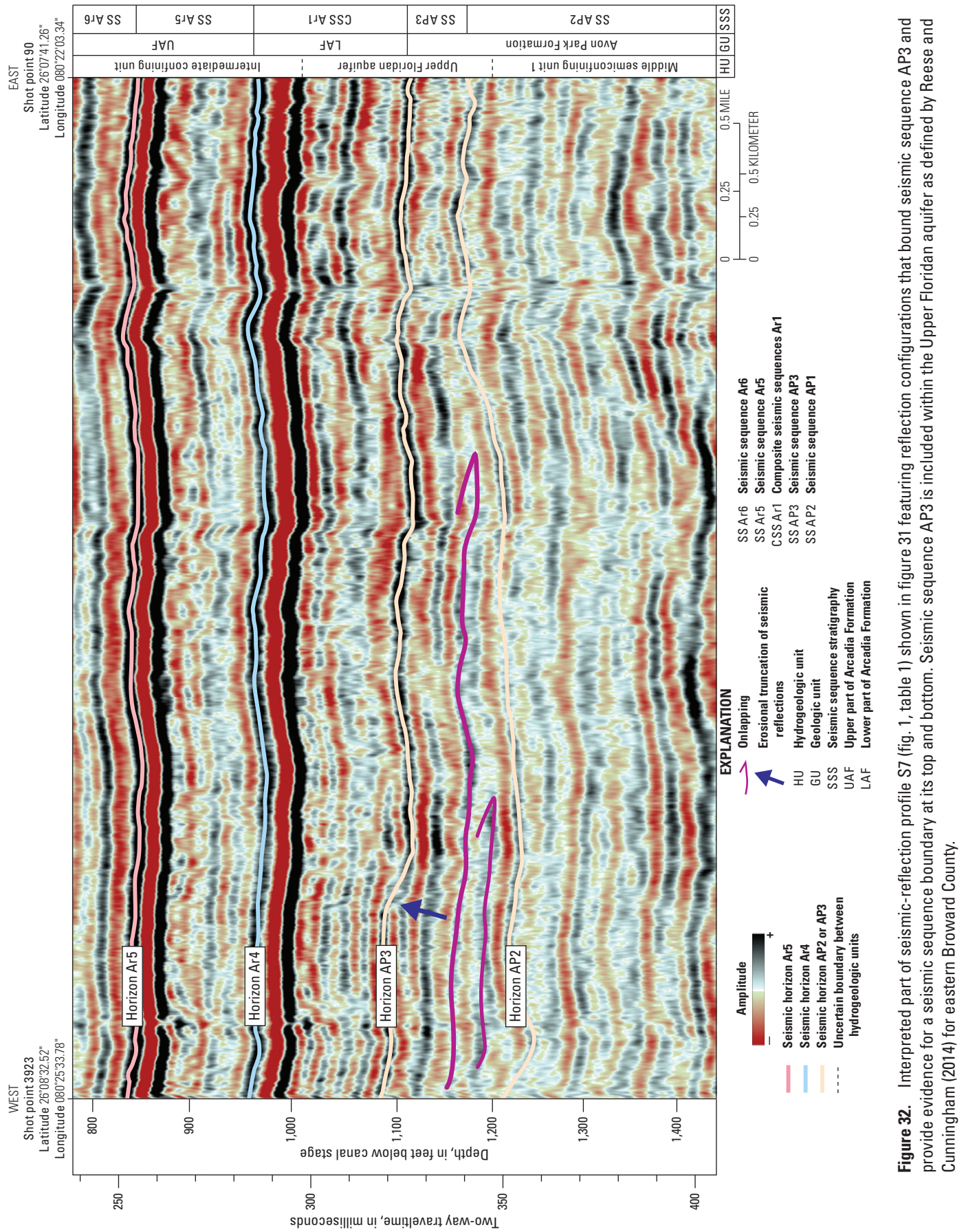

Figure 32. Interpreted part of seismic-reflection profile S7 (fig. 1, table 1) shown in figure 31 featuring reflection configurations that bound seismic sequence AP3 and provide evidence for a seismic sequence boundary at its top and bottom. Seismic sequence AP3 is included within the Upper Floridan aquifer as defined by Reese and Cunningham (2014) for eastern Broward County.

most eastern seismic reflections of seismic sequence Ar5 downlap and terminate at an approximately north-south trend (pls. 6, 7, 14, 15, 18, and 19) near the present-day eastern coastal boundary of the study area. The downlapping seismic reflections show progradation in an easterly direction. Two-way traveltime through seismic sequence Ar5 does not exceed approximately 78 milliseconds or a maximum thickness of about 300 ft in the western part of the study area and seismic sequence Ar5 terminates in seismic-reflection downlap onto composite seismic sequence Ar1 (pls. 6–19).

Seismic Sequence Ar6

Seismic sequence Ar6 is superjacent to seismic sequence Ar5 and subjacent to seismic sequence Ar7 (fig. 4, pls. 6–19). Seismic sequence Ar6 is a bank seismic facies unit (Mitchum and others, 1977; Alley, 1987) throughout the study area. Two-way traveltime through seismic sequence Ar6 is approximately 30 to 42 milliseconds in the western part of the study area, where its thickness ranges from approximately 115 to 160 ft. but reaches its maximum thickness, about 64 milliseconds two-way traveltime or 240 ft, at and near the outer ramp margin slope of the underlying seismic sequence Ar5 (pls. 6, 7, 14, 15, 18, 19). Where seismic-reflection data are good to excellent, seismic sequence Ar6 is composed of mainly continuous, parallel reflection configurations exhibiting high amplitudes in its upper part and relatively lower amplitudes in its lower part (pls. 6–19). Where seismic-reflection data are fair, seismic sequence Ar6 is composed of mostly continuous-to-discontinuous hummocky reflection configurations (pls. 6–19). In the western part of the study area, reflection configurations are parallel to the lower boundary of seismic sequence Ar5 (pls. 6–17). In the eastern part of the study area, seismic reflections downlap onto the upper boundary of seismic sequence Ar5 and overstep seismic sequence Ar5 (pls. 18 and 19). Where the seismic reflections of seismic sequence Ar6 have overstepped seismic sequence Ar5, the seismic reflections of Ar6 downlap onto the upper boundary of composite seismic sequence Ar1 (pls. 18 and 19). The most distal downlapping seismic reflections of seismic sequence Ar6 terminate along an approximately north-south trend (pls. 6, 7, 18, and 19) near the eastern coastal boundary of the study area. Along the eastern side of seismic-reflection profile S1 (fig. 1), seismic sequence Ar6 displays a lowstand wedge above both the most distal part of the outer ramp slope of seismic sequence Ar5 and above part of composite seismic sequence Ar1 (figs. 33 and 34). The paleo-seaward termination of the bank seismic facies unit of seismic sequence Ar6 is located about 1.7 mi east of the paleo-seaward termination of the bank seismic facies unit of underlying seismic sequence Ar5 and overlying seismic sequence Ar7 in the southeastern part of the study area (pls. 18 and 19). As a whole, seismic sequence Ar6 shows eastward progradation of the bank seismic facies unit.

Seismic Sequence Ar7

Seismic sequence Ar7 is superjacent to seismic sequence Ar6 and subjacent to a deltaic depositional system of the Peace River Formation (fig. 5). Seismic sequence Ar7 is a bank seismic facies unit (Mitchum and others, 1977; Alley, 1987) throughout the study area, which has a downward-sloping bank margin along its eastern extent (pls. 18 and 19). The eastern paleo-seaward termination of the bank seismic facies unit trends approximately north-south in eastern Broward County and northeastern Miami-Dade County based on seismic data (pls. 18 and 19) and review of well data within the study area (table 2). The gradient of the eastern ramp margin is about 3.5° (approximately 1.5° more than indicated by Cunningham [2015]). The more western part of the ramp has broad low-relief topography that is roughly flat in the south and dips slightly toward the northeast in the north (pls. 3 and 4). Where seismic-reflection data are of high quality, they indicate that seismic sequence Ar7 is composed of mainly continuous, parallel reflection configurations generally exhibiting high amplitudes in its uppermost part and relatively lower amplitudes in its middle and lower parts (pls. 6–19). In cases where the seismic-reflection data are of fair quality, they indicate that seismic sequence Ar7 is composed of mostly continuous-to-discontinuous hummocky reflection configurations (pls. 6–19). In the western part of the study area, seismic reflections within the lower part of seismic sequence Ar7 are parallel to the upper boundary of seismic sequence Ar6 (pls. 6–17). In the eastern part of the study area, seismic reflections downlap onto the upper boundary of seismic sequence Ar6 (pls. 18 and 19). The paleo-seaward termination of the bank seismic facies unit of seismic sequence Ar7 is located in a landward position and is about 1.7 mi west of the paleo-seaward termination of the bank seismic facies unit of underlying seismic sequence Ar6, indicating a backstepping of seismic sequence Ar7 in relation to the seismic sequence Ar6 ramp (pls. 18 and 19). The downlapping seismic reflections of seismic sequence Ar7 indicate that progradation of the bank seismic facies unit was in an easterly direction (pls. 18 and 19). In most areas, the upper boundary of seismic sequence Ar7 is downlapped by eastward prograding seismic reflections of the Peace River Formation (pls. 6–19), but in the easternmost part of coastal Broward County, seismic reflections of the Stock Island Formation plausibly downlap onto the upper boundary of seismic sequence Ar7 in some areas. Two-way traveltime through seismic sequence Ar7 does not exceed approximately 62 milliseconds and its thickness does not exceed about 270 ft. The thickness of seismic sequence Ar7 thins toward its eastern termination of the seismic-reflection downlap (pls. 6–19).

Seismic Structures

Various tectonic faults and numerous vertical, lengthy, cross-formational seismic-sag (karst collapse) structures (figs. 33–35, pl. 21) have been identified on

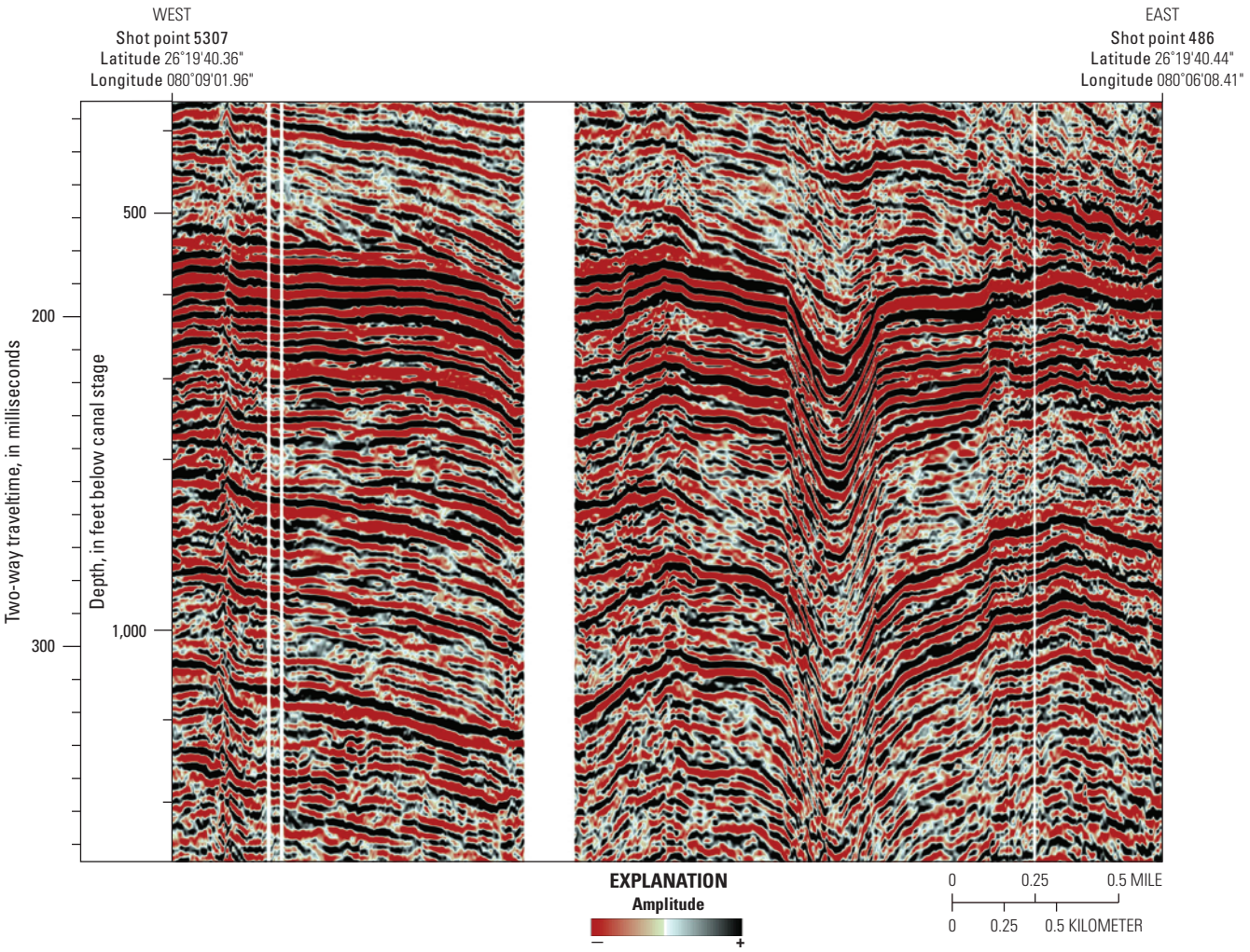

Figure 33. Uninterpreted part of seismic-reflection profile S1 (fig.1, table 1) shown in figure 34.

seismic-reflection profiles in the southeastern part of the Florida Platform (Cunningham and Walker 2009; Cunningham and others, 2012; Cunningham, 2013, 2014; Reese and Cunningham, 2014; Cunningham, 2015). Only one vertical reverse fault of inferred tectonic origin has been directly observed in the seismic-reflection data of the study area (pl. 21), and a second fault has been hypothesized in the southeastern part of the study area (pls. 3 and 4). Seventeen vertical seismic-sag structures of hypogenic karst origin have been identified (figs. 1, 33–35; pls. 6, 7, 12–17) in the study area (fig. 1). Several small-scale unconformity-related paleo-epigenic karst collapse structures at or near the tops of the depositional sequences O1 and O3 were recognized in seismic-reflection profiles (figs. 22, 23, 25–28). Artificial-neural-network-based meta-attribute calculations applied to an eastern part of the S1 seismic-reflection profile (fig. 1, pl. 21) were used to help detect faults, fractures, and fluid-migration pathways. The attribute analysis indicates two heavily faulted seismic-sag structures and the one reverse fault of inferred tectonic origin (pl. 21). In addition, the attribute analysis shows a high probability of potential vertical fluid migration associated with the seismic-sag structures and reverse fault (pl. 21).

Seismic-Sag Structures

Numerous vertical seismic-sag structures have been identified on seismic-reflection profiles from many carbonate provinces worldwide (Popenoe and others, 1984; Hardage and others, 1996; Heubeck and others, 2004; McDonnell and others, 2007; Cunningham and Walker, 2009; Hine and others, 2009; Betzler and others, 2011; Barnett and others, 2015; Burberry and others, 2016). Cunningham and Walker (2009) first described the presence of buried, vertical, lengthy seismic-sag structures on seismic-reflection profiles in Biscayne Bay, southeastern Florida. The seismic-sag structures of the study area herein display concave-upward arrangements of mainly parallel seismic-reflection patterns, with the dip of the reflections generally reducing upward to horizontal at the upward termination of the system (fig. 35, pl. 21).

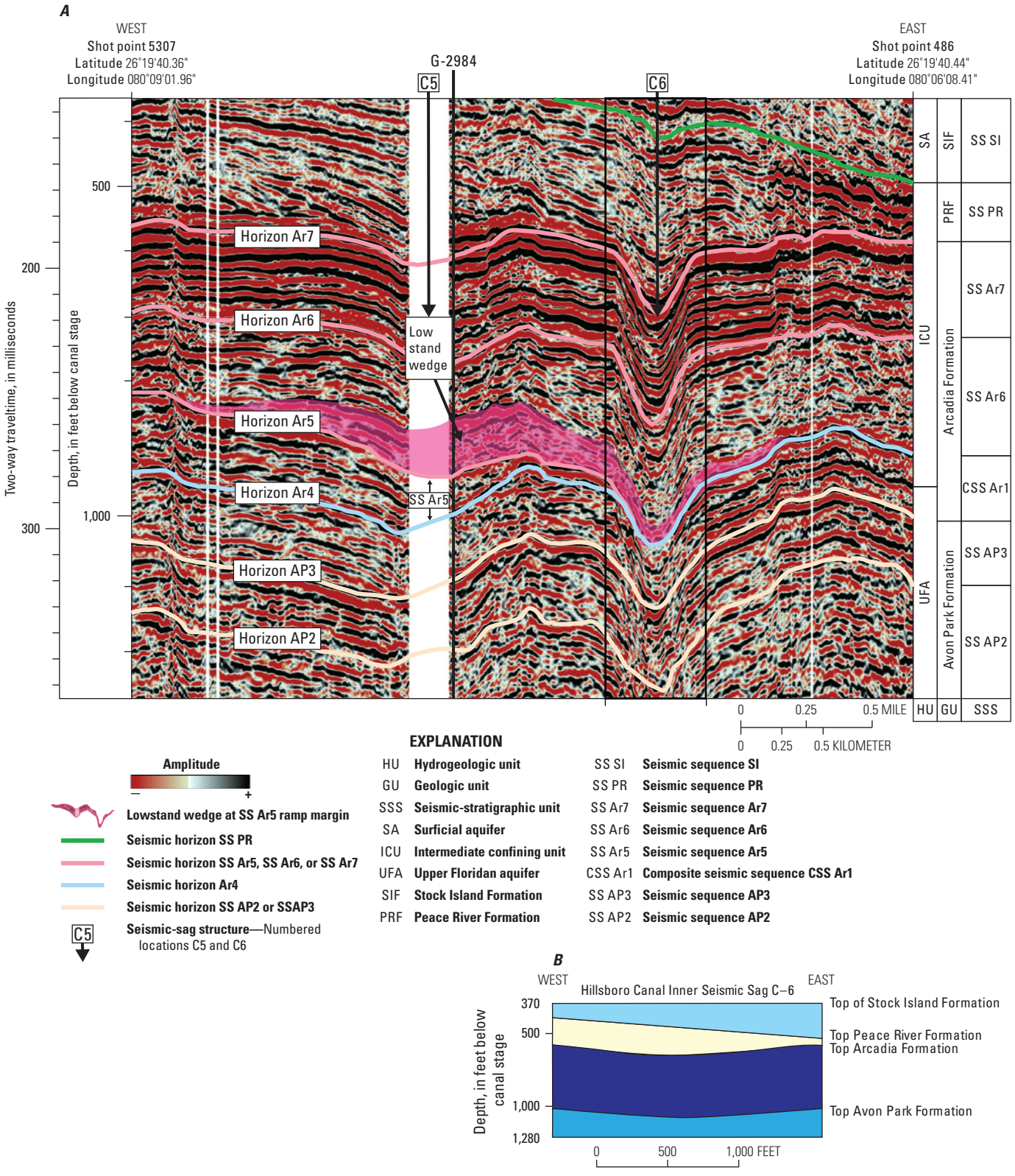

Figure 34. Interpreted part of seismic-reflection profile S1 (fig. 1, table 1) shown in figure 33 acquired along the easternmost part of the Hillsboro Canal with interpreted seismic stratigraphy. Seismic sequence Ar6 contains a lowstand wedge at the ramp margin above the most distal part of the outer ramp margin slope of seismic sequence Ar5 and above part of composite seismic sequence Ar1. Lithology and sequence stratigraphy of the seismic-reflection profile S1 displayed here can be compared to information in appendix 21 and Cunningham and Robinson (2017).

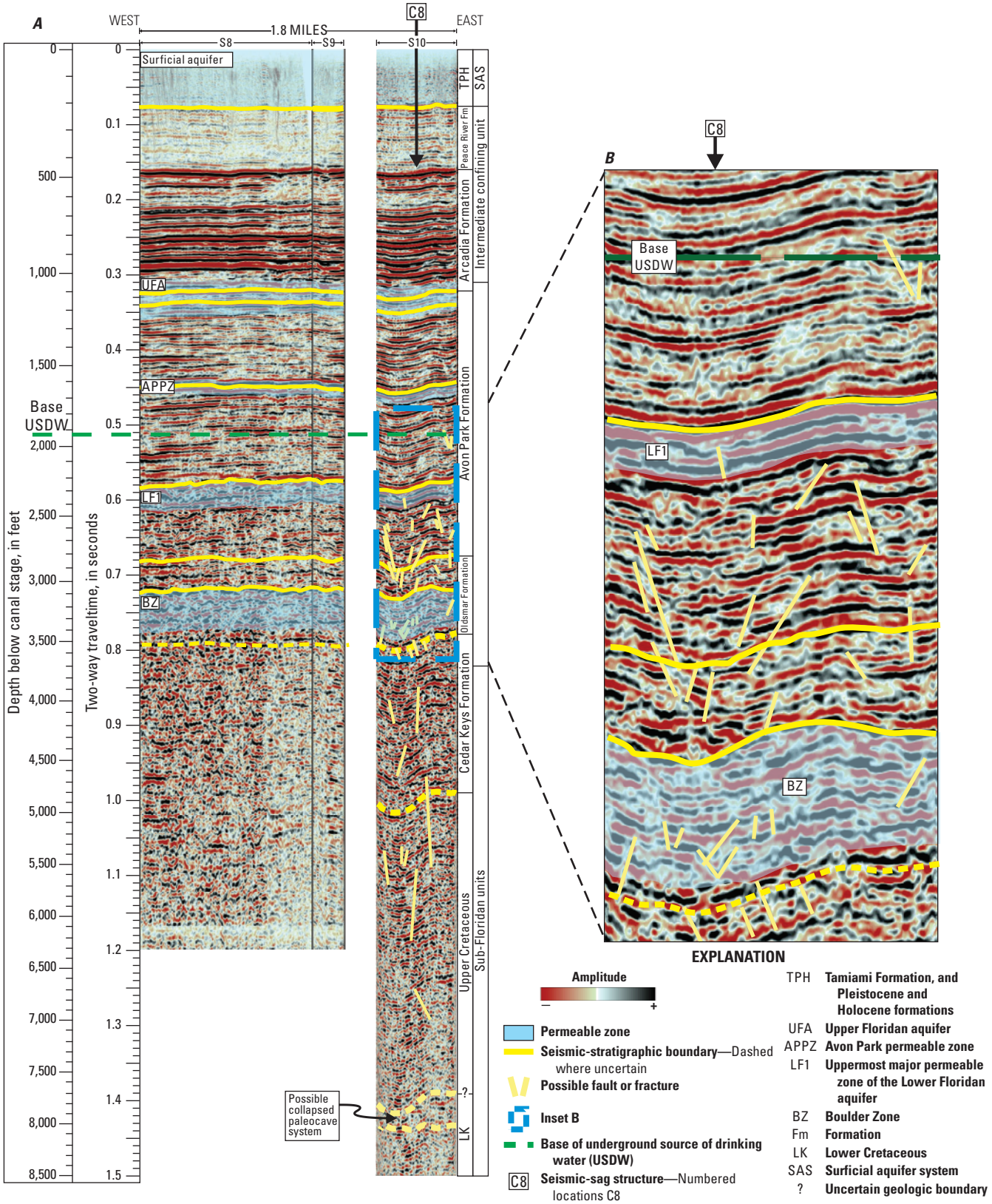

Figure 35. Interpreted seismic-reflection profiles S8, S9, and S10 (fig. 1, table 1). *A*, Sagging seismic reflections on profile S10 delineate a karst collapse structure that extends upward from the upper part of the Lower Cretaceous to the approximate top of the Peace River Formation. Seismic-reflection profiles S8 and S9 overlap, but only the non-overlapping part of S9 is shown. *B*, Inset from *A* showing that faults and fractures within the seismic-sag structure are of greater density in seismic sequences O1 and O3 than in overlying seismic sequence AP1. Modified from Cunningham (2014).

In three dimensions, the sags are conceptualized as having a columniform shape on the basis of comparisons to mapped seismic reflection results in nearby Biscayne Bay (Cunningham and Walker, 2009; Cunningham, 2015), offshore of Miami-Dade County in the Atlantic Ocean (Cunningham and others, 2012), and ancient circular examples of seismic sag structures in other carbonate provinces of the world (for example, Hardage and others, 1996; McDonnell and others, 2007; Betzler and others, 2011). Cunningham and Walker (2009) provided a detailed characterization of the southeastern Florida seismic-sag structures and seismic evidence that the seismic-sag structures are physical structural systems resulting from karst collapse. The bottoms of these structural systems are in many cases not visible on seismic-reflection profiles, because the signal-to-noise ratio of the seismic data decreases with increasing depth, especially below the upper part of seismic sequence O3 and within seismic sequence O1. The presence of karst features causes "noisy" data to persist below the karst (Cai and others, 2011). The base of most seismic-sag structures may be within seismic sequence O1 where chaotic seismic reflection patterns are common, probably indicating widespread occurrence of autogenic breccia and karst collapse. The bottom of one particular seismic-sag structure in eastern Broward County extends much deeper than the others, and the sagging seismic-reflections extend vertically upward about 7,600 ft from carbonate rock within the uppermost Lower Cretaceous to near the top of the Peace River Formation (fig. 35). Other examples of seismic-sag structures in southeastern Florida have been imaged by Cunningham and Walker (2009, figs. 3–5), Cunningham and others (2012, fig. 4), Cunningham (2013, fig. 3), and Cunningham (2015, figs. 7, 9, and 12). Measured heights of other seismic-sag structures in the study area are as great as about 2,500 ft. The great depths of these structures preclude epigenic karst collapse mechanisms (karst related to surface recharge [Klimchouk, 2000]) and indicate hypogenic karst. Hypogenic karst is formed by carbonate dissolution from water whose **aggressiveness** was produced at depth and not at or above the land surface (Palmer, 2007). Hypogenic karstification is the most probable dissolution mechanism, resulting in deeply buried karst collapse structures. Spechler (1994, 2001), Cunningham and Walker (2009), and Audra and Palmer (2015) have speculated on mechanisms involving the dissolution of rocks of the Floridan aquifer system by upward flowing, cross-formational groundwater, a hypogenic karst process.

Attribute Analysis of Seismic Structures

Advanced techniques for attribute analysis were applied to the S1 seismic-reflection profile acquired along the Hillsboro Canal in northeastern Broward County (fig. 1, pl. 21) to better evaluate fault and fracture probabilities within the vertical extent of seismic-sag structures and the associated potential for vertical cross-formational fluid-migration pathways. Neural-network fault-cube attribute analysis of the dip-steered, median-filtered S1 seismic-reflection profile showed vertically oriented zones of high fault probability (pl. 21). Centered on the large sag structure at shot-point 2095 (pl. 21), near the eastern end of the S1 seismic-reflection profile, the fault attribute calculations that used the profile data indicate two approximately 500-ft-wide concentrated zones that have a high probability of faulting and that likely ring the sides of the seismic-sag structure when conceptualized in three dimensions (pl. 21). In addition, the fault-attribute zones extend upward from the lowermost limit of resolvable seismic-reflection data and within the Oldsmar Formation upward into seismic reflections representative of the Peace River Formation (pl. 21). A zone of coherent reflections centered at shot point 2095 is vertically sandwiched by zones that have a high probability of faults and fractures (pl. 21). If imaged in three dimensions, a less-faulted cylindrical core of the seismic-sag structure would be surrounded by extensional ring faults (Bertoni and Cartwright, 2005). The two high-probability fault zones above seismic sequence Ar7 diminish within the thin overlying seismic sequence representing deltaic sediments of the lower part of the Peace River Formation. A few very narrow high-probability fault zones extend farther upward into eastward dipping seismic reflections equivalent to fine-grained carbonate slope deposits of the lower part of the Stock Island Formation (pl. 21).

Located about 1,700 ft to the east of the shot point 2095 seismic-sag structure is a reverse fault defined by minor offset in seismic reflections on either side of where a fault plane would intersect seismic-reflection profile S1 (pl. 21). A very narrow black line indicates a zone of high-probability of faulting and fracturing emphasizes the location of the fault at shot point 1,325 on plate 21. The reverse fault extends upward from the maximum limit of resolvable seismic-reflection data within the Oldsmar Formation into seismic reflections representative of the Peace River Formation and the lower part of the Stock Island Formation (pl. 21). The reverse fault terminates about 75 ft above the top of the Peace River Formation (pl. 21). The high amplitude reflections that represent the Peace River Formation sharply transition to low amplitudes on the western side of the reverse fault (pl. 21). This reverse fault has up to about 19 ft (5 milliseconds two-way traveltime) of upthrown versus downthrown offset between reflections within the Arcadia Formation.

Near the eastern edge of the seismic-reflection profile S1, a third zone of high-probability for faulting is associated with a seismic-sag structure centered on shot point 225 (pl. 21). This approximately 1,500-ft-wide zone of high-probability for faulting gradually widens with depth down to the top of seismic sequence O3, where signal attenuation limits the ability to interpret fault attribute results near the base of the seismic-reflection profile. The seismic-sag structure and associated zone of high-probability for faulting extend upward from about the maximum limit of resolvable seismic-reflection data representative of much of the Oldsmar Formation to an altitude near the top of seismic sequence AP3 (pl. 21). In

addition, a few discrete zones extend upward into composite seismic sequence Ar1 and beyond into seismic reflections representative of the Peace River Formation and Stock Island Formation (pl. 21). Thus, the highest density part of the zone of high-probability for faulting is from within the seismic reflections representative of the Oldsmar Formation upward to near the top of seismic sequence AP3 or top of the Avon Park Formation (pl. 21). Although the eastern limit of this seismic-sag structure is not fully imaged on plate 21 (because of a lack of any seismic-reflection data eastward of this limit), the western side of the seismic-sag structure has a notable concentration of zones of high-probability for faulting (pl. 21), indicating that this seismic-sag structure includes extensional ring faults in its outer perimeter (Bertoni and Cartwright, 2005).

Chimney attribute analysis along part of seismic-reflection profile S1 (fig. 1, pl. 21) yielded a color image of fluid-migration pathway ("chimney") probabilities on the seismic-reflection profile. The fluid-migration pathway probabilities closely correspond to fault attribute results (pl. 21). Fluid-pathway probabilities are highest along probable faults in zones that rim the large seismic-sag structure centered on shot-point 2095 (pl. 21).

Neural-network fault attribute calculations along the seismic-reflection profile S1 (fig. 1) suggest that extensive faulting, concentrated along the sides of the seismic-sag structure centered on shot point 2095, is responsible for the down-dropped, or sagging, pattern observed on the seismic-reflection profile (pl. 21). These dense zones of high-probability for faulting are interpreted to reflect concentrated normal faulting along the sides of a karst collapse structure. This interpretation is consistent with the down-dropped nature of the strata and with the structural interpretations of Cunningham (2014) and Reese and Cunningham (2014). The apparent gradual widening of fault distribution with depth, particularly within and below the Avon Park Formation, is consistent with karstic collapse growth over time reported in other basins (for example, McDonnell and others, 2007) and additional karst collapse structures on the southeastern Florida Platform (Cunningham and Walker, 2009; Cunningham, 2015). Furthermore, the collapse structure appears to be rooted well below the top of seismic sequence O3; however, because of diminished resolution with increasing depth, the exact altitude is uncertain, because the top of seismic sequence O1 is poorly resolvable and underlying seismic-reflection continuity is poor for seismic-reflection profile S1. Slight stratigraphic offsets or reflector sagging observed above the top of composite seismic sequence Ar1 indicates that the collapse structure and associated faults extend upward well into the Peace River Formation and possibly above it into the Stock Island Formation and Ochopee Member of the Tamiami Formation (Cunningham 2013; Reese and Cunningham, 2014). Faults extending into the Tamiami Formation indicate that some of the collapse occurred during the late Pliocene (Reese and Cunningham, 2014, fig. 13) or possibly later. The late timing of the collapse and its deep burial rules out an epigenic origin for the karst collapse and is indicative of hypogenic karst. Sagging seismic reflections within the Peace River Formation siliciclastics that overlie the Arcadia Formation also suggest that karst collapse is the result of hypogenic processes that occurred during late Miocene to early Pliocene time or even possibly later (sag numbers C1, C6, C8, C11; fig. 1, pls. 7, 13, and 15). The zone of dense faulting near shot point 225 on the eastern edge of the profile appears to be the result of deeply buried karstic collapse rooted below the top of seismic sequence O3. Although signal attenuation is relatively higher within the seismic data on seismic-reflection profile S1 compared to overlying data, an overall increase in attribute-derived fault probability within Oldsmar Formation equivalent seismic reflections (figs. 29 and 30, pl. 21) suggests the increased faulting and fracturing within the unit is due to karstification. This probably led to subsequent cave formation and collapse and, in some cases, is the level of origin for other seismic-sag structures in the study area.

The chimney attribute results provide further information about the relations between faulting, karst collapse structures, and potential near-vertical fluid pathways through the carbonate strata. Plate 21 shows that probable fluid pathways are closely correlated to karst collapse features near a tectonic fault that is likely deep-seated, a relationship previously noted elsewhere in northeastern Florida by Popenoe and others (1984). Prominent zones of high chimney probability coincide with the sides of the collapse structure centered on shot point 2095 (pl. 21). Similarly, chimney probability increases below the top of the seismic sequence O3 horizon, indicating there is a substantial increase in fluid pathways below this horizon that could contribute to the potential for upward flow of groundwater and carbonate rock dissolution along vertical pathways.

Summary and Conclusions

The purpose of this study is to characterize the sequence stratigraphy, seismic stratigraphy, and seismic structures of the lower part of the intermediate confining unit and most of the Floridan aquifer, so water managers can better understand the hydrogeologic controls on groundwater movement through these hydrogeologic units. The study included the integration of geologic and geophysical borehole data from 45 wells and approximately 80 miles of seismic-reflection data acquired in canals of eastern Broward County and northeastern Miami-Dade County. These data provide a regional sequence-stratigraphic, hydrogeologic, and structural conceptual framework of the rocks that compose the lower part of the intermediate confining unit downward to the uppermost part of the Boulder Zone. These rocks lie between beds in the upper part of the Boulder Zone and the upper bounding surface of the Arcadia Formation. The association of highly permeable units and unconformities in well data and their correlation to seismic data was critical to producing a unified 3D sequence-stratigraphic and hydrogeologic conceptual geomodel.

The stratigraphic analyses applied to the borehole data and seismic-reflection data were used to map eight uniquely distributed major depositional cycles (seven depositional sequences and one composite sequence) and a corresponding seismic stratigraphy. The depositional sequence stratigraphy was delineated for the Oldsmar Formation (depositional sequences O1 and O3), the Avon Park Formation (depositional sequences AP1, AP2, and AP3), the lower part of the Arcadia Formation (composite depositional sequence Ar1), and the upper part of the Arcadia Formation (depositional sequences Ar5, Ar6, and Ar7). Four additional unmapped depositional sequences (depositional sequences Ar1, Ar2, Ar3, and Ar4) form the composite depositional sequence Ar1.

Upper depositional sequence boundaries and seismic sequence boundaries correspond well or generally to upper surfaces of four major permeability units of the Floridan aquifer system: the Upper Floridan aquifer, Avon Park permeability zone, uppermost major permeable zone of the Lower Floridan aquifer, and the Boulder Zone. The upper boundaries of depositional sequence O1 and seismic sequence O1 correspond to the upper surface of the Boulder Zone, the upper boundaries of depositional sequence O3 and seismic sequence O3 correspond to the upper surface of the uppermost major permeable zone of the Lower Floridan aquifer, the upper boundaries of depositional sequence AP1 and seismic sequence AP1 roughly correspond to the top of the Avon Park permeability zone, and the upper boundaries of composite depositional sequence Ar1 and composite seismic sequence Ar1 are approximate indicators of the top of the Upper Floridan aquifer. Depositional sequence O1 corresponds to a thick dolomite in the lower part of the Oldsmar Formation, depositional sequence O3 corresponds to the upper part of the Oldsmar Formation, depositional sequence AP1 corresponds to the lower part of the Avon Park Formation, and composite depositional sequence Ar1 corresponds to the lower part of the Arcadia Formation. In southeastern Florida, sequence stratigraphy and seismic stratigraphy were useful tools for the correlation of ancient subaerial exposure at unconformities and related secondary porosity at the upper surfaces of carbonate depositional cycles of several hierarchical scales ranging from high-frequency cycles to depositional sequences. Thus, the use of these two stratigraphic methods has enabled a more accurate delineation of aquifer stratigraphy in southeastern Florida than possible with well data alone. In the study area, secondary porosity associated with the upper part of some unconformity-bound seismic sequences has a direct correlation with relatively high permeability hydrogeologic units.

Shallow-marine platform carbonates compose the upper part of the Oldsmar Formation. In the study area, data from core samples indicate that the upper part of the Oldsmar Formation in the study area is composed of thin high-frequency peritidal cycles at a foot- to several-foot-scale and less-common, thicker subtidal cycles deposited on a carbonate platform interior. Dolomite beds, averaging about 100 feet in cumulative thickness and interbedded with limestone, compose the uppermost Oldsmar Formation, which was formed by foot-scale, high-frequency, peritidal cycles. Fractured Oldsmar Formation core samples from the G–2991 City of Davie IW–1 well reflect unconformable geologic relations observed in a nearby seismic-reflection profile. Data from this profile suggest karst solution processes (paleo-sinkholes and vuggy megaporosity), along with a fractured and faulted Oldsmar Formation dolomite, produced a highly irregular paleotopography along a subaerial exposure surface coincident with a major regional unconformity at the upper bounding surface of the formation. The fractured, faulted, vuggy dolomite of the uppermost Oldsmar Formation forms the uppermost major permeable zone of the Lower Floridan aquifer. The substantial acoustic contrast between the dolomite at the top of the Oldsmar Formation and limestone at the base of the overlying Avon Park Formation creates a mappable, high-amplitude seismic reflection that typically provides a good seismic horizon for mapping the top of the Oldsmar Formation and the top of the uppermost major permeable zone of the Lower Floridan aquifer. The absence of dolomite in all Avon Park Formation core samples, in contrast to the common dolomite and thicker, more pervasive desiccation features capping peritidal cycles within the Oldsmar Formation, suggests warmer climatic conditions existed during upper Oldsmar Formation deposition as compared to Avon Park Formation deposition. The presence of a *Fallotella floridana*-*Coskinolina floridana* benthic foraminifer assemblage zone in limestone of the Avon Park Formation above the dolomite as compared to the presence of a *Helicostegina gyralis*-*Thomasella* benthic foraminifer assemble zone below dolomite within an upper part of the Oldsmar Formation also support the presence of a hiatus (major sequence boundary) and change in environmental conditions at the upper bounding surface of depositional sequence O3 that separates the top of the Oldsmar Formation and base of the Avon Park Formation.

The Avon Park Formation is composed of three major depositional sequences, in ascending order, depositional sequence AP1, AP2, and AP3. The two oldest sequences are dominated by highstand deposits composed of three types of ideal high-frequency cycles: (1) microbial laminite-capped grain-rich peritidal cycles; (2) rhizolith- and mud-capped micrite-rich peritidal cycles; and (3) *Glossifungites*-capped subtidal cycles. The uppermost depositional sequence (AP3) is an incomplete depositional cycle and composed of mainly transgressive packstone and grainstone that backstep over underlying depositional sequence AP2. A fourth ideal high-frequency cycle type—an aggradational grain-rich subtidal cycle—dominates the cycles composing depositional sequence AP3. Diffuse flow zones are generally restricted to grainstones and grain-dominated packstone of depositional sequence AP3, and concentrated flow through porous vuggy intervals is generally restricted to the upper part of rhizolith- and mud-capped micrite-rich peritidal cycles in the upper part of depositional sequence AP1.

Composite depositional sequence Ar1 composes the lower part of the Arcadia Formation and consists of four topography-draping, aggradational depositional sequences. The composite sequence is expressed on seismic-reflection profiles as a sheet seismic facies unit and is composed of two shallow-marine carbonate sequences and two shallow-marine mixed carbonate-siliciclastic sequences. The base of the intermediate confining unit and top of the Upper Floridan aquifer lie within composite depositional sequence Ar1. The upper part of the Arcadia Formation contains three depositional sequences, each forming a distally steepened carbonate ramp, with an eastern progradational limit in eastern coastal Broward County and northeastern Miami-Dade County. The three ramps are expressed on seismic-reflection profiles as bank seismic facies units. The progradational ramp margin of depositional sequence Ar6 oversteps the ramp margin of Ar5. The ramp margin slope of both depositional sequence Ar5 and Ar6 downlap onto the upper bounding surface of composite depositional sequence Ar1. Depositional sequence Ar7 backsteps in a paleo-landward direction. The progradational ramp margin of depositional sequence Ar7 and the toe of the ramp margin downlap onto the upper bounding surface of depositional sequence Ar6. The particles of the lower and upper parts of the Arcadia Formation are dominated by a heterozoan particle assemblage, indicating temperate water conditions during deposition of the Arcadia Formation. The upper part of the Arcadia Formation is contained within the lower part of the intermediate confining unit, but the base of the intermediate confining unit is within composite depositional sequence Ar1. Low permeability packstone, wackestone, lime mudstone, marl, and terrigenous mudstone compose the rocks produced by the marginal depositional setting of the three ramps. Compared to 1D well data, the 2D seismic-reflection data provided the most useful information for defining the eastern limit of these three low-permeability confining ramps in eastern Broward County and northeastern Miami-Dade County.

Columniform seismic-sag structures, which have heights as great as 2,500 vertical feet, are the dominant element in the structural landscape of the study area. Seventeen vertical seismic-sag structures were identified on the seismic-reflection profiles. The seismic-sag structures are commonly visible on seismic-reflection profiles that image the early Eocene to Miocene age rocks that compose the Boulder Zone upward to the middle of the intermediate confining unit. One unique seismic-sag structure extends from the upper part of the Lower Cretaceous to rocks and sediment of Pliocene age over a vertical distance of about 7,800 feet.

Seismic-sag structures potentially form passageways for vertical cross-formational groundwater flow through the Floridan aquifer or flow of injected treated wastewater upward from the Boulder Zone into overlying strata. Advanced attribute analysis of two seismic-sag structures show a high probability of faults and fractures associated with karst collapsed seismic-sag structures and a high probability that the faults and fractures provide potential passageways for fluid flow. A seismic-reflection profile acquired along the Hillsboro Canal imaged a single reverse fault of inferred tectonic origin. Advanced attribute analysis of this fault indicates there is a high probability of a potential for vertical cross-formational flow along the fault; however, the low density of tectonic faults in the study area indicates they contribute minimally to upward groundwater flow within the Floridan aquifer system in eastern Broward County. The seismic-sag structures are the result of hypogenic karstification. Thus, the origin of the structures is related to the upward flow of fluids capable of dissolving carbonate rock that was plausibly concentrated along the intersections of deep-seated faults and joints.

References Cited

Alley, A.W. (ed.), 1987, Atlas of seismic stratigraphy: American Association of Petroleum Geologists Studies in Geology 27, v. 1, 125 p.

Aminzadeh, F., and de Groot, P.F., 2005, A neural network based seismic object detection technique: Society of Exploration Geophysicists Technical Program Expanded Abstracts, p. 775–778.

Applin, P.L., and Applin, E.R., 1944, Regional subsurface stratigraphy and structure of Florida and southern Georgia: American Association of Petroleum Geologists Bulletin, v. 28, p. 1673–1753.

Audra, P., and Palmer, A.N., 2015, Research frontiers in speleogenesis, dominant processes, hydrogeological conditions and resulting cave patterns: Acta Carsologica, v. 44, p. 315–348.

Bansal, R., Imhof, M.G., and Daly, T., 2002, Seismic characterization of fractures in a naturally fractured gas reservoir: Society of Exploration Geophysicists Annual Meeting Expanded Abstracts 2002, p. 2233–2236.

Barnett, A.J., Wright, V.P., Chandra, V.S., and Jain, V., 2015, Distinguishing between eogenetic, unconformity-related and mesogenetic dissolution—A case study from the Panna and Mukta fields, offshore, Mumbai, India, *in* Armitage, P.J., Butcher, A.R., Churchill, J.M., Csoma, A.E., Hollis, C., Lander, R.H., Omma, J.E., and Worden, R.H., Reservoir quality of clastic and carbonate rocks— Analysis, modelling and prediction: Geological Society, London, Special Publication 435.

Bashir, Y., Ghosh, D., and Sum, C.W., 2015, Detection of fault and fracture using seismic diffraction and behavior of diffraction hyperbola with velocity and time: European Association of Geoscientists & Engineers symposium, Kuala Lumpur, Malaysia, v. 23618.

Bertoni, C., and Cartwright, J.A., 2005, 3D seismic analysis of circular evaporite dissolution structures, Eastern Mediterranean: London, Journal of the Geological Society, v. 162, p. 909–926.

Betzler, C., Lindhorst, S., Hübscher, C., Lüdmann, T., Fürstenau, J., and Reijmer, J., 2011, Giant pockmarks in a carbonate platform (Maldives, Indian Ocean): Marine Geology, v. 289, p. 1–16.

Brandley, R.T., Krause, F.F., Bamber, E.W., and Marnet, B.L., 1995, Benthic biozones as systems tract and sequence signatures—Lower Cretaceous Mount Head Formation, southwest Alberta and southeast British Colombia, *in* Bell, J.S., Bird, T.D., Hillier, T.L, and Greener, P.L., eds., Proceedings of the Oil and Gas Forum '95 Energy from Sediments: Geological Survey of Canada Open File 3058, p. 7–9.

Brewster-Wingard, G.L., Scott, T.M., Edwards, L.E., Weedman, S.D., and Simmons, K.R., 1997, Reinterpretation of the peninsular Florida Oligocene—An integrated stratigraphic approach: Sedimentary Geology, v. 108, p. 207–228.

Brothers, D.S., Ruppel, C., Kluesner, J.W., ten Brink, U.S., Chaytor, J.D., Hill, J.C., Andrews, B.D., and Flores, C., 2014, Seabed fluid expulsion along upper slope and outer shelf of the U.S. Atlantic continental margin: Geophysical Research Letters, v. 41, p. 1–6.

Brouwer, F.C.G., and Arnaud, H., 2011, An integrated workflow to optimize discontinuity attributes for the imaging of faults, *in* Marfurt, K.J., Gao, Dengliang, Barnes, Art, Chopra, Satinder, Corrao, Antonio, Hart, Bruce, Huw, James, Pacht, Jory, and Rosen, N.C., eds., Attributes: New views on seismic imaging—Their use in exploration and production: 31st Annual Gulf Coast Section Conference Society of Sedimentary Geology, p. 496–532.

Brouwer, F.C.G., Connolly, D., and Tingahl, K.M., 2011, A guide to the practical use of neural networks, *in* Marfurt, K.J., Gao, Dengliang, Barnes, Art, Chopra, Satinder, Corrao, Antonio, Hart, Bruce, Huw, James, Pacht, Jory, and Rosen, N.C., eds., Attributes: New views on seismic imaging—Their use in exploration and production: 31st Annual Gulf Coast Section Society of Sedimentary Geology, p. 440–472.

Broward Water Resources Task Force, 2010, Broward water resources task force report: 50 p., plus appendixes.

Bruns, T.R., Geist, E.L., and Lavoie, D.L., 1994, Synthetic seismograms, migrated seismic reflection profiles, and lithologic correlations for Leg 135 sites in the Lau Basin and Tonga Arc, chap. 21 *of* Hawkins, J.W., Parson, L.M., Allan, J.F., and others, eds., Proceedings of the Ocean Drilling Program, scientific results, Lau Basin, covering Leg 135 of the cruises of the drilling vessel JOIDES Resolution, Suva Harbor, Fiji, to Honolulu, Hawaii, sites 834–841, 17 December 1990–28 February 1991: College Station, Texas, Texas A&M University Ocean Drilling Program, v. 135, p. 331–365.

Budd, D.A., Saller, A.H., and Harris, P.M., 1995, Unconformities and porosity in carbonate strata: American Association of Petroleum Geologists Memoir 63, 313 p.

Burberry, C.M., Jackson, C.A.-L, and Chandler, S.R., 2016, Seismic reflection imaging of karst in the Persian Gulf: Implications for the characterization of carbonate reservoirs: American Association of Petroleum Geologists Bulletin, v. 100, p. 1561–1584.

Cai, J., Xun, H., Li, L., He, Y., Li, Y., Dong, S., Guo, M., and Wang, B., 2011, Detailed velocity model building in a carbonate karst zone and improving sub-karst images in the Gulf of Mexico: Society of Exploration Geophysicists Annual Meeting, Las Vegas, Nev., p. 4030–4034.

Choquette, P.W., and Pray, L.C., 1970, Geologic nomenclature and classification of porosity in sedimentary carbonates: American Association of Petroleum Geologists Bulletin, v. 54, no. 2, p. 207–250.

Connolly, D., and Garcia, R., 2012, Tracking hydrocarbon seepage in Argentina's Neuquén basin: World Oil, v. 233, no. 7, p. 101–104.

Cunningham, K.J., 2013, Integrating seismic-reflection and sequence-stratigraphic methods to characterize the hydrogeology of the Floridan aquifer system in southeastern Florida: U.S. Geological Survey Open-File Report 2013–1181, 8 p.

Cunningham, K.J., 2014, Integration of seismic-reflection and well data to assess the potential impact of stratigraphic and structural features on sustainable water supply from the Floridan aquifer system, Broward County, Florida: U.S. Geological Survey Open-File Report 2014–1136, 5 p.

Cunningham, K.J., 2015, Seismic sequence stratigraphy and geologic structure of the Floridan aquifer system near "Boulder Zone" deep wells in Miami-Dade County, Florida: U.S. Geological Survey Scientific Investigations Report 2015–5013, 28 p.

Cunningham, K.J., Abbott, D.S., and Geokinetics Incorporated, 2017, Synthetic seismogram data for correlation between seismic-reflection profiles and well data, Broward County, Florida: U.S. Geological Survey data release, accessed September 18, 2017, https://doi.org/10.5066/F72R3PVF.

Cunningham, K.J., Locker, S.D., Hine, A.C., Bukry, David, Barron, J.A., and Guertin, L.A., 2003, Interplay of Late Cenozoic siliciclastic supply and carbonate response on the southeast Florida Platform: Journal of Sedimentary Research, v. 73, p. 31–46.

Cunningham, K.J., and Robinson, Edward, 2017, Lithofacies and sequence stratigraphic description of the upper part of the Avon Park Formation and the Arcadia Formation in U.S. Geological Survey G–2984 test corehole, Broward County, Florida: U.S. Geological Survey Open-File Report 2017–1074, 139 p., accessed September 18, 2017, at https://doi.org/10.3133/ofr20171074.

Cunningham, K.J., and Walker, C., 2009, Seismic-sag structures in Tertiary carbonate rocks beneath southeastern Florida, USA: Evidence for hypogenic speleogenesis?, *in* Klimchouk, A.B., and Ford, D.C., eds., Hypogene speleogenesis and karst hydrogeology of artesian basins: Simferopol, Ukraine, Ukrainian Institute of Speleology and Karstology, Special Paper no. 1, p. 151–158, accessed April 11, 2017, at http://institute.speleoukraine.net/libpdf/Cunningham%20Walker_SEISMIC-SAG%20STRUCTURAL%20SYSTEMS%20IN%20FLORIDA_HypoConf_2009.pdf.

Cunningham, K.J. and Walker, Cameron, 2017, Marine seismic profiles used to assess the seismic stratigraphy and structure of the intermediate confining unit and Floridan aquifer system, Broward County, Florida: U.S. Geological Survey data release, accessed September 18, 2017, https://doi.org/10.5066/F77942R3.

Cunningham, K.J., Walker, C., and Westcott, R.L., 2012, Near-surface, marine seismic-reflection data define potential hydrogeologic confinement bypass in the carbonate Floridan aquifer system, southeastern Florida: Society of Exploration Geophysicists Annual Meeting, Las Vegas, Nev., 6 p.

Cushman, J.A., and Ponton, G.M., 1933, A new genus of the foraminifera, *Gunteria*, from the middle Eocene of Florida: Cushman Laboratory for Foraminiferal Research Contributions, v. 9, p. 25–30.

Dausman, A.M., Doherty, J., Langevin, C.D., and Dixon, J., 2009, Hypothesis testing of buoyant plume migration using a highly parameterized variable-density groundwater model at a site in Florida, USA: Hydrogeology Journal, v. 18, p. 147–160.

Decker, L., Janson, X., and Fomel, S., 2015, Carbonate reservoir characterization using seismic diffraction imaging: Interpretation, v. 3, no. 1, p. SF21–SF30.

Droser, M.L., and Bottjer, D.J., 1986, A semiquantitative field classification of ichnofabric: Journal of Sedimentary Petrology, v. 56, p. 558–559.

Droser, M.L., and Bottjer, D.J., 1989, Ichnofabric of sandstones deposited in high-energy nearshore environments: measurement and utilization: Palaios, v. 4, p. 598–604.

Dunham, R.J., 1962, Classification of carbonate rocks according to depositional textures, *in* Ham, W.E., ed., Classification of carbonate rocks: American Association of Petroleum Geologists Memoir 1, p. 108–121.

Embry, A.F., and Klovan, J.E., 1971, A Late Devonian reef tract on northeastern Banks Island, N.W.T.: Bulletin of Canadian Petroleum Geology, v. 19, p. 730–781.

Emerson Process Management, 2017, Reservoir management software: accessed April 11, 2017, at http://www2.emersonprocess.com/en-US/brands/roxar/reservoirmanagement/Pages/ReservoirManagementSoftware.aspx.

Ewing, T.E., 1997, Real answers for synthetic issues: AAPG Explorer, v. 18, no. 8, p. 24–26.

Farfour, M., Woon, W.J., Ferahtia, J., and Djarfour, N., 2012, Seismic attributes combination to enhance detection of bright spot associated with hydrocarbons: Geosystem Engineering, v. 15, p. 143–150.

Federal Register Notice, October 11, 1979, v. 44, no. 198.

Fish, J.E., 1988, Hydrogeology, aquifer characteristics, and ground-water flow of the surficial aquifer system, Broward County, Florida: U.S. Geological Survey Water-Resources Investigations Report 87–4034, 92 p.

Fish, J.E., and Stewart, Mark, 1991, Hydrogeology of the surficial aquifer system, Dade County, Florida: U.S. Geological Survey Water-Resources Investigations Report 90–4108, 50 p.

Geological Society of America, 1991, Rock color chart: Baltimore, Md., Munsell Color.

Godet, A., 2013, Drowning unconformities: paleoenvironmental significance and involvement of global processes: Sedimentary Geology, v. 293, p. 46–66.

Goldman, D., and Mitchell, C.E., 1998, The stratigraphic distribution of graptolites in the classic upper Middle Ordovician Utica Shale of New York State—An evolutionary succession or a response to relative sea-level change?, *in* Gutiérrez-Marco and Rábano, I., eds., Temas Geológico-Mineros, Proceedings 6th International Graptolite Conference and 1998 Field Meeting, v. 23, p. 186–189.

Grasmueck, M., Quintà, M.C., Pomar, K., and Eberli, G.P., 2013, Diffraction imaging of sub-vertical fractures and karst with full-resolution 3D ground-penetrating radar: Geophysical Prospecting, v. 61, p. 907–918.

Guertin, L.A., Missimer, T.M., and McNeill, D.F., 2000, Hiatal duration of correlative sequence boundaries from Oligocene-Pliocene mixed carbonate/siliciclastic sediments of the South Florida Platform: Sedimentary Geology, v. 134, p. 1–26.

Harbaugh, A.W., 2005, MODFLOW-2005, The U.S. Geological Survey modular ground-water model—The Ground-Water Flow Process: U.S. Geological Survey Techniques and Methods book 6, Chap. A16, variously paged, accessed April 11, 2017, at http://pubs.usgs.gov/tm/2005/tm6A16/.

Hardage, B.A., Carr, D.L., Lancaster, D.E., Simmons, J.L., Jr., Elphick, R.Y., Pendleton, V.M., and Johns, R.A., 1996, 3-D seismic evidence of the effects of carbonate karst collapse on overlying clastic stratigraphy and reservoir compartmentalization: Geophysics, v. 61, p. 1336–1350.

Heubeck, C., Story, K., Peng, P., Sullivan, C., and Duff, S., 2004, An integrated reservoir study of the Liuhua 11–1 field using a high-resolution three-dimensional seismic data set, *in* Eberli, G.P., Masaferro, J.L., and Sarg, J.F., eds., Seismic imaging of carbonate reservoirs and systems: American Association of Petroleum Geologists Memoir 81, p. 149–168.

Hine, A.C., Suthard, B.C., Locker, S.D., Cunningham, K.J., Duncan, D.S., Evans, M., and Morton, R.A., 2009, Karst sub-basins and their relationship to the transport of Tertiary siliciclastic sediments on the Florida Platform: International Association of Sedimentologists Special Publication 41, p. 179–197.

Heggland, R., 2005, Using gas chimney in seal integrity analysis—A discussion based on case histories, *in* Boult, P., and Kaldi, J., eds., Evaluating fault and cap rock seals: AAPG Hedberg Series, no. 2, p. 237–245.

James, N.P., 1997, The cool-water carbonate depositional realm, *in* James, N.P., and Clarke, J.A.D., eds., Cool-water carbonates: Society for Sedimentary Geology Special Publication 56, p. 1–20.

Janson, X., Kerans, C., Loucks, R., Marhx, M.A., Reyes, C., and Murguia, F., 2011, Seismic architecture of a Lower Cretaceous platform-to-slope system, Santa Agueda and Poza Rica fields, Mexico: American Association of Petroleum Geologists, v. 95, no. 1, p. 105–146.

Kerans, C., and Tinker, S.W., 1997, Sequence stratigraphy and characterization of carbonate reservoirs: Tulsa, Okla., Society of Economic Paleontologists and Mineralogists Short Course Notes no. 40, 130 p.

Klimchouk, Alexander, 2000, Speleogenesis under deep-seated and confined settings, *in* Klimchouk, A.B., Ford, D.C., Palmer, A.N., and Dreybrodt, W., eds., Speleogenesis: evolution of karst aquifers: Huntsville, Ala., National Speleological Society, Inc., p. 244–260.

Kluesner, J.W., and Brothers, D.S., 2016, Seismic attribute detection of faults and fluid pathways within an active strike-slip shear zone: New insights from high-resolution 3D P-Cable seismic data along the Hosgri Fault, offshore California: Interpretation, v. 4, no. 1, p. 1–18.

Ligtenberg, J.H., 2005, Detection of fluid migration pathways in seismic data—Implications or fault seal analysis: Basin Research, v. 17, no. 1, p. 141–153, accessed April 11, 2017, at, http://dx.doi.org/10.1111/j.1365–2117.2005.00258.x.

Loeblich, A.R., Jr., and Tappan, H., 1987, Foraminiferal genera and their classification: New York, Van Nostrand Reinhold, 2 v., 1059 p., 847 pls.

Løseth, Helge, Gading, Marita, and Wensass, Lars, 2009, Hydrocarbon leakage interpreted on seismic data: Marine and Petroleum Geology, v. 26, p. 1304–1319.

Loucks, R.G., 1999, Paleocave carbonate reservoirs—Origins, burial-depth modifications, spatial complexity, and reservoir implications: American Association of Petroleum Geologists Bulletin, v. 83, p. 1795–1834.

Lucia, F.J., 1995, Rock-fabric/petrophysical classification of carbonate pore space for reservoir characterization: American Association of Petroleum Geologists Bulletin, v. 79, no. 9, p. 1275–1300.

Lucia, F.J., 1999, Carbonate reservoir characterization: Berlin, Springer-Verlag, 226 p.

MacEachern, J.A., Bann, K.L., Pemberton, S.G., and Gingras, M.K., 2007, The ichnofacies paradigm—High-resolution paleoenvironmental interpretation of the rock record, *in* MacEachern, J.A., Bann, K.L., Gingras, M.K., and Pemberton, S.G., eds., Applied ichnology: Society of Economic Paleontologists and Mineralogists Short Course Notes, v. 52, p. 27–93.

MacEachern, J.A., and Burton, J.A., 2000, Firmground *Zoophycos* in Lower Cretaceous Viking Formation, Alberta: A distal expression of the *Glossifungites* Ichnofacies: Palaios, v. 15, p. 387–398.

Macurda, D.B., Jr., 1997, Carbonate seismic facies analyses, *in* Palaz, Ibrahim, and Marfurt, K.J., eds., Carbonate seismology: Society of Exploration Geophysicists, Geophysical Developments Series, no. 6, p. 95–119.

Maliva, R.G., Guo, W., and Missimer, T., 2007, Vertical migration of municipal wastewater in deep injection well systems, South Florida, USA: Hydrogeology Journal, v. 15, p. 1387–1396.

McDonnell, A., Loucks, R.G., and Dooley, T., 2007, Quantifying the origin and geometry of circular sag structures in northern Fort Worth Basin, Texas—Paleocave collapse, pull-apart fault systems, or hydrothermal alteration?: American Association of Petroleum Geologists Bulletin, v. 91, p. 1295–1318.

Meyer, F.W., 1974, Evaluation of hydraulic characteristics of a deep artesian aquifer from natural water-level fluctuations, Miami, Florida: Florida Bureau of Geology Report of Investigations 75, 32 p.

Meyer, F.W., 1989, Hydrogeology, ground-water movement, and subsurface storage in the Floridan aquifer system in southern Florida: U.S. Geological Survey Professional Paper 1403–G, 59 p.

Miller, J.A., 1986, Hydrogeologic framework of the Floridan aquifer system in Florida, and in parts of Georgia, Alabama, and South Carolina: U.S. Geological Survey Professional Paper 1403-B, 91 p., 33 pls.

Miller, J.A., 1990, Ground water atlas of the United States—Segment 6, Alabama, Florida, Georgia, and South Carolina: U.S. Geological Survey Hydrologic Atlas 730-G, 28 p.

Mitchum, R.M., Jr., Vail, P.R., and Sangree, J.B., 1977, Seismic stratigraphy and global changes of sea level, Part 6: Stratigraphic interpretation of seismic reflection patterns in depositional sequences, *in* Payton, C.E., ed., Seismic stratigraphy—Applications to hydrocarbon exploration: American Association of Petroleum Geologists Memoir 26, p. 117–133.

Palmer, A.N., 2007, Hydrogeologic control of cave patterns: *in* Klimchouk, A.B., Ford, D.C., Palmer, A.N., and Dreybrodt, W., eds., Speleogenesis—Evolution of karst aquifers: Huntsville, Ala., National Speleological Society, Inc., p. 77–90.

Pomar, L., 2001, Types of carbonate platforms—A genetic approach: Basin Research, v. 31, p. 313–334.

Popenoe, P., Kohout, F.A., and Manheim, F.T., 1984, Seismic-reflection studies of sinkholes and limestone dissolution features on the northeastern Florida shelf, *in* Beck, B.F., ed., Sinkholes—Their geology, engineering, and environmental impact: Proceedings of First Multidisciplinary Conference on Sinkholes, p. 43–57.

Pratt, B.R., and James, N.P., 1992, Peritidal carbonates, *in* Walker, R.G., and James, N.P., eds., Facies models—Response to sea level change: St. John's, Newfoundland, Geological Association of Canada, p. 303–322.

Reese, R.S., 1994, Hydrogeology and the distribution and origin of salinity in the Floridan aquifer system, southeastern Florida: U.S. Geological Survey Water-Resources Investigations Report 94–4010, 56 p.

Reese, R.S., 2002, Inventory and review of aquifer storage and recovery in southern Florida: U.S. Geological Survey Water-Resources Investigations Report 02–4036, 56 p.

Reese, R.S., and Alvarez-Zarikian, C.A., 2007, Hydrogeology and aquifer storage and recovery performance in the Upper Floridan aquifer, southern Florida: U.S. Geological Survey Scientific Investigations Report 2006–5239, 117 p. (appendixes on CD).

Reese, R.S., and Cunningham, K.J., 2013, Preliminary stratigraphic and hydrogeologic cross sections and seismic profile of the Floridan aquifer system of Broward County, Florida: U.S. Geological Survey Open-File Report 2013–1141, 10 p., accessed April 11, 2017, at http://pubs.usgs.gov/of/2013/1141.

Reese, R.S., and Cunningham, K.J., 2014, Hydrogeologic framework and salinity distribution of the Floridan aquifer system of Broward County, Florida: U.S. Geological Survey Scientific Investigations Report 2014–5029, 60 p.

Reese, R.S., and Memberg, S.J., 2000, Hydrogeology and distribution of salinity in the Floridan aquifer system, Palm Beach County, Florida: U.S. Geological Survey Water-Resources Investigations Report 99–4061, 52 p.

Reese, R.S., and Richardson, E., 2008, Synthesis of the hydrogeologic framework of the Floridan aquifer system and delineation of a major Avon Park permeable zone in central and southern Florida: U.S. Geological Survey Scientific Investigations Report 2007–5207, 60 p., 4 pls., (appendixes on CD).

Reese, R.S., and Wacker, M.A., 2009, Hydrogeologic and hydraulic characterization of the surficial aquifer system, and origin of high salinity groundwater, Palm Beach County, Florida: U.S. Geological Survey Scientific Investigations Report 2009–5113, 83 p., (appendixes on CD).

Roberts-Ashby, T.L., Stewart, M.T., and Ashby, B.N., 2013, An evaluation of porosity and potential use for carbon dioxide storage in the Upper Cretaceous Lawson Formation and Paleocene Cedar Keys Formation of south-central and southern Florida: Environmental Geology, v. 20, p. 109–135.

Schlager, W., 1989, Drowning unconformities on carbonate platforms, *in* Crevello, P.D., Wilson, J.L., Sarg, J.F., and Read, J.F., eds., Controls on carbonate platform and basin development: Society of Economic Paleontologists and Mineralogists Special Publication 44, p. 15–25.

Scott, T.M., 1988, The lithostratigraphy of the Hawthorn Group (Miocene) of Florida: Florida Geological Survey Bulletin 59, 148 p.

Spechler, R.M., 1994, Saltwater intrusion and quality of water in the Floridan aquifer system, northeastern Florida: U.S. Geological Survey Water-Resources Investigations Report 92–4174, 76 p.

Spechler, R.M., 2001, The relation between structure and saltwater in the Floridan aquifer system, northeastern Florida, *in* U.S. Geological Survey Karst Interest Group Proceedings, February 13–16, 2001: U.S. Geological Survey Water-Resources Investigations Report 01–4011, p. 25–29.

Schwarz, Ernesto, and Buatois, L.A., 2012, Substrate-controlled ichnofacies along a marine sequence boundary: The intra-Valanginian discontinuity in central Neuquén Basin (Argentina): Sedimentary Geology, v. 277–278, p. 72–87.

Tingdahl, K.M., Bril, A.H., and de Groot, P.F., 2001, Improving seismic chimney detection using directional attributes: Journal of Petroleum Science and Engineering, v. 29, p. 205–211.

Tingdahl, K.M., and de Rooij, M., 2005, Semi-automatic detection of faults in 3D seismic data: Geophysical Prospecting, v. 53, p. 533–542.

Walsh, Virginia, and Price, R.M., 2010, Determination of vertical and horizontal pathways of injected fresh wastewater into a deep saline aquifer (Florida, USA) using natural chemical tracers: Hydrogeology Journal, v. 18, p. 1027–1042.

Williams, L.J., and Kuniansky, E.L., 2015, Revised hydrogeologic framework of the Floridan aquifer system in Florida and parts of Georgia, Alabama, and South Carolina: U.S. Geological Survey Professional Paper 1807, 140 p.

Winston, G.O., 1994, The Paleogene of Florida, Volume 3: Lithostratigraphy of the Cedar Keys Formation of Paleocene and Upper Cretaceous age—Peninsular Florida and environs: Coral Gables, Fla., Miami Geological Society, 50 p.

Zeng, H., Loucks, R., Janson, X., Wang, G., Xia, Y., Yuan, B., and Xu, L., 2011a, Three-dimensional seismic geomorphology and analysis of the Ordovician paleokarst drainage system in the central Tabei Uplift, northern Tarim Basin, western China: American Association of Petroleum Geologists Bulletin, v. 95, no. 12, p. 2061–2083.

Zeng, H., Wang, G., Janson, X., Loucks, R., Xia, Y., Xu, L., and Yuan, B., 2011b, Characterizing seismic bright spots in deeply buried, Ordovician paleokarst strata, Central Tabei Uplift, Tarim Basin, Western China: Geophysics, v. 76, no. 4, p. B127–B137.

Glossary

aggressiveness A measure of the relative capacity of water to dissolve rock material. In the context of karstification and speleogenesis, this usually concerns the dissolution of limestone or dolomite through the action of dissolved carbon dioxide (carbonic acid), although other acids may also be involved (Lowe and Waltham, 1995).

average energy A post-stack seismic-reflection attribute that computes the sum of the squared amplitudes, divided by the number of samples within the specified window used. This provides a measure of reflectivity and allows the analysis and interpretation of geologic features within a zone of interest (Chopra and Marfurt, 2007).

chimney Seismic noise caused by upward migration of fluids, most commonly gas, which degrades the quality of seismic reflection events and delineates a fluid-migration pathway (Aminzadeh and others, 2002).

composite sequence Relatively conformable sets of strata bounded by subaerial unconformities and their correlative conformities arranged in distinctive retrogradational, aggradational, or progradational patterns. These higher order sequences stack into lowstand, transgressive, and highstand sets (Kerans and Kempter, 2002). In this report, a composite depositional sequence was defined in the lower part of the Arcadia Formation and consists of only four aggradational, unconformity-bound, sheet-like depositional sequences, and thus is considered an incomplete composite sequence, because it lacks a complete suite of systems tracts.

depositional sequence "A stratigraphic unit composed of a relatively conformable succession of genetically related strata and bounded at its top and base by unconformities or their correlative conformities." (Mitchum and others, 1977b).

dip steering The process of auto-tracking seismic data by following the precalculated, local dip and azimuth of seismic reflections.

epigenic karst Formed by acid dissolution by water recharged from the surface (Klimchouk, 2000).

horizon-point data All known x, y, z coordinates (including depths) from well or seismic-reflection data that are used for the interpolation process to create horizon surfaces.

hypogenic karst "Hypogenic caves" and herein, karst "are formed by water in which the aggressiveness has been produced at depth beneath the surface, independent of surface or soil CO_2 or other near-surface acid sources" (Palmer, 2000)

inner sag width For seismic sag structures, inner sag width for an incremental seismic horizon in the overburden represents the distance between inflection points (that is, where the shape of the subsidence profile changed from concave to convex) on both sides of the sag (McDonnell and others, 2007).

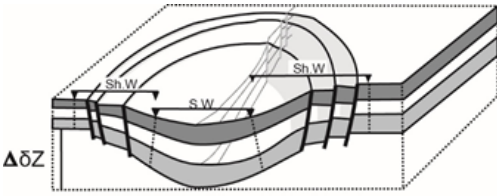

Modified from McDonnell and others (2007).

karst "A fluid flow system (geohydrodynamic system) with a permeability structure evolved as a consequence of dissolutional enlargement of initial preferential flow pathways, dominated by interconnected voids and conduits, and organized to facilitate the circulation of fluid in the downgradient direction due to the positive feedback between flow and conduit growth" (Klimchouk, 2015).

marl A lithology consisting of 35 to 65 percent carbonate and 65 to 35 percent clay (Pettijohn, 1957, p. 410; Flügel, 2004).

meta-attribute An attribute created from multiple input attributes.

reflection continuity A seismic reflection parameter that "is closely associated with the continuity of strata; continuous reflections suggest widespread, uniformly stratified deposits." (Mitchum and others, 1977a, p. 121).

seismic attribute A seismic attribute extracts information from seismic reflection data that can be used for quantitative and qualitative interpretation (Chopra and Marfurt, 2008)—seismic amplitude is an example.

seismic facies unit A "mappable, three-dimensional seismic unit composed of groups of reflections whose parameters differ from those of adjacent facies units." (Mitchum and others, 1977a).

seismic sequence "A depositional sequence . . . identified on a seismic section. It is a relatively conformable succession of reflections on a seismic section, interpreted as genetically related strata; this succession is bounded at its top and base by surfaces of discontinuity marked by reflection terminations and interpreted as unconformities or their correlative conformities. Seismic sequences have all the properties of depositional sequences subject only to the condition that these properties may be recognized and interpreted from the seismic reflection data." (Mitchum and others, 1977a).

sequence stratigraphy The study of rock relationships within a chronostratigraphic framework of repetitive, genetically related strata bounded by surfaces of erosion or nondeposition, or their correlative conformities (Van Wagoner and others, 1990).

shoulder width For seismic-sag structures, shoulder width (see figure accompanying definition of **inner sag width**) is the distance from the inflection point to the point where the horizon flattens out (McDonnell and others, 2007).

Underground Source of Drinking Water The U.S. Environmental Protection Agency designation for an aquifer, or that part of an aquifer, that contains a sufficient quantity of groundwater to supply a public water system, contains fewer than 10,000 mg/L of total dissolved solids, and is not an exempted aquifer (U.S. Environmental Protection Agency, 2015).

Walther's Law of facies The principle that facies that occur in conformable vertical successions of strata also occur in laterally adjacent environments (Middleton, 1973).

Glossary References Cited

Aminzadeh, F., Connolly, D., and de Groot, P., 2002, Interpretation of gas chimney volumes: Society of Exploration Geophysicists Technical Program Expanded Abstracts, p. 440–443.

Chopra, Santinder, and Marfurt, K.J., 2007, Seismic attributes for prospect identification and reservoir characterization: Society of Exploration Geophysical Development Series, no. 11, 464 p.

Chopra, Satinder, and Marfurt, K.J., 2008, Emerging and future trends in seismic attributes: The Leading Edge, v. 27, p. 298–318.

Flügel, Erik, 2004, Microfacies of carbonate rocks—Analysis, interpretation and application: Springer, New York, 976 p.

Kerans, C., and Kempter, K., 2002, Hierarchical stratigraphic analysis of a carbonate platform Permian of the Guadalupe Mountains: American Association of Petroleum Geologists, Datapages Discovery Series no. 5. (CD–ROM and color plate.)

Klimchouk, Alexander, 2000, Speleogenesis under deep-seated and confined settings, *in* Klimchouk, A.B., Ford, D.C., Palmer, A.N., and Dreybrodt, W., eds., Speleogenesis: evolution of karst aquifers: Huntsville, Ala., National Speleological Society, Inc., p. 244–260.

Klimchouk, Alexander, 2015, The karst paradigm: changes, trends and perspectives: Acta Carsologica, v. 44, p. 289–313.

Lowe, D., and Waltham, T., 1995, A dictionary of karst and caves—A brief guide to the terminology and concepts of cave and karst science: London, British Cave Research Association, Cave Studies Series no. 6, 41 p.

McDonnell, A., Loucks, R.G., and Dooley, T., 2007, Quantifying the origin and geometry of circular sag structures in northern Fort Worth Basin, Texas: Paleocave collapse, pull-apart fault systems, or hydrothermal alteration?: American Association of Petroleum Geologists Bulletin, v. 91, p. 1295–1318.

Middleton, G.V., 1973, Johannes Walther's law of the correlation of facies: Geological Society of America Bulletin, v. 84, p. 979–988.

Mitchum, R.M., Jr., Vail, P.R., and Sangree, J.B., 1977a, Seismic stratigraphy and global changes of sea level, Part 6: Stratigraphic interpretation of seismic reflection patterns in depositional sequences, *in* Payton, C.E., ed., Seismic stratigraphy—Applications to hydrocarbon exploration: American Association of Petroleum Geologists Memoir 26, p. 117–133.

Mitchum, R.M., Jr., Vail, P.R., and Thompson, S., III 1977b, Seismic stratigraphy and global changes of sea level, Part 2: Depositional sequence as a basic unit for stratigraphic analysis, *in* Payton, C.E., ed., Seismic stratigraphy—Applications to hydrocarbon exploration: American Association of Petroleum Geologists Memoir 26, p. 53–62.

Palmer, A.N., 2000, Hydrogeologic control of cave patterns: *in* Klimchouk, A.B., Ford, D.C., Palmer, A.N., and Dreybrodt, W., eds., Speleogenesis—Evolution of karst aquifers: Huntsville, Ala., National Speleological Society, Inc., p. 77–90.

Pettijohn, F.J., 1957, Sedimentary rocks: New York, Harper, 718 p.

U.S. Environmental Protection Agency, 2015, Aquifer exemptions in the underground injection control program, accessed April 11, 2017, at https://www.epa.gov/uic/aquifer-exemptions-underground-injection-control-program.

Van Wagoner, J.C., Mitchum, R.M., Campion, K.M., and Rahmanian, V.D., 1990, Siliciclastic sequence stratigraphy in well logs, cores and outcrops: concepts for high-resolution correlation of time and facies: American Association of Petroleum Geologists Methods in Exploration Series, no. 7, 55 p.

Prepared by the Lafayette Publishing Service Center

For more information about this publication, contact
Director, Caribbean-Florida Water Science Center
U.S. Geological Survey
4446 Pet Lane, Suite 108
Lutz, FL 33559
(813) 498-5000

For additional information visit
https://www2.usgs.gov/water/caribbeanflorida/index.html

ISSN 2328-0328 (online)
https://doi.org/10.3133/sir20175109